DISTRIBUTED RESOURCE ALLOCATION AND PERFORMANCE ANALYSIS IN 5G WIRELESS CELLULAR NETWORKS

Chuan Ma

A THESIS SUBMITTED IN FULFILLMENT OF THE REQUIREMENTS OF THE DEGREE OF DOCTOR of PHILOSOPHY

SCHOOL OF ELECTRICAL AND INFORMATION ENGINEERING
The UNIVERSITY OF SYDNEY

June, 2018

To my parents and wife,

Baili Ma, Sanxian Fu, and Yu Su

Acknowledgements

There are so many people who I would like to thank for their great support in this tough but exciting Ph.D journey. They inspired me, encouraged me, and fought with me to achieve this first milestone in my research career. Maybe I will miss some of their names here, but I am sure that all of them will be remembered for life.

My gratitude should be firstly given to my supervisor, Dr. Zihuai Lin. I am really grateful for his appreciation, for offering me the opportunity to study in Sydney and the financial support during the entire Ph.D program. Those valuable discussions and constructive suggestions were the indispensable parts of my research. His deep insight enlightened me at various aspects including but no limited to the research. His attitudes to life helped me to face the ups and downs in these years and will continuously encourage me to take on challenges in the future.

I wish to express my special thanks to my co-supervisors, Dr. Ming Ding and Prof. Jun Li. I will never forget the days when I worked with them. Their brilliant inspiration and excellent suggestions guided me through the difficult times of my study. Their passion and dedication for work motivated me to conquer the research problems during the past years.

I would like to express my sincere thanks to Prof. Guoqiang Mao, for his great inspiration, intelligent suggestions, and helpful comments.

I would like to thank all my co-authors, Dr. David López- Pérez, Dr. He(Henry) Chen, Prof. Branka Vucetic, and Loris Marini, for their passionate discussions, constructive suggestions, and useful comments.

I am also indebted to all my friends in the University of Sydney, Di Zhai, Dezhou Zhang, Xuefeng Yao, Yi Zhou, Allen, Emma, Rui Zhang, and Zhanwei Hou, for all their help and companionship they provided to me, and to my nine lovely friends who we met in the trip to Carins, Yubo Liu, Jing Wang, Jiao Liu, Juejun Chen, Jason, Zhengtai Xiao, Miaomiao Zheng, Ying Ying, and Yu Su, for the happiness and lives

we shared, and to my familiar but almost never met friends on the Internet, Eric, God A, Ibox, OMG, Savage, TB, RyaNIng, Baozi, and Damon, for the special time that we spent at nights. I will always cherish these beautiful memories with you all and hold you in special places in my heart.

Last and most importantly, I would like to express my deepest gratitude to my parents and my wife. Without your selfless love and constant support and encouragement, I would never have embarked on this journey and completed the Ph.D study.

Chuan Ma
Sydney, Australia
April, 2018

Statement of Originality

This thesis, submitted in fulfillment of the requirements for the degree of Doctor of Philosophy, is the original work of the author unless otherwise stated, while enrolled in the school of Electrical and Information Engineering at the University of Sydney. The content in this thesis has not been previously submitted for the award of any other academic qualification in any other university or educational institution. Most of the results contained herein have been published in journals or conference of international standing. The author's contribution in terms of published material is listed in the chapter "List of Publication".

There studies were conducted under the supervision of Dr. Zihuai Lin from the University of Sydney, Dr. Ming Ding from Data61, CSIRO, Prof. Jun Li from Nanjing University of Science and Technology, China, and Prof. Guoqiang Mao from the University of Technology Sydney.

Chuan Ma
School of Electrical and Information Engineering
The University of Sydney
April, 2018

Abstract

This thesis focuses on the study of Heterogeneous Networks (HetNets), Device-to-device (D2D) communication networks, and unmanned aerial vehicle (UAV) networks in fifth generation wireless communication (5G) systems. HetNets that consist of macro-cells and small-cells have become increasingly popular in current wireless networks and 5G systems to meet the exponentially growing demand for higher data rates. Compared to conventional homogeneous cellular networks, the disparity of transmission power among different types of base stations (BSs), the relatively random deployment of SBSs, and the densifying networks, bring new challenges, such as the imbalanced load between macro and small cells and severe inter-cell interference. In the other hand, with the skyrocketing number of tablets and smart phones, the notion of caching popular content in the storage of BSs and users' devices is proposed to reduce duplicated wireless transmissions.

To fulfill multi-fold communication requirements from humans, machine, and things, the 5G systems which include D2D communications, UAV communications, and so on, can improve the network performance. Among them, the performance analyses of these emerging technologies are attracting much attention and should be investigated first.

This thesis focuses on these hot issues and emerging technologies in 5G systems, analyzing the network performance and conducting the allocation of available resources, such as serving BSs, spectrum resources, and storage resources. Specifically, three main research focuses are included in the thesis.

The first focus of this thesis is the impact of the BS idle mode capacity (IMC) on the network performance of multi-tier and dense HCNs with both line-of-sight (LoS) and non-line-of-sight (NLoS) transmissions. I consider a more practical set-up with a finite number of UEs in the analysis. Moreover, the SBSs apply a positive power bias in the cell association procedure, so that macrocell UEs are actively encouraged to use the more lightly loaded SBSs. In addition, to address the severe interference that these

cell range expanded UEs may suffer, the MBSs apply enhanced inter-cell interference coordination (eICIC), in the form of almost blank subframe (ABS) mechanism. For this model, I derive the coverage probability and the rate of a typical UE in the whole network or a certain tier. The impact of the IMC on the performance of the network is shown to be significant. In particular, it is important to note that there will be a surplus of BSs when the BS density exceeds the UE density, and thus a large number of BSs switch off. As a result, the overall coverage probability, as well as the area spectral efficiency (ASE), will continuously increase with the BS density, addressing the network outage that occurs when all BSs are active and the interference becomes LoS dominated. Finally, the optimal ABS factors are investigated in different BS density regions. One of major findings is that MBSs should give up all resources in favor of the SBSs when the small cell networks go ultra-dense. This reinforces the need for orthogonal deployments, shedding new light on the design and deployment of the future 5G dense HCNs.

The second focus of this thesis is the content caching in D2D communication networks. In practical deployment, D2D content caching has its own problem that is not all of the user devices are willing to share the content with others due to numerous concerns such as security, battery life, and social relationship. To solve this problem, I consider the factor of social relationship in the deployment of D2D content caching. First, I apply stochastic geometry theory to derive an analytical expression of downloading performance for the D2D caching network. Specifically, a social relationship model with respect to the physical distance is adopted in the analysis to obtain the average downloading delay performance using random and deterministic caching strategies. Second, to achieve a better performance in more practical and specific scenarios, I develop a socially aware distributed caching strategy based on a decentralized learning automaton, to optimize the cache placement operation in D2D networks. Different from the existing caching schemes, the proposed algorithm not only considers the file request probability and the closeness of devices as measured by their physical distance, but also takes into account the social relationship between D2D users. The simulation results show that the proposed algorithm can converge quickly and outperforms the random and deterministic caching strategies. With these results, the work sheds insights on the design of D2D caching in the practical deployment of 5G networks.

The third focus of this thesis is the performance analysis for practical UAV-enabled networks. By considering both LoS and NLoS transmissions between aerial BSs and

ground users, the coverage probability and the ASE are derived. Considering that there is no consensus on the path loss model for studying UAVs in the literature, in this focus, three path loss models, i.e., high-altitude model, low-altitude model, and ultra-low-altitude model, are investigated and compared. Moreover, the lower bound of the network performance is obtained assuming that UAVs are hovering randomly according to homogeneous Poisson point process (HPPP), while the upper bound is derived assuming that UAVs can instantaneously move to the positions directly overhead ground users. From the analytical and simulation results for a practical UAV height of 50 meters, I find that the network performance of the high-altitude model and the low-altitude model exhibit similar trends, while that of the ultra-low-altitude model deviates significantly from the above two models. In addition, the optimal density of UAVs to maximize the coverage probability performance has also been investigated.

Contents

List of Figures

Acronyms

ABS	almost blank subframe
ASE	area spectral efficiency
AWGN	additive white gaussian noise
BS	base station
CRE	cell range expansion
DC	deterministic caching
DGPA	discrete generalized pursuit algorithm
D2D	device-to-device
eICIC	enhanced inter-cell interference coordination
HCN	heterogeneous cellular networks
HPPP	homogeneous poisson point process
IMC	idle mode capacity
IU	important user
LoS	line-of-sight
LTE	long term evolution
MBS	macro base station
NLoS	non-line-of-sight
OC	optimal cacaing
PDF	probability distribution function
QoE	quality-of-experience
RC	random caching
REB	resource expanded bias
RV	random variable
SBS	small base station
SINR	signal-to-interference-plus-noise-ratio
TDD	time-division duplexing
UAV	unmanned aerial vehicle

UDN	ultra-dense networks
UE	user equipment
5G	fifth generation wireless communication systems

List of Publications

The following is a list of publications in refereed journals and conference proceedings produced during my Ph.D. candidature. In some cases, the journal papers contain materials overlapping with the conference publications.

Journal Papers

[J1] C. Ma, M. Ding, D. López- Pérez, Z. Lin, J. Li and G. Mao, "Performance Analysis of the Idle Mode Capability in a Dense Heterogeneous Cellular Network," in *IEEE Transactions on Communications*. [Early Access]. April. 2018. doi: 10.1109/TCOMM.2018.2822805.

[J2] C. Ma, M. Ding, H. Chen, Z. Lin, G. Mao, Y. Liang and B. Vucetic, "Socially Aware Caching Strategy in Device-to-Device Communication Networks," in *IEEE Transactions on Vehicular Technology,* vol. 67, no. 5, pp. 4615-4629, May 2018. doi: 10.1109/TVT.2018.2796575.

[J3] P. Cheng, C. Ma, M. Ding, Y. Hu, Z. Lin, Y. Li and B. Vucetic, "Localized Small Cell Caching: A Machine Learning Approach Based on Rating Data", submitted to *IEEE Transactions on Communications*, Minor Revision,2018.

Conference Papers

[C1] C. Ma, M. Ding, H. Chen, Z. Lin, G. Mao and D. López- Pérez, "On the Performance of Multi-tier Heterogeneous Cellular Networks with Idle Mode Capability", in Proceedings of IEEE Wireless Communications and Networking Conderence (WCNC), Barcelona, April 2018. **Best Student Paper** of the track "Wireless Networks".

[C2] C. Ma, M. Ding, H. Chen, Z. Lin, G. Mao and X. Li, "Socially Aware Distributed Caching in Device-to-Device Communication Networks," in *IEEE Globecom Workshops (GC Wkshps)*, Washington, DC, 2016, pp. 1-6. doi: 10.1109/GLOCOMW.2016.7849047.

[C3] C. Ma, Z. Lin, L. Marini, J. Li and B. Vucetic, "Learning Automaton Based Distributed Caching for Mobile Social Networks," in *IEEE Wireless Communications and Networking Conference (WCNC)*, Doha, 2016, pp. 1-6. doi: 10.1109/WCNC.2016.7564817.

[C4] C. Liu, M. Ding, C. Ma, Q. Li, Z. Lin and Y. Liang, "Performance Analysis for Practical Unmanned Aerial Vehicle Networks with LoS/NLoS Transmissions", in *Proceedings of IEEE International Conference on Communications Workshops (ICC Wkshps)*, Kansas City, MO, 2018.

Chapter 1

Introduction

This chapter firstly describes the history and motivation for the research work in this thesis. Then the major research problems and the main contributions in this issue are summarized.

1.1 History and Motivation

Since Alexander Graham Bell carried out the first bi-directional telephone transmission in 1876, the development of telecommunication has changed people's lives incredibly. Meanwhile, requirements for higher speed and better service have kept pushing forward advancements in communication theory.

Voice services were the dominant application at the beginning of this century, demanding tens of Kbps for each user, while data traffic constitutes more than 90% of the total bits in many wireless networks nowadays [1], needing tens of Mbps or even Gbps per user. According to Cisco, an unprecedented worldwide growth of mobile data traffic is expected to continue at an annual rate of 45% over the next decade, surpassing 30 exabytes per month by 2020 [2]. With the fast development of mobile data applications such as wireless video streaming and social networking, the huge

demand pushes operators to provide high-throughput wireless access services in 5th generation (5G) networks.

To meet the explosively increasing demand for more mobile data traffic [2], commercial wireless networks are evolving to looking for every possible tool to improve network capacity. In [3], the existing tools are classified into paradigms:

- Increase node density to enhance spatial reuse gain;
- Exploit new spectrum resources to enlarge the available bandwidth;
- Enhance spectral efficiency through multi-antenna transmissions, cooperative communications, dynamic Time-Division Duplexing (TDD) techniques, etc.

Among them, higher frequency reusing by deploying more and more small cells [3] is a straightforward way to improve wireless capacity. A major part of the mobile throughput growth has already been supplied by the so-called network densification during the past few years, and this trend is expected to continue in the years to come. Thus, the emerging fifth generation (5G) cellular network deployments are envisaged to be heterogeneous and dense. Such a dense heterogeneous cellular network (HCN) will be comprised of a conventional cellular network overlaid with a variety of small cells, metro, pico, and femtocells. This will greatly help to realize the 5G requirement of a 100x increase in mobile network throughput with respect to the current 4G one.

However, with the increasing amount of node' density, the cell splitting gain significantly reduces inter-cell interference [4]. More importantly, how to allocate the radio frequency and bandwidth resource to macro base stations (MBSs) and small base stations (SBSs) should be seriously considered and carefully designed in the

future ultra-dense HetNets. Andrews *et al.* in [5] first analyzed the coverage probability of a single-tier small cell network by modeling BS locations as a homogeneous point Poisson process (HPPP). That study concluded that the coverage probability of the network did not depend on the density of BSs in interference-limited scenarios. Following [5], Dhillon *et al.* in [6] also reached the same conclusion for each BS tier in a multi-tier HCN, but it is important to note that the aforementioned studies assumed an unlimited number of user equipment (UE) in the network, which implies that all BSs would always be active and transmit in all time and frequency resources. Obviously, this may not be the case in practice, especially in ultra-dense networks (UDNs).

To attain a more practical network performance, Lee *et al.* in [7] first analyzed the coverage probability of a single-tier small cell network with a finite number of UEs, and derived the optimal BS density accordingly. This was done considering the tradeoff between the performance gain and the resultant network cost. Moreover, a system-level analysis of cellular networks with respect to the density of BSs and blockages was conducted in [8], which showed the validity for the footprints of buildings in dense urban environments. A trackable performance analysis was proposed in [9], and they found that the increasing trend of the ASE was highly related to the density of BSs and UEs. Recently, the authors in [10] studied the coverage probability and ASE of a single-tier small cell network with probabilistic line-of-sight (LoS) and non-LoS (NLoS) transmissions, in which the UE number is finite and the small cell BS has an idle mode capability (IMC). More specifically, if there is no active UE within the coverage area of a certain BS, the BS will be turned off and will not transmit. The IMC switches off unused BSs, and thus can improve the UEs' coverage probability

and network energy efficiency as the network density increases. This is because UEs can receive stronger signals from the closer BSs, while the interference power remains constant or even decreases thanks to the IMC. This conclusion in [10] - the coverage probability depends on the density of BSs in an interference-limited network - is fundamentally different from the previous results in [5] and [6], and presents new insights for the design and deployment of 5G networks [11]. To realize the aggressive 5G version, milimeter-wave (mmWave) massive MIMO used for the access and backhaul in UDN has been considered as a promising technique to enable gigabit-per-second user experience, seamless coverage, and green communication [12]. Due to the ultra-dense deployment, each user may receive the signal from multiple BSs. To exploit the advantage of this architecture, the accurate channel state information (CSI) associated with multiple cells is essential for the joint beamforming, scheduling and cooperation among the ultra-dense small-cell BSs. To require the reliable CSI with low overhead, [13], [14] have proposed a multilevel codebook based joint channel estimation and beamforming for mmWave access and backhaul, and in [15] the hybrid analog-digital beamforming scheme is proposed to support the multi-stream transmission with low hardware cost and energy consumption. Motivated by the gap that none of the aforementioned works considered the IMC in the dense HetNets, in Chapter 3, a basic analysis of the network performance has been derived by considering practical setting, and the results can shed light on the design and the deployment of the future ultra-dense HetNets.

Although the spectrum efficiency is improved with the densifying network, the current wireless access technologies have almost approached their theoretical limits and it is imperative to develop new communication strategies to meet the ever-increasing

demand from mobile subscribers [1]. To tackle this problem, several new technologies are proposed to show their high effectiveness. One of the promising approaches in 5G is content caching, as this technology can significantly offload the network traffic by optimally and intelligently storing the content files in the small base stations (SBSs) [4] and/or in mobile users' devices [11, 16, 17] that are closer to end-users. As a result, network congestion can be eased and users' quality-of-experience (QoE) can be significantly improved. With the emergence of 5G, exchanging the cached files among mobile devices through D2D communications, termed as D2D caching, has attracted considerable attention recently [18]. In [19], Ji *et al.* considered the D2D caching from the perspective of information theory and proposed deterministic and random caching schemes, both of which are shown to be able to achieve the information theoretic bound within a constant multiplicative factor. In addition, Ji *et al.* in [20] analyzed the basic principle and system performance of the D2D caching networks, and demonstrated that the gain from the unicast transmission is comparable to the gain from the coded BS multicast in [21]. However, in device-to-device (D2D) caching, due to limited memory and energy resources, users may be unwilling to serve data over the aforementioned D2D transmission unless they can obtain benefits (e.g., monetary incentives) from the operator [22] or other incentives (e.g., social relationship) from the users [23]. Furthermore, the social interactions between users should also be carefully taken into consideration. To make full advantage of the social characters as well as the content request probability, which needs to solve a complicated combinatorial optimization problem, the classical optimization methods are not suitable to address such a challenging problem. This motivate me to design a reinforcement learning based iterative algorithm, by simulating the exact content

requested by the user, and then observing the resultant reward or penalty. To the best of my knowledge, how to design the content placement in D2D caching by incorporating the social characters between users remains an open question, and there is a lack of performance analysis for the socially aware D2D caching networks, which motivated Chapter 4 of this thesis.

Another focus of this thesis is the performance analysis of the unmanned aerial vehicles (UAVs)-mounted networks. Due to the flying nature of unmanned aerial vehicles (UAVs), base stations (BSs) can be mounted on the UAV to support wireless communications and boost the network performance of the 5G systems. For example, UAV-mounted base stations (UAV-BSs) are introduced when a natural disaster interrupts communications or ground base stations are overloaded [24]. Compared with ground BSs, the flexibility of UAV-BSs allows them to adapt their locations to the demand of users.

In the analysis of the network performance, although the path loss model has been considered as a key factor in the performance analysis for UAV networks, there is no consensus on this issue yet. For example, the work in [24] and [25] only considered the UAV hovering in a LoS-dominated network for simplicity. To conduct a practical analysis for UAV, the authors of [26] proposed a general path loss model which considers both LoS and NLoS connections and their occurrence probabilities, depending on the elevation angle between a UAV and a user. Despite that this model has been widely adopted as the high-altitude model (a typical height is around 1000 meters), the network performance has not been investigated due to the complexity of the proposed model. On the other hand, the work in [27] provided a network analysis of the terrestrial cellular network where the antenna height between BSs and users

is around 10m∼30m, together with 3GPP LoS and NLoS models. Considering that the height of UAVs is comparable with that of ground base stations in future UAV networks, the curent macrocell-to-UE model (a typical height is around 32 meters) and picocell-to-UE model (a typical height is around 10 meters) proposed for terrestrial communication in 3GPP standards can also be applied to the UAV-based network. Such macrocell-to-UE model and picocell-to-UE model are referred to as the low-altitude model and the ultra-low-altitude model hereafter. To the best of my knowledge, the path loss model for UAV-BSs has not been adequately explored in the literature, which motivated Chapter 5 of this thesis.

1.2 Research Problems and Contributions

The main topics of the thesis are the performance analysis of the 5G wireless network and the design of the resource allocation. Specially, the performance analysis of the dense HetNets and the D2D-enabled cellular networks are presented in Chapter 3, 4, and 5. Additionally, the corresponding design of the radio frequency resource allocation is discussed in Chapter 3 and a novel caching strategy for D2D users is proposed in Chapter 4. In the sequel of this section, I elaborate the thesis research problems and the corresponding contributions.

The first research problem in this thesis is the theoretical study of the dense HCNs. It is commonly assumed that there is an unlimited number of UEs in the network, which is not the case in practice for the dense or ultra-dense networks. To attain a more practical network performance, the idle mode capacity (IMC) of the BSs should be considered. Moreover, to encourage UEs to take advantage of the large amount of resource at the SBSs, cell range expansion (CRE) combined with

the enhanced intercell interference coordination (eICIC) scheme has been introduced to the networks, which can significantly reduce interference among UEs. One such eICIC strategy implemented in the time-domain, called almost blank subframe (ABS), received a lot of attention for the easy implementation. To the best of my knowledge, the theoretical study of dense HCNs with a realistic path loss model, a finite number of UEs as well as CRE together with ABSs has not been conducted before, although some preliminary simulation results can be found in [3] and [28]. Motivated by this theoretical gap, in Chapter 3, I analyze for the first time the coverage probability and ASE of a HCN with *i)* two BS tiers, *ii)* a general and practical path loss model, *iii)* a finite number of UEs, *iv)* an IMC at small cell BSs, and *v)* a flexible cell association strategy with CRE and ABS.

This results in a completely new modelling and analysis, through which I provide the following theoretical contributions:

- I calculate an analytical expression to derive the density of active BSs in a two tier HCN. Based on this, I compute the analytical expressions of the coverage probability and ASE for such two tier HCN, while considering the IMC.

- The optimal ABS factor, i.e., the ratio between the number of ABS to the number of total subframes, is showed numerically and obtained by simulations for scheduling in MBSs for different SBS density regions. Moreover, I prove that ASE can achieve the maximum value if the ABS factor is set to one when the small cell networks go ultra-dense.

- I perform an extensive simulation campaign to validate the accuracy of the analytical results. Both simulation and analytical results match and shed new

insights on the design and deployment of BSs in 5G UDNs. One important finding is that MBSs should give up all resources in favour of the SBSs when the small cell network goes ultra-dense. This reinforces the need for orthogonal spectrum assignments for macrocell and ultra-dense small cell deployments.

The second research problem in this thesis is to investigate the system design and performance analysis of the D2D caching networks. Exchanging the cached files among mobile devices through D2D communications, termed D2D caching, has attracted considerable attention. However, how to activate users to share the cached contents always is a problem. To solve this, the concept of the social network is proven to be a useful tool in this application. By using the social relationship among users, D2D communications should be able to promote and the corresponding caching scheme could be implemented. To the best of my knowledge, how to design the content placement in D2D caching by incorporating the social characters between users remains an open question, and there is a lack of performance analysis for the socially aware D2D caching networks. Motivated by the above observations, it is interesting and challenging to investigate the system design and performance analysis of the D2D caching networks. In Chapter 4, I study the caching placement problem among D2D users. First, using the stochastic geometry tool, a probabilistic caching scheme is analyzed when the social relationship between users is distance-dependent. Then, a distributed caching algorithm is proposed for a deterministic network scenario.

It is important to note that the first contribution is regarding the theoretical performance bounds using the random and deterministic caching strategies. However, it still remains unclear how to implement the 5G D2D caching in practice. And more importantly, can we even do better than the derived analytical results by means of

more advanced algorithms? In practice, it is desirable and might be feasible to optimize the D2D content placement on the fly, and popular content can be thus placed in particular devices to achieve high performance gains in particular areas. Therefore, the second contribution is related to devising a distributed algorithm for D2D caching with known number and locations of users in realistic scenarios. Specifically, the following contributions are made:

- I derive an analytical expression of downloading performance for the D2D caching network using stochastic geometry. Specifically, by adopting the physical distance-dependent social model wherein the probability that two users have a social relationship is assumed to be a decreasing function of their physical distance, the average transmission probability for a D2D user is analyzed and the average downloading delay performance of the proposed scheme is derived using random and deterministic caching strategies. An interesting finding is that the successful transmission probability will become stable when the density of users is large enough.

- Following the theoretical finding, in order to reduce the downloading delay, I optimize the caching strategy in a deterministic network scenario. More specifically, I develop a content caching algorithm based on a decentralized learning approach, termed DGPA. Different from most papers on D2D caching (e.g., [29]-[30]), I embrace several practical features of D2D communications, such as different cache sizes, different requesting distribution and social interaction among users, into the design of the caching algorithm. To the best of my knowledge, the proposed caching algorithm is the first one that considers not only the file request probability and the closeness of devices as measured by their

physical distance, but also takes into account the social relationship among D2D users. Furthermore, to increase the diversity of the cached contents in the network, the mutual impact between the different cached D2D users is considered. The convergence of the proposed caching algorithm is also analyzed.

- Simulations are conducted to validate the accuracy of the analytical results. Both simulation and analytical results show that the proposed algorithm not only outperforms its counterpart using deterministic caching, but also outperforms that in the existing literature.

The third research problem in this thesis is to conduct the performance analysis of the UAV-enabled network. By utilising the flexibility of the UAVs, the UAV mounted BSs can provide an enhanced cover to remedy the shortage of the ground BSs and improve the service quality of users. Before the UAV deployments are designed, the performance of this 3D network should be conducted first and the path loss model is one of the key factors in the system model. Although several works have considered different path loss models, there is no consensus on this issue yet. Motivated by the above theoretical gap and to answer such a fundamental question, in this paper, I analyze the performance of UAV-enabled networks on the condition of different path loss models. Specifically, the following contributions are made:

- I provide three path loss models, i.e., high-altitude model, low-altitude model, and ultra-low-altitude model, for different ranges of UAV's height in the system. The analytical results of the coverage probability and ASE are investigated and compared.

- I provide the lower and upper bounds of the network performance by assuming

that UAVs are hovering randomly or moving instantaneously to the positions directly overhead ground users.

- The optimal density of UAVs to maximize the coverage probability performance is also investigated.

Chapter 2

Background

This chapter introduces several basic point processes in stochastic geometry as math preliminary. Then HetNets in the 5G systems are introduced, including their structures, challenges, and related works. At last, the basic, and the concepts of caching and UAV-communication are included.

2.1 Stochastic Geometry / Point Process

Stochastic geometry deals with random spatial patterns. Point processes are the most basic and important objects in stochastic geometry, which are defined as follows [31].

Definition 2.1.1. A point process is a countable random collection of points that reside in some measure space, usually the Euclidean space $\mathbb{R}^d,\ d \geq 1$. The associated σ-algebra consists of the Borel sets $\mathcal{B}^d$, and the measure is the Lebesgue measure.

Following this definition, the point process can be viewed as a countable random set $\Phi = x_1, x_2, \cdots \subset \mathbb{R}^d$, consisting of random variables $x_i \in \mathbb{R}^d$ as elements. There are several important properties related to a point process.

Counting Measure

The counting measure N denotes the number of points falling in set $B \subset \mathbb{R}^d$. As we know, $N(B)$ is a random non-negative integer, which can be calculated as

$$N(B) = \sum_{i=1}^{\infty} \mathbf{1}(x_i \in B), \tag{2.1.1}$$

where $\mathbf{1}(\cdot)$ is the indicator function.

Intensity Measure

The intensity measure Λ represents the expected number of points falling in the set B, which is defined as

$$\Lambda(B) \triangleq \mathbb{E}[N(B)]. \tag{2.1.2}$$

If there exists a density λ of Λ, then λ is called the intensity function. That is,

$$\Lambda(B) = \int_B \lambda(\xi) d\xi. \tag{2.1.3}$$

The intensity function λ represents the expected number of points in the process per unit volume.

Void Probability

The distribution of a simple point process can be uniquely determined by its void probabilities of bounded Borel sets. The void probability of $B \subset \mathbb{R}^d$ is

$$v(B) \triangleq \Pr[N(B) - 0]. \tag{2.1.4}$$

Probability Generating Functional

The probability generating functional plays the same role for a point process as the probability generating functional plays for a non-negative integer-valued random variable. The probability generating functional for a point process Φ is defined as

$$G_\Phi(f) = \mathbb{E}\left[\exp\left(\int_{\mathbb{R}^d} \ln f(\xi) dN(\xi)\right)\right] = \mathbb{E}\left[\prod_{\xi \in \Phi} f(\xi)\right], \tag{2.1.5}$$

where function $f : \mathbb{R}^d \longrightarrow [0, 1]$ with $\{\xi \in \mathbb{R}^d : f(\xi) < 1\}$.

Moreover, there are a few dichotomies concerning point processes.

1) simple: A point process is simple if only one point can exist at a given location, i.e., no coincident points.

2) stationary: A point process is stationary if its distribution is translation invariant, i.e., $\Phi + s = \{x + s : x \in \Phi\}$ has the same distribution as $\Phi, \forall s \in \mathbb{R}^d$.

3) isotropic: A point process is isotropic if its distribution is invariant under rotations around the origin, i.e., $\mathcal{O}\Phi = \{\mathcal{O}x : x \in \Phi\}$ has the same distribution as Φ for any rotation $\mathcal{O}$ around the origin.

4) homogeneous: A point process is homogeneous if its intensity function λ exists and is constant.

In the following, I briefly introduces several point processes used to model wireless networks in this thesis.

2.1.1 Poisson Point Process

The Poisson point process (PPP) offers a computational framework, so it is widely used in the analysis of wireless networks. Its formal definition is given as follows.

Definition 2.1.2. A point process Φ is a Poisson point process if the following two properties hold:

- For all $B \subset \mathbb{R}^d$, $N(B)$ has a Poisson distribution. That is, with the intensity measure $\Lambda(B)$,
$$\Pr[N(B) = k] = \exp(-\Lambda(B)) \cdot \frac{\Lambda^k(B)}{k!}. \tag{2.1.6}$$
- For all disjoint bounded sets $B_1, B_2, \cdots, B_m$ in $\mathbb{R}^d$, $N(B_1), N(B_2), \cdots, N(B_m)$ are independent random variables.

From this definition, we can see that the key property of a PPP is complete spatial randomness. That is, all the points are independently located in the space.

With the intensity measure $\Lambda(B)$ for $B \subset \mathbb{R}^d$, because $N(B)$ follows a Poisson distribution, the void probability of a Poisson point process can be calculated as

$$\Pr[N(B) = 0] = \frac{\exp(-\Lambda(B))\Lambda^0(B)}{0!} = \exp(-\Lambda(B)). \tag{2.1.7}$$

The probability generating function of a PPP is

$$G_\Phi(f) = \exp\left(-\int_{\mathbb{R}^d}(1 - f(\xi))\lambda(\xi)d\xi\right), \tag{2.1.8}$$

which can be used to calculate the Laplace transform related to Φ.

There are several appealing features of a PPP.

- A disjoint union $\bigcup_{i=1}^{\infty}\Phi_i$ of the point processes $\Phi_1, \Phi_2, \cdots$ is called a superposition. The superposition of two or more mutually independent Poisson point processes is again a PPP.

- The thinned point process $\Phi_{thin} \subset \Phi$ is obtained by including $\xi \subset \mathbb{R}^d$ in Φ_{thin} with retention probability $p(\xi)$, where the points are included or excluded independently on each other, said to be an independent thinning. The independent thinning of a PPP with intensity function $\lambda(\xi)$ is again a PPP with intensity function $p(\xi)\lambda(\xi)$.

- Given that a PPP Φ has a point x_0, the law of point process $\Phi - x_0$ is the same as the law of Φ. That is, the reduced Palm probability of a PPP is the distribution of this PPP itself.

Moreover, a PPP is homogeneous or uniform if its intensity function is constant across the space. Given the intensity λ, $N(B)$ follows a Poisson distribution with mean $\lambda|B|$. The homogeneous Poisson point process (HPPP) is simple, stationary, and isotropic. It is considered as one of the simplest point processes.

Given mutually independent HPPPs Φ_i with intensity $\lambda_i, i = 1, 2, \cdots$, the superposition $\Phi = \bigcup_i \Phi_i$ is an HPPP with intensity $\lambda = \sum_i \lambda_i$. Moreover, let an HPPP with intensity λ subject to an independent thinning with a constant retention probability p, and then the point processes Φ_{thin} and $\Phi \backslash \Phi_{thin}$ are both HPPPs, with intensities $p\lambda$ and $(1-p)\lambda$, respectively.

2.1.2 Cluster Processes

A general cluster process is generated by taking a parent point process and daughter point processes, one per parent, and translating the daughter processes to the position of their parent [32]. The cluster process is then the union of all the daughter points. Denote the parent point process by $\Phi_P = \{x_1, x_2, ...\}$, and let $n = \#\Phi_P \in N \bigcup \{\infty\}$ be the number of parent points. Further, let Φ_i be a family of finite point sets, the untranslated clusters or daughter processes. The cluster process is then the union of the translated clusters:

$$\Phi \triangleq \bigcup \Phi_i + x_i. \tag{2.1.9}$$

In terms of random counting measures, letting N_i be the family of counting measures for the clusters, the cluster process is given by

$$N \triangleq \sum N_i + x_i. \tag{2.1.10}$$

Alternatively, the counting measure may be expressed using the cluster field $N_c(\cdot|y)$ for $y \in \mathbb{R}^d$, which is sampled at the points of the parent process, i.e.,

$$N(A) = \int N_c(A|y)\Phi_P(dy) = \sum N_c(A|y)). \tag{2.1.11}$$

In this representation, $N_c(\cdot|y_i)$, which is indexed by the cluster centers or parent points, assumes the role of Φ_i, which is indexed by the cardinal i.

If the parent process is a lattice, the process is called a lattice cluster process.

Analogously, if the parent process is a PPP, the resulting process is a Poisson cluster process.

2.1.3 Gibbs process

Gibbs processes are related to Gibbs distributions in statistical physics. The main idea is to shape the distribution of a basic point process, usually a PPP, using a density on the space of counting measures $\mathcal{N}$.

Definition 2.1.3. Let Φ be a PPP with intensity measure Λ such that $\Lambda(\mathbb{R}^d) = 1$ and denote its distribution by Q. Define a new point process distribution P_f by

$$P_f(Y) = \int_Y f_\lambda(\varphi) Q(d\varphi), \tag{2.1.12}$$

where $f_\lambda : \mathbb{N} \mapsto R^+$ is given by

$$f_\lambda(\varphi) = \lambda^{\psi(\mathbb{R}^d)} \exp(1 - \lambda). \tag{2.1.13}$$

The new distribution P_f defines a PPP of intensity measure $\lambda\Lambda$. To see this, let P be the distribution of a PPP Φ of intensity measure $\lambda\Lambda$, and compare the measures that P and P_f give to the event

$$Y_K = \{\varphi \in \mathcal{N} : \varphi(\mathbb{R}^d) = n, \varphi(K) = 0\}. \tag{2.1.14}$$

Since $P(Y_K) = P_f(Y_K)$ for all $n \in \mathcal{N}$ and compact K, the void probabilities agree, and the distributions are equal.

2.1.4 Voronoi Polygon

Definition 2.1.4. For a simple point process $\Phi \subset \mathbb{R}^d$ and any point $u \in \Phi$, the Voronoi polygon $\mathcal{V}(u)$ with the center u is the subset

$$\mathcal{V}(u) = \left\{x \in \mathbb{R}^d : \| x - u \| < \| x - x_j \|, \forall x_j \in \Phi, x_j \neq u\right\}. \tag{2.1.15}$$

In other words, the Voronoi Polygon or Voronoi cell associated with the point $u \in \Phi$ is the set of all points in the space whose distance to u is smaller than their distance to the other points in Φ.

2.2 Heterogeneous Networks

2.2.1 Heterogeneous LTE/LTE-A Networks

In LTE/LTE-Advanced, HetNets contain conventionally deployed HPNs, (i.e., MBSs) and overlapping LPNs, which are generally known as SBSs, e.g., pico, femto, and relay base stations [33]. As mentioned in the previous chapter, HetNets in LTE/LTE-A systems are usually classified as intra-HetNets. That is, HPNs and LPNs use the same RAT. The aim of these low-power and flexibly deployed SBSs is to eliminate coverage holes and increase capacity in hot spots. Usually, the locations of MBSs are carefully chosen, and properly configured to minimize interference among them, while SBSs are deployed in a relatively unplanned manner. The three different types of SBSs in LTE/LTE-A HetNets are introduced as follows [4]:

- Pico-cells: Pico BSs are regular eNBs with the distribution of having lower transmission power than conversional MBSs. They are typically equipped with omnidirectional antennas, i.e., not sectorized, and are deployed indoors or outdoors in a planned manner. Their transmission power ranges from 250mW to 2W for outdoor deployments, while it is typically 100mW or less for indoor deployments. Because pico BSs are regular eNBs, they can benefit from X-2 based inter-cell interference coordination (ICIC).

- Femto-cells: Femto BSs, also known as the Home evolved NodeB, are typically deployed in indoor environments. The installation of femto BSs is usually subscriber deployed based on a simple "plug and play" method, which is typically unplanned. The backhaul of femto-cells can be carried via subscribers'

broadband wireline (such as digital subscriber line, fiber optic, and cable modem). Femto BSs are typically equipped with omni-directional antennas, and their transmission power is 100mW or less. However, the absence of the X2 interference makes ICIC impossible for them.

- Relay nodes: The backhaul that connects relay nodes to the rest of the network, is wireless and uses spectrum resource as well. If back-haul communication uses the same frequency as communication with MU, the relays are referred to as out-of-band relays. Usually relay nodes are deployed at the cell-edge area to enhance the coverage. Relay nodes are typically equipped with directional antennas in the back-haul link and omnidirectional antennas in the link with MUs.

Although the deployment of HetNets benefits LTE/LTE-A systems in many ways, technical challenges and issues also arise due to their characteristics, i.e., the large disparities of transmission power used by different types of BSs and the relatively random locations of SBSs.

User Association

As mentioned before, one major issue in HetNets is how to associate each MU with a proper BS, i.e., user association, to achieve optimal performance. Due to the large transmission power of MBSs, the conventional association criterion, i.e., maximum received pilot signal, pushes many MUs to MBSs even if they are located close to SBSs. In such cases, MBSs may struggle to supper so many MUs, which SBSs only serve a small portion of MUs and become under-utilized. This imbalanced load among BSs leads to system performance loss and uneven user experience. Much effort has been invested in this issue.

An effective association scheme is to adapt the coverage of SBSs to control the number of MUs connecting to them. This kind of solution is firstly used in WLANs. In details, a cell breathing technique was proposed to balance the load of APs by tuning transmission power [34]. However, this technique is not suitable for HetNets, because transmission power is quite different between MBSs and SBSs. Instead, cell range expansion (CRE) was introduced in long term evolution (LTE) networks to proactively offload UEs from MBSs to SBSs. This is done by adding a positive offset to the pilot RSS of the SBSs during the cell selection procedure [3]. CRE allows UE not associating with the BS that provides the strongest signal strength, but with those with more resources. Intuitively speaking, more UEs will be offloaded to the SBSs with a larger range expansion bias (REB). CRE without interference management has been shown to increase the sum capacity of the macrocell UEs due to the offloading, but decrease the overall throughput of the network due to strong cell-edge interference [35]. The offloaded UEs do not connect to the strongest cell anymore. To address this cell-edge performance issue, the use of enhanced intercell interference coordination (eICIC) schemes was also introduced in LTE networks [36], [37]. One such eICIC strategy implemented in the time-domain, called almost blank subframe (ABS), received a lot of attention. No control or data signals but only reference signals are transmitted in an ABS. Thus, when an MBS schedules ABSs, SBSs can schedule their offloaded UEs in subframes overlapping with the MBS ABSs. This significantly reduces interference towards those offloaded UEs.

One extension to the eICIC in 5G is ultra-reliable low latency communication (URLLC), which is the hottest research topic [38]. From a physical-layer perspective, the URLLC design is challenging as it ought to satisfy two conflicting requirements:

low latency and ultra-high reliability [39]. On the one hand, minimizing latency mandates the use of short packets which in turns causes a severe degradation in channel coding gain [40]. On the other hand, ensuring reliability requires more resources (e.g., parity, redundancy, and re-transmissions) albeit increasing latency (notably for time-domain redundancy). This ranges from users connected to the radio access network which must receive equal grade of service, to vehicles reliably transmitting their safety messages and industrial plants whereby sensors, actuators and controllers communicate within very short cycles [41].

Deployment Scenarios

There are several deployment options in LTE/LTE-A HetNets [4], [42].

- Orthogonal Deployment: In this scenario, orthogonal frequency resources are allocated to MBSs and SBSs. For instance, pico BSs are allocated with carriers that are not being used by MBSs. In such scenarios, each frequency resource utilization ratio is low, which limits system performance.

- Co-channel Deployment: In this scenario, all BSs are deployed in the same frequency tier to avoid bandwidth segmentation. MBSs and SBSs can both access the entire spectrum bandwidth, and the spectrum is reused as long as the interference constraint is satisfied. This kind of deployment improves the frequency resource utilization ratio. However, the co-tier interference between MBSs and SBSs is more challenging.

- Mixed: In this scenario, a portion of spectrum bandwidth is shared between MBSs and SBSs, while another portion of the spectrum bandwidth is assigned to MBSs and SBSs separately.

As spectrum resources available for an LTE/LET-A system become rare and expensive, co-channel deployment is more desirable to operators [43]. However, co-channel transmissions will lead to severe inter-tier interference, and the interference is further exacerbated due to the random locations of SBSs. Therefore, to mitigate the interference and highlight the benefits of co-channel deployment, it is necessary to consider interference management techniques in such scenarios.

In addition, a high level network deployment is introduced in [44]. As the popularity of new information technologies grows dramatically, personal requirement has become more and more diversified. To meet this requirement, service network (SV) is a feasible approach to deal with this problem [45]. An SN is considered as a persistent social service infrastructure consisting of massive interconnected small services. When a specific requirement is raised, the SN is customized by dynamically looking for a sub-network, which satisfies the requirement exactly. In this way, massive personalized with traditional service composition approaches, especially in mass customization scenarios [46].

2.2.2 Heterogeneous Networks for 5G Systems

The 5G system to be deployed initially in 2020 is expected to provide approximately 1000 times higher wireless area capacity and save up to 90% energy consumption per service compared with the current LTE-A system. More than 1000 Gbps/km^2 area spectral capacity in dense urban environments, ten times higher battery life of connected devices, and five times reduced end-to-end latency are anticipated in 5G system [47].

Among many advanced technologies, 5G HetNets have been presented as a potential solution to provide universal high-rate coverage and seamless user experience.

Besides more RATs considered, such as D2D communications, M2M communications and the Internet of Things, the ultra-dense SBSs are provided in the deployment of the 5G systems. In this context, the co-channel deployment of macro cell BSs (MBSs) and small cell BSs (SBSs) in HCNs, i.e., all BS tiers operating on the same frequency spectrum, have recently attracted considerable attention, e.g., [48, 49] and [50]. Using a dual slope path loss model, Zhang *et al.* in [51] demonstrated that the coverage probability strongly depends on the BS density. In the same line, using a multi-slope path loss model and the smallest path loss association rule, the authors in [52] showed that the coverage probability first increases with the BS density and then decreases, while the area spectral efficiency (ASE) will grow almost linearly as the BS density goes asymptotically large. In [53], a stretched exponential path loss model was proposed for the short-range communication, and they proved that the ASE is non-decreasing with the BS density and converges to a constant for high densities. These works all show that the density of the BS plays an important role in estimating and analysing the performance of the 5G dense or ultra-dense HetNets.

2.2.3 Caching in Heterogeneous Networks

Caching Strategies in Wireless Networks Video traffic will be the major traffic source due to the growing success of on-demand video streaming services. The huge demand pushes operators to provide high-throughput wireless access services in 5th generation (5G) networks. However, the current wireless access technologies have almost approached their theoretical limits and it is imperative to develop new communication strategies to meet the ever-increasing demand from mobile subscribers [1].

One of the promising approaches to tackle this problem in 5G is content caching,

as this technology can significantly offload the network traffic by optimally and intelligently storing the content files in the small base stations (SBSs) [4],[29], [54] and/or in mobile users' devices [11], [18], which are closer to end-users. As a result, network congestion can be eased and users' quality-of-experience (QoE) can be significantly improved. The authors in [4] introduced the ideas of caching in heterogeneous networks, wherein one macro cell is divided into multiple small cells. Within each small cell, one low power base station, termed as SBS, is deployed to serve the users within its coverage. The requested files by users are first transmitted from the MBS to the SBSs through the backhaul connections between them in off-peak period and then transmitted from the SBSs to the users. To optimize the cache content placement in the SBSs, two algorithms have been proposed in the literature: a) discrete generalized pursuit algorithm (DGPA)-based scheme proposed in [29] for which the SBSs can place the content according to the local demands; b) belief propagation (BP) algorithm based on the factor graph [54], which allows the file placement to be arranged in a distributed manner between the users and SBSs. Also, the caching is investigated in wireless network virtualization [55].

D2D Caching

In HetNets, D2D caching attracts lots of attention, because (i) The large number of users' devices in 4G and 5G networks have the capability to provide a promising basis for caching [56]; and (ii) Compared to SBS caching, D2D caching has several advantages. For example, it may be costly to set up and maintain the SBSs as well as the backhaul. Furthermore, the SBS caching may suffer from long latency and slow update of popular contents, which could hinder its application in practice.

With the emergence of 5G, exchanging the cached files among mobile devices

through D2D communications, termed D2D caching, has attracted considerable attention recently [18]. In [21], probalistic content placement was proposed and analyzed in the context of D2D caching, where each mobile terminal caches a specific subset of contents with a given caching probability. The throughput versus outage trade-off was analyzed and the optimal caching distribution was derived for a grid network relying on a particular protocol model.

However, in practice, due to limited memory and energy resources, users may be unwilling to serve data over the aforementioned D2D transmission unless they can obtain benefits (e.g., monetary incentives) from the operator [22] or other incentives (e.g., social relationship) from the users [11], [57], and [23]. In [58], Chen *et al.* proposed an incentive mechanism in which the BS rewards those users that share contents with others using D2D communication. But the social relationships among users are not considered. Compared with SBSs, the storage capacities at users are much smaller. In this context, different from the existing works on SBS and D2D caching, it is not optimal and practical to store same files in all users, and hence the optimization of the content placement becomes more critical and complex in the design of D2D caching strategies. Furthermore, the interactions between users should also be carefully taken into consideration [59].

To address the aforementioned issues, social relationship among mobile users can be a useful tool. The ideas of applying social characters to promote D2D communications and to design D2D caching was first proposed in [56]. In By using the close social ties in the same community, the resource allocation problem of D2D pairs was formulated and optimized by a two-step coalitional game. Besides, the use of positive social relationship among mobile users was investigated in [11], which helps to

reduce malicious or irrational users in the system. Moreover, a content dissemination scheme based on the common interest of users in a social group was proposed in [30]. A considerable delay reduction can be obtained when there are a large number of users in the same social group. In addition, in [60], a socially incentive mechanism for content distribution through D2D communications has been proposed. The contract theory investigated in this work can effectively incentivize user's participation, and increase capacity of the cellular network. In [61] the traffic fluctuation has already been derived as an important social characteristic to indicate the similarity of traffic variation of BSs. By utilizing the social relationship between BSs, the cache can be appropriately deployed to improve the network performance.

2.2.4 UAVs in Heterogeneous Networks

A drone is an unmanned aerial vehicle (UAV) designed to be flown either through remote control or autonomously using embedded software and sensors. Historically, drones were used mainly in military for reconnaissance purposes, but with recent developments in light-weight battery-powered drones, many civilian applications are emerging [62]. Using drones to deploy small cells in the HetNets of urgent needs is one of the most interesting applications. The greatest advantage of this approach is that drones can be equipped with small cell base station module and sent to a specific target location immediately to establish emergency communication links without having to deploy any infrastructure. For example, UAV-mounted base stations (UAV-BSs) are introduced when a natural disaster interrupts communications or ground base stations are overloaded [63].

Most of the literature on the UAV-BS focuses on its deployment. The work in [64] proposed that fixed-wing UAVs at a constant height are more applicable for aerial

networks due to less power consumption. Positions of UAV-BSs were modeled as a 3D Poisson Point Process (3D-PPP) distribution with a limited height in [24], but the analysis in [65] showed that the flexible height of UAV is not as helpful as a well-chosen fixed altitude. In [25], UAV-mounted mobile base stations were deployed in a fixed altitude and placed along an optimal trajectory to cover as much as user equipment (UE) whose locations are already known in a given area. Finding the 3D optimal location for deploying a drone cell was studied in [66]. When some users with QoS requirements are distributed in an area, a 3D location could be found for deploying a drone cell to provide services for the maximum number of users satisfying the SNR constraints.

Beyond the UAV deployment, the performance of 3D networks also attracts much attention in the existing literature. The work in [65] analyzed the average downlink spectral efficiency without considering the environment noise, while the authors of [67] evaluated the performance of UAV at a low altitude platform in terms of the coverage area, and transmit power. Similarly, the optimal deployment model in [68] led to the analysis of coverage and transmit power. Furthermore, the analysis in [69] introduced a tractable analytical framework for the coverage and the rate in UAV based network with the coexistence of device-to-device (D2D) network. Moreover, applying stochastic tools to 3D UAV-mounted HetNets, different coverage probability and throughput scaling behaviors in terms of the path loss components using a dual path-loss model are discussed in [70].

Besides the performance analysis, exploiting the UAV's high mobility in the mobile-UAV enabled wireless networks is anticipated to unlock the full controllable

UAV-ground communications. With the fully controllable UAV mobility, the communication distance between the UAV and ground users can be significantly shortened by proper UAV trajectory design and user scheduling. This is analogous and yet in sharp contrast to the existing small-cell technology [71]. Motivated by this, the UAV trajectory design is rigorously studied in [72] and [73] for a mobile relaying system and a point-to-point energy-efficient system, respectively, where sequential convex optimization techniques are applied to solve the non-convex trajectory optimization problems therein. For UAV-enabled multi-user systems, a novel cyclical multiple access scheme is proposed in [74], where the UAV communicates with ground users when it flies sufficiently close to each of them in a periodic time-division manner. An interesting throughput-access delay tradeoff is revealed and it has been shown that significant throughput gains can be achieved over the case of a static UAV for delay-tolerant applications.

Chapter 3

Performance Analysis of the Idle Mode Capability in a Dense Heterogeneous Cellular Network

In this chapter, the impact of the BS IMC on the multi-tier and dense HCNs is conducted to investigate the network performance. To be more practical, a finite number of UEs is considered and the mechanism of the ABS is applied by the MBSs to enhance the ICIC. As a result, the developing trend of the coverage probability and ASE are shown with the densifying network. Finally, the optimal ABS factors are investigated in different BS density regions.

3.1 System Model

In this chapter, I assume a wireless network consisting of two BS tiers. The locations of the BSs of the kth tier ($k = 1, 2$) are modeled as a two-dimensional HPPP Φ_k with a density λ_k. Without loss of generality, I denote the macrocell tier and the small cell tier as tier 1 and tier 2. The locations of UEs (denoted by $\mathcal{U}$) in the network are modeled as another independent HPPP Φ_u with a density λ_u. In most existing works, λ_u was assumed to be sufficiently large, so that each BS in each

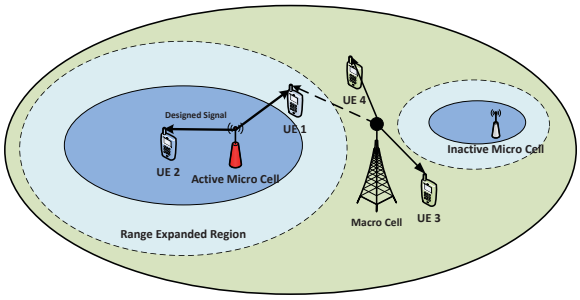

Figure 3.1: A network scenario consisting of two BS tiers. Each UE is connected to the BS that provides the strongest average signal, which is marked by the designed signal. BSs with no UE associated are in idle mode.

tier always has at least one associated UE. However, in the model with finite BS and UE densities, a BS might serve no UE, and thus be turned off thanks to the IMC[1]. Following [52], I adopt a general and practical path loss model, in which the path loss $\zeta(r)$ associated with distance r is calculated as

$$\zeta_k(r) = \begin{cases} \zeta_k^{\mathrm{L}}(r) = A_k^{\mathrm{L}} r^{-\alpha_k^{\mathrm{L}}}, & \text{LoS: } \mathrm{Pr}_k^{\mathrm{L}}(r); \\ \zeta_k^{\mathrm{NL}}(r) = A_k^{\mathrm{NL}} r^{-\alpha_k^{\mathrm{NL}}}, & \text{NLoS: } \mathrm{Pr}_k^{\mathrm{NL}}(r) = 1 - \mathrm{Pr}_k^{\mathrm{L}}(r), \end{cases} \tag{3.1.1}$$

where A_k^{L} and A_k^{NL} are the path losses at a reference distance $r = 1$ for the kth tier and for the LoS and the NLoS cases, respectively, and α_k^{L} and α_k^{NL} are the path loss exponents for the kth and for the LoS and NLoS cases, respectively. Moreover, $\mathrm{Pr}_k^{\mathrm{L}}(r)$ is the LoS probability function with a distance r. For example, as recommended by the 3GPP, $\mathrm{Pr}_k^{\mathrm{L}}(r)$ can be computed as

$$\mathrm{Pr}_k^{\mathrm{L}}(r) = \begin{cases} \min\left(0.018/r, 1\right) * (1 - \exp(-r/0.063)) + \exp(-r/0.063), \\ \text{when k=1;} \\ 0.5 - \min(0.5, 5\exp(-0.156/r)) + \min(0.5, 5\exp(-r/0.03)), \\ \text{when k=2.} \end{cases} \tag{3.1.2}$$

[1]The mobility of UEs is not considered in the work. It is worth noting that if mobility is present, MBSs may not be turned off easily, as the MBSs need to support the UE handover. Several works considering the mobility can be found in [75] and [76].

Moreover, I consider a cell association based on the maximum received power, where a UE is associated with the strongest BS:

$$\mathcal{X}_k = P_k \zeta_k(r) D_k, \tag{3.1.3}$$

where P_k and D_k denote the transmit power and the REB of a BS in the kth tier, where $D_1 = 0$ dB for the macrocell tier and $D_2 = D$ dB for the small cell tier.

Because UEs are randomly and uniformly distributed in the network, I adopt a common assumption that the activated BSs in each tier also follows an independent HPPP distribution $\widetilde{\Phi}_i$, the density of which is denoted by $\widetilde{\lambda}_i$ BSs/km^2 [77], [78].

Finally, I assume that each UE/BS is equipped with an isotropic antenna, and as a common practice in the field, that the multi-path fading between an arbitrary UE and an arbitrary BS is modeled as independently identical distributed (i.i.d) Rayleigh fading.

The SINR of the typical UE with a random distance r to its associated BS in the kth tier is given by

$$\mathrm{SINR}_k(r) = \frac{P_k h_{k0} \zeta_k(r)}{\sum_{j=1}^{K} \sum_{i \in \widetilde{\Phi} \backslash b_0} P_j h_{ji} \zeta_j(|Y_{ji}|) + \sigma^2}, \tag{3.1.4}$$

where h_{k0} and h_{ji} are the exponentially distributed channel power with unit mean from the serving BS and the i-th interfering BS in the j-th tier, respectively. $|Y_{ji}|$ is the distance from the activated BS in the j-th tier to the origin, and b_0 is the serving BS in the k-th tier. Note that only the activated BSs in $\widetilde{\Phi} \backslash b_0$ inject effective interference into the network, because the other BSs are turned off thanks to the IMC.

In Fig. 3.1, I show an illustration of the proposed network, which consists of two BS tiers. In this case, UE 1 is offloaded from the MBS to the SBS because of the REB. The other SBS is in idle mode in that there is no UE associated to it.

3.2 Density of the activated BSs

To evaluate the impact of the IMC on the performance of each BS tier, I first analyze the probability of having a given average number of UEs in each cell. Then, I derive expressions for the density of active BSs in each tier.

3.2.1 Average Number of UEs in Each Cell

The coverage area of each small cell is a random variable V, representing the size of a Poisson Voronoi cell. Although there is no known closed-form expression for V's probability distribution function (PDF), some accurate estimates of this distribution have been proposed in the literature, e.g., [79] and [80].

In [79], a simple gamma distribution derived from Monte Carlo simulations was used to approximate the PDF of V for the kth BS tier, given by

$$f_{V_k}(x) = (b\lambda_k)^q x^{q-1} \frac{\exp(-b\lambda_k x)}{\Gamma(q)}, \tag{3.2.1}$$

where q and b are fixed values, $\Gamma(x) = \int_0^{+\infty} t^{x-1} e^{-t} dt$ is the standard gamma function and λ_k is the BS density of the kth BS tier.

Remind here I assume that the coverage area of each cell has not considered the associating relation to users, where each user may be covered by multiple BSs in different tiers, and the average number of UEs in each cell may be a little larger than the actual one. This inaccuracy is shown to be ignorable in the Sec. V-A. If the association probability is considered here, each user can only be covered by one BS, then the Poisson Voronoi cell will change to be a weighted cell, and the shape of cell will become irregular. The works in [81] show how to calculate the weighted Poisson Voronoi cell and are useful for further discussion.

In that the distribution of UEs follows an HPPP with a density of λ_u, given a

Voronoi cell with size x, the number of UEs located in this Voronoi cell is a Poisson random variable with a mean of $\lambda_u x$. Denoting by N_k the number of UEs located in a Voronoi cell of the kth BS tier, I have that

$$\begin{aligned}\mathbb{P}[N_k = n] &= \int_0^{+\infty} \frac{(\lambda_u x)^n}{n!} \exp(-\lambda_u x) f_{V_k}(x) dx \\ &\overset{(a)}{=} \frac{\Gamma(n+q)}{\Gamma(n+1)\Gamma(q)} \left(\frac{\lambda_u}{\lambda_u + b\lambda_k}\right)^n \left(\frac{b\lambda_k}{\lambda_u + b\lambda_k}\right)^q, \quad n \geq 0\end{aligned} \tag{3.2.2}$$

where step *(a)* is computed by using the definition of the gamma function.

3.2.2 Probability of a UE Associated to the kth Tier

According to Eq. (3.1.3), each BS tier density and transmit power determine the probability that a typical UE is associated with a BS in this tier. The following Lemmas provide the per-tier association probability, which is essential for deriving the main results in the sequel.

If one UE connects to one MBS ($k = 1$), this MBS can be a MBS with a LoS path or a NLoS path. In the following, I provide the probability that one such UE is associated with a LoS MBS in Lemma 3.2.1.

Lemma 3.2.1. *The probability that the UE is associated with a LoS MBS can be written as*

$$\mathbb{P}_1^{\mathrm{L}} = \int_0^{\infty} p_{11}^{\mathrm{L}}(r) \times p_{12}^{\mathrm{L}}(r) \times p_{13}^{\mathrm{L}}(r) \times f_1^{\mathrm{L}}(r) dr, \tag{3.2.3}$$

where $p_{11}^{\mathrm{L}}(r) = \exp\left(-\int_0^{\Delta_{11}^{\mathrm{L}}(r)} \mathrm{Pr}_1^{\mathrm{NL}}(u) \times 2\pi u \lambda_1 du\right)$, $\Delta_{11}^{\mathrm{L}}(r) = (\frac{A_1^{\mathrm{NL}}}{A_1^{\mathrm{L}}})^{\frac{1}{\alpha_1^{\mathrm{NL}}}} r^{\frac{\alpha_1^{\mathrm{L}}}{\alpha_1^{\mathrm{NL}}}}$, *and* $p_{12}^{\mathrm{L}}(r) = \exp\left(-\int_0^{\Delta_{12}^{\mathrm{L}}(r)} \mathrm{Pr}_2^{\mathrm{L}}(u) \times 2\pi u \lambda_2 du\right)$, $\Delta_{12}^{\mathrm{L}}(r) = \left(\frac{DP_2 A_2^{\mathrm{L}}}{P_1 A_1^{\mathrm{L}}}\right)^{\frac{1}{\alpha_2^{\mathrm{L}}}} r^{\frac{\alpha_1^{\mathrm{L}}}{\alpha_2^{\mathrm{L}}}}$, *and* $p_{13}^{\mathrm{L}}(r) = \exp\left(-\int_0^{\Delta_{13}^{\mathrm{L}}(r)} \mathrm{Pr}_2^{\mathrm{NL}}(u) \times 2\pi u \lambda_2 du\right)$, $\Delta_{13}^{\mathrm{L}}(r) = \left(\frac{DP_2 A_2^{\mathrm{NL}}}{P_1 A_1^{\mathrm{L}}}\right)^{\frac{1}{\alpha_2^{\mathrm{NL}}}} r^{\frac{\alpha_1^{\mathrm{L}}}{\alpha_2^{\mathrm{NL}}}}$, *respectively, and* $f_1^{\mathrm{L}}(r)$ *is the PDF that the UE is associated with a LoS MBS, which can be written as*

$$f_1^{\mathrm{L}}(r) = \exp\left\{-\int_0^r \mathrm{Pr}_1^{\mathrm{L}}(u) 2\pi\lambda_1 u du\right\} \times \mathrm{Pr}_1^{\mathrm{L}}(r) 2\pi\lambda_1 r. \tag{3.2.4}$$

Proof. See Appendix A.1. □

Following the same logic, I provide the probability that the UE is associated with a NLoS MBS in Lemma 3.2.2.

Lemma 3.2.2. *The probability that the UE is associated with a NLoS MBS can be written as*

$$\mathbb{P}_1^{\mathrm{NL}} = \int_0^\infty p_{11}^{\mathrm{NL}}(r) \times p_{12}^{\mathrm{NL}}(r) \times p_{13}^{\mathrm{NL}}(r) \times f_1^{\mathrm{NL}}(r)dr, \tag{3.2.5}$$

where $p_{11}^{\mathrm{NL}}(r) = \exp\left(-\int_0^{\Delta_{11}^{\mathrm{NL}}(r)} \mathrm{Pr}_1^{\mathrm{L}}(u) \times 2\pi u\lambda_1 du\right)$, $\Delta_{11}^{\mathrm{NL}}(r) = (\frac{A_1^{\mathrm{L}}}{A_1^{\mathrm{NL}}})^{\frac{1}{\alpha_1^{\mathrm{L}}}} \times r^{\frac{\alpha_1^{\mathrm{NL}}}{\alpha_1^{\mathrm{L}}}}$, *and* $p_{12}^{\mathrm{NL}}(r) = \exp\left(-\int_0^{\Delta_{12}^{\mathrm{NL}}(r)} \mathrm{Pr}_2^{\mathrm{L}}(u) \times 2\pi u\lambda_2 du\right)$, $\Delta_{12}^{\mathrm{NL}}(r) = \left(\frac{DP_2A_2^{\mathrm{L}}}{P_1A_1^{\mathrm{NL}}}\right)^{\frac{1}{\alpha_2^{\mathrm{L}}}} \times r^{\frac{\alpha_1^{\mathrm{NL}}}{\alpha_2^{\mathrm{L}}}}$, *and* $p_{13}^{\mathrm{NL}}(r) = \exp\left(-\int_0^{\Delta_{13}^{\mathrm{NL}}(r)} \mathrm{Pr}_2^{\mathrm{NL}}(u) \times 2\pi u\lambda_2 du\right)$, $\Delta_{13}^{\mathrm{NL}}(r) = \left(\frac{DP_2A_2^{\mathrm{NL}}}{P_1A_1^{\mathrm{NL}}}\right)^{\frac{1}{\alpha_2^{\mathrm{NL}}}} \times r^{\frac{\alpha_1^{\mathrm{NL}}}{\alpha_2^{\mathrm{NL}}}}$, *respectively, and* $f_1^{\mathrm{NL}}(r)$ *is the PDF that the UE is associated with a NLoS MBS, which can be written as*

$$f_1^{\mathrm{NL}}(r) = \exp\left\{-\int_0^r \mathrm{Pr}_1^{\mathrm{NL}}(u)2\pi\lambda_1 u du\right\} \times \mathrm{Pr}_1^{\mathrm{NL}}(r)2\pi\lambda_1 r. \tag{3.2.6}$$

Proof. See Appendix A.2. □

If one UE connects to one SBS ($K = 2$), this SBS can also be a SBS with a LoS path or a NLoS path. Similarly, the corresponding UE association probabilities are derived in Lemma 3.2.3 and Lemma 3.2.4.

Lemma 3.2.3. *The probability that the UE is associated with a LoS SBS can be written as*

$$\mathbb{P}_2^{\mathrm{L}} = \int_0^\infty p_{21}^{\mathrm{L}}(r) \times p_{22}^{\mathrm{L}}(r) \times p_{23}^{\mathrm{L}}(r) \times f_2^{\mathrm{L}}(r)dr, \tag{3.2.7}$$

where $p_{21}^{\mathrm{L}}(r) = \exp(-\int_0^{\Delta_{21}^{\mathrm{L}}} \mathrm{Pr}_1^{\mathrm{NL}}(u) \times 2\pi u\lambda_1 du)$, $\Delta_{21}^{\mathrm{L}}(r) = (\frac{P_1A_1^{\mathrm{L}}}{DP_2A_2^{\mathrm{L}}})^{\frac{1}{\alpha_1^{\mathrm{L}}}} \times r^{\frac{\alpha_2^{\mathrm{L}}}{\alpha_1^{\mathrm{L}}}}$, *and* $p_{22}^{\mathrm{L}}(r) = \exp(-\int_0^{\Delta_{22}^{\mathrm{L}}} \times \mathrm{Pr}_1^{\mathrm{L}}(u)2\pi u\lambda_1 du)$, $\Delta_{22}^{\mathrm{L}}(r) = (\frac{P_1A_1^{\mathrm{NL}}}{DP_2A_2^{\mathrm{L}}})^{\frac{1}{\alpha_1^{\mathrm{NL}}}} r^{\frac{\alpha_2^{\mathrm{L}}}{\alpha_1^{\mathrm{NL}}}}$, *and* $p_{23}^{\mathrm{L}}(r) = \exp(-\int_0^{\Delta_{23}^{\mathrm{L}}} \mathrm{Pr}_2^{\mathrm{NL}}(u) \times 2\pi u\lambda_2 du)$, $\Delta_{23}^{\mathrm{L}}(r) = (\frac{A_2^{\mathrm{NL}}}{A_2^{\mathrm{L}}})^{\frac{1}{\alpha_2^{\mathrm{NL}}}} \times r^{\frac{\alpha_2^{\mathrm{L}}}{\alpha_2^{\mathrm{NL}}}}$, *respectively, and*
$f_2^{\mathrm{L}}(r) = \mathrm{Pr}_2^{\mathrm{L}}(r)2\pi\lambda_2 r \times \exp\left\{-\int_0^r \mathrm{Pr}_2^{\mathrm{L}}(u)2\pi\lambda_2 u du\right\}$.

Lemma 3.2.4. *The probability that the UE is associated with a NLoS SBS can be written as*

$$\mathbb{P}_2^{\mathrm{NL}} = \int_0^\infty p_{21}^{\mathrm{NL}}(r) \times p_{22}^{\mathrm{NL}}(r) \times p_{23}^{\mathrm{NL}}(r) \times f_2^{\mathrm{NL}}(r)dr, \tag{3.2.8}$$

where $p_{21}^{\mathrm{NL}}(r) = \exp(-\int_0^{\Delta_{21}^{\mathrm{NL}}} \times \mathrm{Pr}_1^{\mathrm{L}}(u) 2\pi u \lambda_1 du)$, $\Delta_{21}^{\mathrm{NL}}(r) = (\frac{P_1 A_1^{\mathrm{L}}}{D P_2 A_2^{\mathrm{NL}}})^{\frac{1}{\alpha_1^{\mathrm{L}}}} \times r^{\frac{\alpha_2^{\mathrm{NL}}}{\alpha_1^{\mathrm{L}}}}$, *and* $p_{22}^{\mathrm{NL}}(r) = \exp(-\int_0^{\Delta_{22}^{\mathrm{NL}}} \times \mathrm{Pr}_1^{\mathrm{NL}}(u) 2\pi u \lambda_1 du)$, $\Delta_{22}^{\mathrm{NL}}(r) = (\frac{P_1 A_1^{\mathrm{NL}}}{D P_2 A_2^{\mathrm{NL}}})^{\frac{1}{\alpha_1^{\mathrm{NL}}}} \times r^{\frac{\alpha_2^{\mathrm{NL}}}{\alpha_1^{\mathrm{NL}}}}$, *and* $p_{23}^{\mathrm{NL}}(r) = \exp(-\int_0^{\Delta_{23}^{\mathrm{NL}}} \mathrm{Pr}_2^{\mathrm{L}}(u) \times 2\pi u \lambda_2 du)$, $\Delta_{23}^{\mathrm{NL}}(r) = (\frac{A_2^{\mathrm{L}}}{A_2^{\mathrm{NL}}})^{\frac{1}{\alpha_2^{\mathrm{L}}}} \times r^{\frac{\alpha_2^{\mathrm{NL}}}{\alpha_2^{\mathrm{L}}}}$, *respectively, and* $f_2^{\mathrm{NL}}(r) = \exp\left\{-\int_0^r \mathrm{Pr}_2^{\mathrm{NL}}(u) 2\pi \lambda_2 u du\right\} \times \mathrm{Pr}_2^{\mathrm{NL}}(r) 2\pi \lambda_2 r$.

Proof. The proofs of Lemma 3.2.3 and Lemma 3.2.4 are similar to Lemma 3.2.1 and Lemma 3.2.2, so the proof are omitted here. □

3.2.3 Density of activated BSs in the kth tier

After attaining the probability of one UE associating to a BS in the kth tier, I am ready to derive the density of active BSs in the kth tier.

Defining by $\mathbb{P}_k^{\mathrm{off}}(n)$ the probability that a BS in the kth tier is inactive when there are n UEs in its coverage, then $\mathbb{P}_k^{\mathrm{off}}(n)$ can be calculated by

$$\mathbb{P}_k^{\mathrm{off}}(n) = \mathbb{P}[N_k = n](1 - A_k)^n, \tag{3.2.9}$$

where $\mathbb{P}[N_k = n]$ is the probability of having n UEs located in a cell of the kth tier, which can be obtained from Eq. (3.2.2), and $A_k = \mathbb{P}_k^{\mathrm{L}} + \mathbb{P}_k^{\mathrm{NL}}$, which denotes the per-tier association probability.

With this result, the density of active BSs in the kth tier $\widetilde{\lambda}_k$ can now be derived as

$$\widetilde{\lambda}_k = \lambda_k \left(1 - \sum_{n=0}^{\infty} \mathbb{P}_k^{\mathrm{off}}(n)\right), \tag{3.2.10}$$

where $\mathbb{P}_k^{\mathrm{off}}(n)$ is the probability that the kth tier is inactive when there are n UEs in its coverage.

3.3 Main Results

Recall that in this paper, The REB for the first tier (macro tier) is $D_1 = 0\ dB$ and that for the second tier is simply denoted by D, where $D \geq 0\ dB$.

With the modelling, a UE $u \in \mathcal{U}$ belongs to the following six disjoint sets:

$$u \in \begin{cases} \mathcal{U}_1 \begin{cases} \mathcal{U}_1^{\mathrm{L}}, \text{The UE connects to a LoS MBS;} \\ \mathcal{U}_1^{\mathrm{NL}}; \text{The UE connects to a NLoS MBS;} \end{cases} \\ \mathcal{U}_2 \begin{cases} \mathcal{U}_2^{\mathrm{L}}, \text{The UE connects to a LoS SBS without} \\ \quad \text{power bias;} \\ \mathcal{U}_2^{\mathrm{NL}}; \text{The UE connects to a NLoS SBS without} \\ \quad \text{power bias;} \end{cases} \\ \mathcal{U}_3 \begin{cases} \mathcal{U}_3^{\mathrm{L}}, \text{The UE is offloaded from a MBS to a LoS} \\ \quad \text{SBS;} \\ \mathcal{U}_3^{\mathrm{NL}}; \text{The UE is offloaded from a MBS to a NLoS} \\ \quad \text{SBS,} \end{cases} \end{cases} \tag{3.3.1}$$

where $\mathcal{U}_1 \bigcup \mathcal{U}_2 \bigcup \mathcal{U}_3 = \mathcal{U}$. The set $\mathcal{U}_1$ is the set of macrocell UEs and the set $\mathcal{U}_2$ is the set of unbiased small cell UEs. The UEs offloaded from macrocells to small cells due to CRE constitute set $\mathcal{U}_3$, and are referred to as *range expanded (RE) UEs.*

Moreover, an ABS approach to eICIC is considered, in which MBSs shut their transmissions on certain fraction of time/frequency resources, and SBSs schedule their RE UEs on the corresponding resources, which are free from macrocell interference.

Definition 3.3.1. η: The resource partitioning fraction η is the fraction of resources on which the MBSs are inactive, where $0 < \eta < 1$. η is also known as the ABS factor.

Thus, with resource partitioning, $1 - \eta$ is the fraction of resources that the MBSs and the SBSs allocate to UEs in $\mathcal{U}_1$ and $\mathcal{U}_2$, respectively, while η is the fraction of

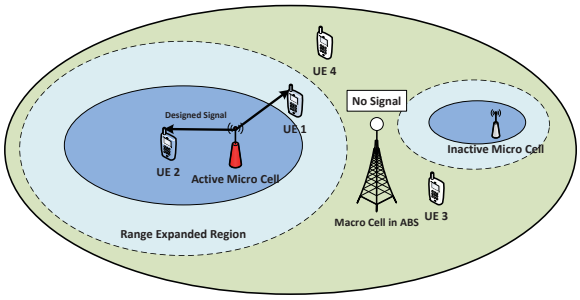

Figure 3.2: MBS schedules ABSs, and the UEs associated with it cannot get service in such subframes.

resources in which the MBSs do not transmit and the SBSs can schedule UEs in $\mathcal{U}_2$ and $\mathcal{U}_3$.

In Fig. 3.2, I show an illustration of the proposed network when the ABS framework is in place. When the MBS schedules ABSs and mutes its transmission, UE 3 and UE 4 will not receive any signal from their serving MBS. In contrast, the UEs associated with the SBS, i.e., UE 1 (the RE SBS UE) and UE 2 (the native SBS UE), can be served without the interference from the MBS.

As a result of resource partitioning, the SINR of a typical UE u, when it belongs to $\mathcal{U}_k$, can be written as

$$\text{SINR} = \mathbf{1}(k \in 1,2)\frac{P_k h_{k,0}\zeta_k(r)}{\sum_{k=1}^{2} I_k + \sigma^2} + \mathbf{1}(k \in 2,3)\frac{P_2 h_{2,0}\zeta_2(r)}{I_2 + \sigma^2}, \tag{3.3.2}$$

where $\mathbf{1}(A)$ is the indicator of the event A, and I_k is the interference from the kth tier.

3.3.1 The Coverage Probability

Let us define the coverage probability $\mathcal{S}$ as the probability that the instantaneous SINR of a randomly located UE is larger than a target SINR (τ). In that the typical

UE is associated with at most one BS, the coverage probability can be calculated by

$$\mathcal{S} = \sum_{k=1}^{3} \mathcal{S}_k = \sum_{k=1}^{3} \mathbb{P}(\mathrm{SINR}_k > \tau). \tag{3.3.3}$$

The results of the coverage probability is presented in Theorem 3.3.1.

Theorem 3.3.1. *(Coverage Probability) For a typical UE in the presented framework, the* SINR *coverage probability is*

$$\mathcal{S}(\tau) = \mathcal{S}_1^{\mathrm{L}}(\tau) + \mathcal{S}_1^{\mathrm{NL}}(\tau) + \mathcal{S}_2^{\mathrm{L}}(\tau) + \mathcal{S}_2^{\mathrm{NL}}(\tau) + \mathcal{S}_3^{\mathrm{L}}(\tau) + \mathcal{S}_3^{\mathrm{NL}}(\tau), \tag{3.3.4}$$

where $\mathcal{S}_1^{\mathrm{L/NL}}(\tau) = \int_0^\infty \Pr\left[\frac{S_1^{\mathrm{L/NL}}(x)h}{I_{\mathrm{agg}}+\sigma^2} > \tau\right] \mathcal{F}_1^{\mathrm{L/NL}}(x)dx$, $S_2^{\mathrm{L/NL}}(\tau) =$ $\theta \int_0^\infty \Pr\left[\frac{S_2^{\mathrm{L/NL}}(x)h}{I_{\mathrm{agg}_1}+\sigma^2} > \tau\right] \mathcal{F}_2^{\mathrm{L/NL}}(x)dx + (1-\theta) \int_0^\infty \Pr\left[\frac{S_2^{\mathrm{L/NL}}(x)h}{I_{\mathrm{agg}_2}+\sigma^2} > \tau\right] \mathcal{F}_2^{\mathrm{L/NL}}(x)dx$, *and* $\mathcal{S}_3^{\mathrm{L/NL}}(\tau) = \int_0^\infty \Pr\left[\frac{S_3^{\mathrm{L/NL}}(x)h}{I_{\mathrm{agg}}+\sigma^2} > \tau\right] \mathcal{F}_3^{\mathrm{L/NL}}(x)dx$, *where* θ *represents the ABS fraction, and* $\theta = 1-\eta$. *Moreover,* $\mathcal{F}_1^{\mathrm{L/NL}}(x)dx$, $\mathcal{F}_2^{\mathrm{L/NL}}(x)dx$ *and* $\mathcal{F}_3^{\mathrm{L/NL}}(x)dx$ *are represented by*

$$\begin{aligned}
\mathcal{F}_1^{\mathrm{L/NL}}(x) &= p_{11}^{\mathrm{L/NL}}(x) \times p_{12}^{\mathrm{L/NL}}(x) \times p_{13}^{\mathrm{L/NL}}(x) \times f_1^{\mathrm{L/NL}}(x),\\
\mathcal{F}_2^{\mathrm{L/NL}}(x) &= p_{21}^{\mathrm{L'/NL'}}(x) \times p_{22}^{\mathrm{L'/NL'}}(x) \times p_{23}^{\mathrm{L/NL}}(x) \times f_2^{\mathrm{L/NL}}(x),\\
\mathcal{F}_3^{\mathrm{L}}(x) &= p_{21}^{\mathrm{L}}(x) \times p_{22}^{\mathrm{L}}(x) \times p_{23}^{\mathrm{L}}(x) \times \left(\mathfrak{p}_1^{\mathrm{L}}(x) + \mathfrak{p}_1^{\mathrm{NL}}(x)\right) \times f_2^{\mathrm{L}}(x), \text{ and}\\
\mathcal{F}_3^{\mathrm{NL}}(x) &= p_{21}^{\mathrm{NL}}(x) \times p_{22}^{\mathrm{NL}}(x) \times p_{23}^{\mathrm{NL}}(x) \times \left(\mathfrak{p}_2^{\mathrm{L}}(x) + \mathfrak{p}_2^{\mathrm{NL}}(x)\right) \times f_2^{\mathrm{NL}}(x).
\end{aligned} \tag{3.3.5}$$

In addition, $\Pr\left[\frac{S_1^{\mathrm{L/NL}}(x)h}{I_{\mathrm{agg}}+\sigma^2} > \tau\right]$, $\Pr\left[\frac{S_2^{\mathrm{L/NL}}(x)h}{I_{\mathrm{agg}_{1,2}}+\sigma^2} > \tau\right]$, *and* $\Pr\left[\frac{S_3^{\mathrm{L/NL}}(x)h}{I_{\mathrm{agg}}+\sigma^2} > \tau\right]$ *are respectively computed by*

$$\begin{aligned}
\Pr\left[\frac{S_1^{\mathrm{L/NL}}(x)h}{I_{\mathrm{agg}}+\sigma^2} > \tau\right] &= \exp\left(-\frac{\sigma^2\tau}{S_1^{\mathrm{L/NL}}(x)}\right) \times \mathcal{L}_{I_1^{\mathrm{L/NL}}}\left(\frac{\tau}{S_1^{\mathrm{L/NL}}(x)}\right),\\
\Pr\left[\frac{S_2^{\mathrm{L/NL}}(x)h}{I_{\mathrm{agg}_1}+\sigma^2} > \tau\right] &= \exp\left(-\frac{\sigma^2\tau}{S_2^{\mathrm{L/NL}}(x)}\right) \times \mathcal{L}_{I_{21}^{\mathrm{L/NL}}}\left(\frac{\tau}{S_2^{\mathrm{L/NL}}(x)}\right),\\
\Pr\left[\frac{S_2^{\mathrm{L/NL}}(x)h}{I_{\mathrm{agg}_2}+\sigma^2} > \tau\right] &= \exp\left(-\frac{\sigma^2\tau}{S_2^{\mathrm{L/NL}}(x)}\right) \times \mathcal{L}_{I_{22}^{\mathrm{L/NL}}}\left(\frac{\tau}{S_2^{\mathrm{L/NL}}(x)}\right), \text{and}\\
\Pr\left[\frac{S_3^{\mathrm{L/NL}}(x)h}{I_{\mathrm{agg}}+\sigma^2} > \tau\right] &= \exp\left(-\frac{\sigma^2\tau}{S_2^{\mathrm{L/NL}}(x)}\right) \times \mathcal{L}_{I_3^{\mathrm{L/NL}}}\left(\frac{\tau}{S_2^{\mathrm{L/NL}}(x)}\right).
\end{aligned} \tag{3.3.6}$$

Proof. See Appendix A.3. □

In Theorem 3.3.1, $\mathcal{L}_I(s)$ in Eq. (3.3.6) are the Laplace transform of I_{agg} evaluated

at s for LoS or NLoS transmissions in each BS tier, respectively. For clarity, they are presented in the following Lemmas.

Lemma 3.3.1. *In Theorem 1,* $\mathcal{L}_{I_1^{\mathrm{L/NL}}}(s)$ *are given by*

$$\begin{aligned}\mathcal{L}_{I_1^{\mathrm{L}}}(s) = &\exp\left(-2\pi\tilde{\lambda}_1 \int_x^\infty \mathrm{Pr}_1^{\mathrm{L}}(u)\frac{u}{1+\frac{S_1^{\mathrm{L}}(x)}{\tau S_1^{\mathrm{L}}(u)}}du\right)\times \\ &\exp\left(-2\pi\tilde{\lambda}_1 \int_{\Delta_{11}^{\mathrm{L}}(x)}^\infty \mathrm{Pr}_1^{\mathrm{NL}}(u)\frac{u}{1+\frac{S_1^{L}(x)}{\tau S_1^{\mathrm{NL}}(u)}}du\right)\times \\ &\exp\left(-2\pi\tilde{\lambda}_2 \int_{\Delta_{12}^{\mathrm{L}}(x)}^\infty \mathrm{Pr}_2^{\mathrm{L}}(u)\frac{u}{1+\frac{S_1^{\mathrm{L}}(x)}{\tau S_2^{\mathrm{L}}(u)}}du\right)\times \\ &\exp\left(-2\pi\tilde{\lambda}_2 \int_{\Delta_{13}^{\mathrm{L}}(x)}^\infty \mathrm{Pr}_2^{\mathrm{NL}}(u)\frac{u}{1+\frac{S_1^{\mathrm{L}}(x)}{\tau S_2^{\mathrm{NL}}(u)}}du\right),\end{aligned} \tag{3.3.7}$$

and

$$\begin{aligned}\mathcal{L}_{I_1^{\mathrm{NL}}}(s) = &\exp\left(-2\pi\tilde{\lambda}_1 \int_x^\infty \mathrm{Pr}_1^{\mathrm{NL}}(u)\frac{u}{1+\frac{S_1^{\mathrm{NL}}(x)}{\tau S_1^{\mathrm{NL}}(u)}}du\right)\times \\ &\exp\left(-2\pi\tilde{\lambda}_1 \int_{\Delta_{11}^{\mathrm{NL}}(x)}^\infty \mathrm{Pr}_1^{\mathrm{L}}(u)\frac{u}{1+\frac{S_1^{\mathrm{NL}}(x)}{\tau S_1^{\mathrm{L}}(u)}}du\right)\times \\ &\exp\left(-2\pi\tilde{\lambda}_2 \int_{\Delta_{12}^{\mathrm{NL}}(x)}^\infty \mathrm{Pr}_2^{\mathrm{L}}(u)\frac{u}{1+\frac{S_1^{\mathrm{NL}}(x)}{\tau S_2^{\mathrm{L}}(u)}}du\right)\times \\ &\exp\left(-2\pi\tilde{\lambda}_2 \int_{\Delta_{13}^{\mathrm{NL}}(x)}^\infty \mathrm{Pr}_2^{\mathrm{NL}}(u)\frac{u}{1+\frac{S_1^{\mathrm{NL}}(x)}{\tau S_2^{\mathrm{NL}}(u)}}du\right).\end{aligned} \tag{3.3.8}$$

In Lemma 3.3.1, the interference from a LoS/NLoS channel for a UE $u \in \mathcal{U}_1$ is represented by Eq. (3.3.7) and Eq. (3.3.8), respectively. Moreover, the interference for $\mathcal{L}_{I_1^L}$ is composed of four parts, which are from other LoS MBSs, NLoS MBSs, LoS SBSs, and NLoS SBSs as shown in Eq. (3.3.7), and $\mathcal{L}_{I_1^{NL}}$ is shown as the similar components.

Lemma 3.3.2. *In Theorem 3.3.1,* $\mathcal{L}_{I_{21}^{\mathrm{L/NL}}}(s)$ *and* $\mathcal{L}_{I_{22}^{\mathrm{L/NL}}}(s)$ *are given by*

$$\begin{aligned}\mathcal{L}_{I_{21}^{\mathrm{L}}}(s) = &\exp\left(-2\pi\tilde{\lambda}_1 \int_{\Delta_{21}^{\mathrm{L}'}(x)}^{\infty} \mathrm{Pr}_1^{\mathrm{L}}(u) \frac{u}{1+\frac{S_2^{\mathrm{L}}(x)}{\tau S_1^{\mathrm{L}}(u)}} du\right) \times \\ &\exp\left(-2\pi\tilde{\lambda}_1 \int_{\Delta_{22}^{\mathrm{L}'}(x)}^{\infty} \mathrm{Pr}_1^{\mathrm{NL}}(u) \frac{u}{1+\frac{S_2^{\mathrm{L}}(x)}{\tau S_1^{\mathrm{NL}}(u)}} du\right) \times \\ &\exp\left(-2\pi\tilde{\lambda}_2 \int_{x}^{\infty} \mathrm{Pr}_2^{\mathrm{L}}(u) \frac{u}{1+\frac{S_2^{\mathrm{L}}(x)}{\tau S_2^{\mathrm{L}}(u)}} du\right) \times \\ &\exp\left(-2\pi\tilde{\lambda}_2 \int_{\Delta_{23}^{\mathrm{L}}(x)}^{\infty} \mathrm{Pr}_2^{\mathrm{NL}}(u) \frac{u}{1+\frac{S_2^{\mathrm{L}}(x)}{\tau S_2^{\mathrm{NL}}(u)}} du\right),\end{aligned} \tag{3.3.9}$$

$$\begin{aligned}\mathcal{L}_{I_{22}^{\mathrm{L}}}(s) = &\exp\left(-2\pi\tilde{\lambda}_2 \int_{x}^{\infty} \mathrm{Pr}_2^{\mathrm{L}}(u) \frac{u}{1+\frac{S_2^{\mathrm{L}}(x)}{\tau S_2^{\mathrm{L}}(u)}} du\right) \times \\ &\exp\left(-2\pi\tilde{\lambda}_2 \int_{\Delta_{23}^{\mathrm{L}}(x)}^{\infty} \mathrm{Pr}_2^{\mathrm{NL}}(u) \frac{u}{1+\frac{S_2^{\mathrm{L}}(x)}{\tau S_2^{\mathrm{NL}}(u)}} du\right);\end{aligned} \tag{3.3.10}$$

and

$$\begin{aligned}\mathcal{L}_{I_{21}^{\mathrm{NL}}}(s) = &\exp\left(-2\pi\tilde{\lambda}_1 \int_{\Delta_{21}^{\mathrm{NL}'}(x)}^{\infty} \mathrm{Pr}_1^{\mathrm{L}}(u) \frac{u}{1+\frac{S_2^{\mathrm{NL}}(x)}{\tau S_1^{\mathrm{L}}(u)}} du\right) \times \\ &\exp\left(-2\pi\tilde{\lambda}_1 \int_{\Delta_{22}^{\mathrm{NL}'}(x)}^{\infty} \mathrm{Pr}_1^{\mathrm{NL}}(u) \frac{u}{1+\frac{S_2^{\mathrm{NL}}(x)}{\tau S_1^{\mathrm{NL}}(u)}} du\right) \times \\ &\exp\left(-2\pi\tilde{\lambda}_2 \int_{\Delta_{23}^{\mathrm{NL}}(x)}^{\infty} \mathrm{Pr}_2^{\mathrm{L}}(u) \frac{u}{1+\frac{S_2^{\mathrm{NL}}(x)}{\tau S_2^{\mathrm{L}}(u)}} du\right) \times \\ &\exp\left(-2\pi\tilde{\lambda}_2 \int_{x}^{\infty} \mathrm{Pr}_2^{\mathrm{NL}}(u) \frac{u}{1+\frac{S_2^{\mathrm{NL}}(x)}{\tau S_2^{\mathrm{NL}}(u)}} du\right),\end{aligned} \tag{3.3.11}$$

$$\mathcal{L}_{I_{22}^{\mathrm{NL}}}(s) = \exp\left(-2\pi\tilde{\lambda}_2 \int_{\Delta_{23}^{\mathrm{NL}}(x)}^{\infty} \mathrm{Pr}_2^{\mathrm{L}}(u) \frac{u}{1+\frac{S_2^{\mathrm{NL}}(x)}{\tau S_2^{\mathrm{L}}(u)}} du\right) \times \exp\left(-2\pi\tilde{\lambda}_2 \int_{x}^{\infty} \mathrm{Pr}_2^{\mathrm{NL}}(u) \frac{u}{1+\frac{S_2^{\mathrm{NL}}(x)}{\tau S_2^{\mathrm{NL}}(u)}} du\right). \tag{3.3.12}$$

In Lemma 3.3.2, the interference from a LoS/NLoS channel for a UE $u \in \mathcal{U}_2$ is represented in Eq. (3.3.9)-Eq. (3.3.12), respectively. Moreover, from Eq. (3.3.10) I can find that when the ABS is working, only the interference from the other SBSs is valid. This is because all the MBSs are not transmitting in the ABS, and this brings about two parts of interference in Eq. (3.3.10). Similar components are shown in Eq. (3.3.11) and Eq. (3.3.12).

Lemma 3.3.3. *In Theorem 1,* $\mathcal{L}_{I_3^{\mathrm{L/NL}}}(s)$ *are given by*

$$\mathcal{L}_{I_3^{\mathrm{L}}}(s) = \exp\left(-2\pi\tilde{\lambda}_2 \int_{x}^{\infty} \mathrm{Pr}_2^{\mathrm{L}}(u) \frac{u}{1+\frac{S_2^{\mathrm{L}}(x)}{\tau S_2^{\mathrm{L}}(u)}} du\right) \times \exp\left(-2\pi\tilde{\lambda}_2 \int_{\Delta_{23}^{\mathrm{L}}(x)}^{\infty} \mathrm{Pr}_2^{\mathrm{NL}}(u) \frac{u}{1+\frac{S_2^{\mathrm{L}}(x)}{\tau S_2^{\mathrm{NL}}(u)}} du\right), \tag{3.3.13}$$

and

$$\mathcal{L}_{I_3^{\mathrm{NL}}}(s) = \exp\left(-2\pi\tilde{\lambda}_2 \int_{\Delta_{23}^{\mathrm{NL}}(x)}^{\infty} \mathrm{Pr}_2^{\mathrm{L}}(u) \frac{u}{1+\frac{S_2^{\mathrm{NL}}(x)}{\tau S_2^{\mathrm{L}}(u)}} du\right) \times \exp\left(-2\pi\tilde{\lambda}_2 \int_{x}^{\infty} \mathrm{Pr}_2^{\mathrm{NL}}(u) \frac{u}{1+\frac{S_2^{\mathrm{NL}}(x)}{\tau S_2^{\mathrm{NL}}(u)}} du\right). \tag{3.3.14}$$

In Lemma 3.3.3, the interference from a LoS/NLoS channel for a UE $u \in \mathcal{U}_3$ is represented in Eq. (3.3.13) and Eq. (3.3.14), respectively. Similar to Eq. (3.3.10) and Eq. (3.3.12), the components of them are two pars, as the interference only comes from SBSs.

It is important to note that the impact of the tier and BS selection on the coverage probability is measured in Eq. (3.3.5), the expressions of which are based on λ_1 and λ_2. This is because all the BSs can be chosen by the UEs. Moreover, the impact of the interference on the coverage probability is measured in Lemma 3.3.1, 3.3.2, and 3.3.3. Note that instead of λ_1 and λ_2, I use $\tilde{\lambda}_1$ and $\tilde{\lambda}_2$. This is because the IMC is applied, and thus only the activated BSs emit effective interference into the network.

3.3.2 Area Spectral Efficiency

In this subsection, I investigate the network capacity performance in terms of the area spectral efficiency (ASE) in bps/HZ/km^2, which is defined as

$$R = \sum_{k \in 1,2,3} \mathbf{1}(u \in \mathcal{U}_k)\eta_k \mathcal{R}_k, \tag{3.3.15}$$

where $\mathbf{1}(A)$ is the indicator of the event A, $\eta_1 = 1 - \eta$, $\eta_3 = \eta$, and $\eta_2 = 1 - \eta$ when ABS is engaged, while $\eta_2 = \eta$ when ABS is not engaged.

Then, the per tier $\mathcal{R}_k$ is defined by

$$\mathcal{R}_k \triangleq \lambda_u \mathbb{E}_x \left\{ \mathbb{E}_{\mathrm{SINR}_k}[\log_2(1 + \mathrm{SINR}_k(x))] \right\}. \tag{3.3.16}$$

It is important to note that the average is taken over both the spatial PPP and the channel fading distribution. The ASE is first averaged on the condition that the typical UE is at a distance x from its serving BS in the kth tier. Then it is averaged by calculating the expectation over the distance x. The following Theorem 3.3.2 gives the ASE over the entire network.

Theorem 3.3.2. *(Area Spectral Efficiency) For a typical user in the setup, the* ASE *is computed by*

$$R = \mathcal{R}_1^{\mathrm{L}} + \mathcal{R}_1^{\mathrm{NL}} + \mathcal{R}_2^{\mathrm{L}} + \mathcal{R}_2^{\mathrm{NL}} + \mathcal{R}_3^{\mathrm{L}} + \mathcal{R}_3^{\mathrm{NL}}, \tag{3.3.17}$$

where the conditional rate coverage $\mathcal{R}_k$ is given by the following equations:

$$\mathcal{R}_1^{\mathrm{L}} = (1-\eta)\lambda_u \int_{x=0}^{\infty} \int_{\rho_0}^{\infty} \exp\left(-\frac{\sigma^2 t(\rho)}{S_1^{\mathrm{L}}(x)}\right) \times \mathcal{L}_{I_1^{\mathrm{L}}}\left(\frac{t(\rho)}{S_1^{\mathrm{L}}(x)}\right) d\rho \mathcal{F}_1^{\mathrm{L}}(x) dx; \tag{3.3.18}$$

$$\mathcal{R}_1^{\mathrm{NL}} = (1-\eta)\lambda_u \int_{x=0}^{\infty}\int_{\rho_0}^{\infty} \exp\left(-\frac{\sigma^2 t(\rho)}{S_2^{\mathrm{L}}(x)}\right) \times \mathcal{L}_{I_1^{\mathrm{NL}}}(\frac{t(\rho)}{S_1^{\mathrm{NL}}(x)}) d\rho \mathcal{F}_2^{\mathrm{L}}(x)dx; \tag{3.3.19}$$

$$\begin{aligned}\mathcal{R}_2^{\mathrm{L}} =&(1-\eta)\lambda_u \int_{x=0}^{\infty}\int_{\rho_0}^{\infty} \exp\left(-\frac{\sigma^2 t(\rho)}{S_2^{\mathrm{L}}(x)}\right) \times \mathcal{L}_{I_{21}^{\mathrm{L}}}(\frac{t(\rho)}{S_2^{\mathrm{L}}(x)}) d\rho \mathcal{F}_2^{\mathrm{L}}(x)dx \\ &+ \eta\lambda_u \int_{x=0}^{\infty}\int_{\rho_0}^{\infty} \exp\left(-\frac{\sigma^2 t(\rho)}{S_2^{\mathrm{L}}(x)}\right) \times \mathcal{L}_{I_{22}^{\mathrm{L}}}(\frac{t(\rho)}{S_2^{\mathrm{L}}(x)}) d\rho \mathcal{F}_2^{\mathrm{L}}(x)dx;\end{aligned} \tag{3.3.20}$$

$$\begin{aligned}\mathcal{R}_2^{\mathrm{NL}} =&(1-\eta)\lambda_u \int_{x=0}^{\infty}\int_{\rho_0}^{\infty} \exp\left(-\frac{\sigma^2 t(\rho)}{S_2^{\mathrm{NL}}(x)}\right) \times \mathcal{L}_{I_{21}^{\mathrm{NL}}}(\frac{t(\rho)}{S_2^{\mathrm{NL}}(x)}) d\rho \mathcal{F}_2^{\mathrm{NL}}(x)dx; \\ &+ \eta\lambda_u \int_{x=0}^{\infty}\int_{\rho_0}^{\infty} \exp\left(-\frac{\sigma^2 t(\rho)}{S_2^{\mathrm{NL}}(x)}\right) \times \mathcal{L}_{I_{22}^{\mathrm{NL}}}(\frac{t(\rho)}{S_2^{\mathrm{NL}}(x)}) d\rho \mathcal{F}_2^{\mathrm{NL}}(x)dx\end{aligned} \tag{3.3.21}$$

$$\mathcal{R}_3^{\mathrm{L}} = \eta\lambda_u \int_{x=0}^{\infty}\int_{\rho_0}^{\infty} \exp\left(-\frac{\sigma^2 t(\rho)}{S_2^{\mathrm{L}}(x)}\right) \times \mathcal{L}_{I_3^{\mathrm{L}}}(\frac{t(\rho)}{S_2^{\mathrm{L}}(x)}) d\rho \mathcal{F}_3^{\mathrm{L}}(x)dx; \tag{3.3.22}$$

$$\mathcal{R}_3^{\mathrm{NL}} = \eta\lambda_u \int_{x=0}^{\infty}\int_{\rho_0}^{\infty} \exp\left(-\frac{\sigma^2 t(\rho)}{S_2^{\mathrm{NL}}(x)}\right) \times \mathcal{L}_{I_3^{\mathrm{NL}}}(\frac{t(\rho)}{S_2^{\mathrm{NL}}(x)}) d\rho \mathcal{F}_3^{\mathrm{NL}}(x)dx, \tag{3.3.23}$$

where $\rho_0 = \log_2(\tau+1)$*, defining the minimum working* SINR*, and* $t(\rho) = 2^{\rho} - 1$ *and the* PDFs *in each equation are given in Theorem 3.3.2.*

Proof. See Appendix A.4. □

Although the results for the coverage probability and ASE are not in closed-form, they can be numerically evaluated in a simple form. Moreover, they can be presented in closed-form expressions in several cases, for example, the 3GPP Case 1 mentioned in [52].

3.3.3 Special Case for ASE

In this subsection, a special case is used to show the analysis results for the ASE, and obtain insights from it.

I consider a very dense network where $\lambda_2 \to +\infty$, then the signal coming from the NLoS BSs can be neglected, and all UEs can be assumed to connect with BSs in a LoS channel. Thus, the ASE for the considered very dense network does not actually

depend on the LoS and NLoS propagation, and it can be described as the following Lemma.

Lemma 3.3.4. *In a very dense network where $\lambda_2 \to +\infty$, the ASE can be shown as*

$$\begin{aligned} R &= \mathcal{R}_1^{\mathrm{L}} + \mathcal{R}_2^{\mathrm{L}} + \mathcal{R}_3^{\mathrm{L}} \\ &= (1-\eta)\lambda_u(\Theta_1 + \Theta_{21}) + \eta\lambda_u(\Theta_{22} + \Theta_3), \end{aligned} \tag{3.3.24}$$

where

$$\Theta_1 = \int_{x=0}^{\infty}\int_{\rho_0}^{\infty} \exp\left(-\frac{\sigma^2 t(\rho)}{S_1^{\mathrm{L}}(x)}\right) \times \mathcal{L}_{I_1^{\mathrm{L}}}(\frac{t(\rho)}{S_1^{\mathrm{L}}(x)}) d\rho \mathcal{F}_1^{\mathrm{L}}(x) dx, \tag{3.3.25}$$

$$\Theta_{21} = \int_{x=0}^{\infty}\int_{\rho_0}^{\infty} \exp\left(-\frac{\sigma^2 t(\rho)}{S_2^{\mathrm{L}}(x)}\right) \times \mathcal{L}_{I_{21}^{\mathrm{L}}}(\frac{t(\rho)}{S_2^{\mathrm{L}}(x)}) d\rho \mathcal{F}_2^{\mathrm{L}}(x) dx, \tag{3.3.26}$$

$$\Theta_{22} = \int_{x=0}^{\infty}\int_{\rho_0}^{\infty} \exp\left(-\frac{\sigma^2 t(\rho)}{S_2^{\mathrm{L}}(x)}\right) \times \mathcal{L}_{I_{22}^{\mathrm{L}}}(\frac{t(\rho)}{S_2^{\mathrm{L}}(x)}) d\rho \mathcal{F}_2^{\mathrm{L}}(x) dx, \tag{3.3.27}$$

and

$$\Theta_3 = \int_{x=0}^{\infty}\int_{\rho_0}^{\infty} \exp\left(-\frac{\sigma^2 t(\rho)}{S_2^{\mathrm{L}}(x)}\right) \times \mathcal{L}_{I_3^{\mathrm{L}}}(\frac{t(\rho)}{S_2^{\mathrm{L}}(x)}) d\rho \mathcal{F}_3^{\mathrm{L}}(x) dx. \tag{3.3.28}$$

Besides, to compute the interference power for different tiers, $\mathcal{L}_{I_1^L}(\frac{t(\rho)}{S_1^L(x)})$,$\mathcal{L}_{I_{21}^L}(\frac{t(\rho)}{S_2^L(x)})$, $\mathcal{L}_{I_{22}^L}(\frac{t(\rho)}{S_2^L(x)})$, and $\mathcal{L}_{I_3^L}(\frac{t(\rho)}{S_2^L(x)})$, Lemma 3.3.5 is proposed.

Lemma 3.3.5. *The interference power for different tiers can be calculated by*

$$\begin{aligned} \mathcal{L}_{I_1^{\mathrm{L}}}(\frac{t(\rho)}{S_1^{\mathrm{L}}(x)}) &= \exp\left(-2\pi\widetilde{\lambda}_1 \times \rho\left(\alpha_1^L, 1, t(\rho)^{-1}x^{-\alpha_1^L}, x\right)\right) \\ &\times \exp\left(-2\pi\widetilde{\lambda}_2 \times \rho\left(\alpha_2^L, 1, \frac{P_1 A_1^L}{P_2 A_2^L} t(\rho)^{-1} x^{-\alpha_1^L}, \Delta_{12}^{L\cdot}(x)\right)\right), \end{aligned} \tag{3.3.29}$$

$$\begin{aligned} \mathcal{L}_{I_{21}^{\mathrm{L}}}(\frac{t(\rho)}{S_2^{\mathrm{L}}(x)}) &= \exp\left(-2\pi\widetilde{\lambda}_1 \times \rho\left(\alpha_1^L, 1, \frac{P_2 A_2^L}{P_1 A_1^L} t(\rho)^{-1} x^{-\alpha_2^L}, \Delta_{21}^{L\cdot\prime}(x)\right)\right) \\ &\times \exp\left(-2\pi\widetilde{\lambda}_2 \times \rho\left(\alpha_2^L, 1, t(\rho)^{-1}x^{-\alpha_2^L}, x\right)\right), \end{aligned} \tag{3.3.30}$$

and

$$\mathcal{L}_{I_{22}^{\mathrm{L}}}(\frac{t(\rho)}{S_2^{\mathrm{L}}(x)}) = \mathcal{L}_{I_3^{\mathrm{L}}}(\frac{t(\rho)}{S_2^{\mathrm{L}}(x)}) = \exp\left(-2\pi\widetilde{\lambda}_2 \times \rho\left(\alpha_2^L, 1, t(\rho)^{-1}x^{-\alpha_2^L}, x\right)\right), \tag{3.3.31}$$

where

$$\rho(\alpha,\beta,t,d) = \left[\frac{d^{-(\alpha-\beta-1)}}{t(\alpha-\beta-1)}\right] {}_2F_1\left[1, 1-\frac{\beta+1}{\alpha}; 2-\frac{\beta+1}{\alpha}; -\frac{1}{td^{\alpha}}\right], \quad (\alpha > \beta+1), \tag{3.3.32}$$

where ${}_2F_1[\cdot,\cdot;\cdot;\cdot]$ is the hyper-geometric function [82].

Proof. See Appendix A.5. □

From Lemma 3.3.4 and 3.3.5, the expression of the special case can be obtained, where the expressions of the interference power are much simpler than in the general case. To get more insights, I provide Lemma 3.3.6 to show that the ASE achieves the maximum value when the ABS factor is set to one.

Lemma 3.3.6. *In a very dense network, ASE achieves the maximum value when the ABS factor is set to one.*

Proof. Take the derivative of R with respect to η, then I get $\frac{\Delta R}{\Delta \eta} = \Theta_{22} + \Theta_3 - \Theta_1 - \Theta_{21}$. As the $\lambda_2 \to +\infty$, for the UE associated with a MBS, the interference power is increasing while the source power keeps stable. For the UE associated with a SBS, the UE can get stronger signal from a closer SBS. So intuitively speaking, $\Theta_{22} + \Theta_3$, which represents the UE connecting the SBS and receiving interference only from SBSs, should be larger than $\Theta_1 + \Theta_{21}$, which suffers interferences from all BSs. As a result, $\frac{\Delta R}{\Delta \eta} > 0$ and the optimal ABS factor should be one to get the maximum ASE. □

3.4 Simulation and Discussion

In this section, I use numerical results to establish the accuracy of the analysis, and further study the performance of dense HCNs.

3.4.1 Validation and Discussion on the Active BS Probability

I consider the 2-tier HCN, following the 3GPP definitions [83], to show the accuracy of our analysis. Table 3.1 summarizes the most important assumptions and parameter values.

In Fig. 3.3, I plot $\mathbb{P}_i^{\text{on}}$ versus λ_2, where $\lambda_2 \in [10, 1000]$ BSs/km^2. As can be observed from this figure, the analytical results match well with the simulation results. Moreover, they also show that, within the 5 dB power bias allocation to the small cell

Table 3.1: Parameter values Summary

Parameter	Values
Macro BS transmit power P_1	46 dBm
Micro BS transmit power P_2	24 dBm
Macro BS density λ_1	10 BSs/km^2
User density λ_u	300 UEs/km2
A_1^{L}	$10^{-10.34}$
α_1^{L}	2.42
A_1^{NL}	$10^{-13.11}$
α_1^{NL}	4.28
A_2^{L}	$10^{-10.38}$
α_2^{L}	2.09
A_2^{NL}	$10^{-14.54}$
α_2^{NL}	3.75
Power bias allocation D	5 dB
Noise Power σ^2	-95 dBm
$q = b$	4.18 [10]
Resource partitioning fraction η	0.4

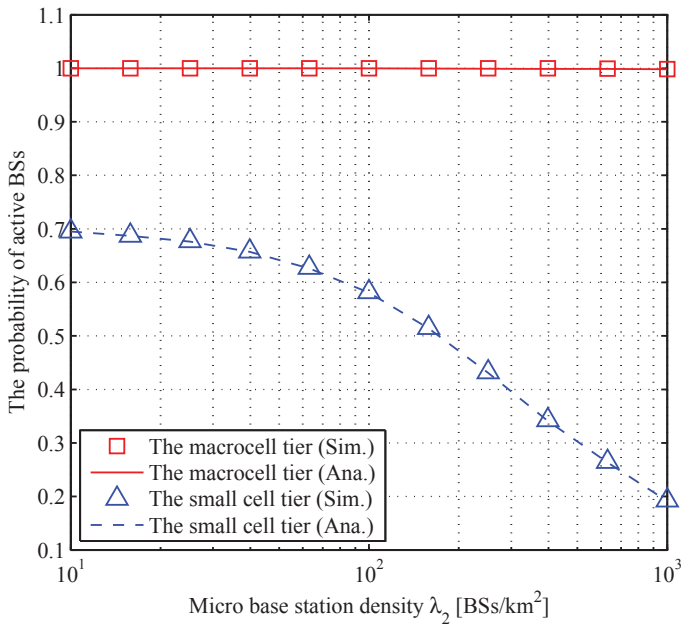

Figure 3.3: The active BS probability for each tier

BSs, *i)* the probability of a BS being active in the small cell BS tier decreases with λ_2, when λ_u is a finite value, and that *ii)* the BSs with a lower transmit power have lower activation probability. For example, more than 60% of the BSs in the small cell BS tier are idle when $\lambda_2 > 300$ BSs/km^2. This means that a large number of UEs are associated with the BSs in the macrocell tier, as they can provide stronger signals to these UEs.

3.4.2 Validation and Discussion on the Coverage Probability

In this subsection, I first validate the accuracy of Theorem 3.3.1. As in the previous subsection, the network consists of 2 tiers of BSs, represented by $\mathcal{U}_1$ and $\mathcal{U}_2$, respectively, and $\mathcal{U}_3$ is defined by the small cell tier, contributed by the range expanded (RE) UEs. All the simulation results are represented by the solid line.

In Fig. 3.4, I show the results of $\mathcal{S}$ with respect to λ_2. As can be seen from the figure, there are some small misalignments between the simulation and analytical results in each tier. For example, there is about 1.5% inaccuracy when λ_2 is about 16 BSs/km^2 as shown in Fig. 3.4. With the increasing number of BSs in the small cell tier, the error becomes negligible. The reason of such an error is that the spatial correlation in the UE association process is not considered in the analysis. More specially, when performing simulations, nearby UEs have a high probability of being covered and served by the same BS. However, for tractability, I consider the BS association of different UEs as independent process in Eq. (3.2.9) in the analysis, which underestimates the active BS density, as their no channel correlation. Because the accuracy of $\mathcal{S}$ is good enough, about 1.5%, I will only use analytical results of $\mathcal{S}$ for the figures in the sequel.

Fig. 3.4 also shows that with the increasing number of BSs in the small cell tier,

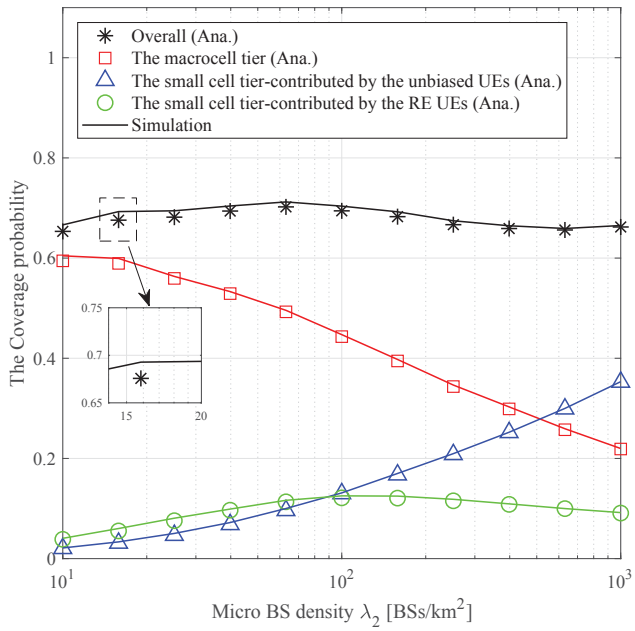

Figure 3.4: The coverage probability with respect to small cell BS density λ_2

the coverage probability of $\mathcal{U}_1$ decreases while that of $\mathcal{U}_2$ increases. The coverage probability of $\mathcal{U}_3$ first increases to a peak point and then decreases afterwards. As a result, the overall coverage probability first increases, then decreases, and finally increases again. The reason behind this phenomenon is that:

- The overall coverage probability first increases because UEs can connect to the stronger BSs.
- Then, the overall coverage probability decreases since the interference power grows faster than the signal power as many interfering paths transit from NLoS to LoS.
- Finally, the overall coverage probability performance continuously increases as the network densifies. The intuition is that the interference power will remain

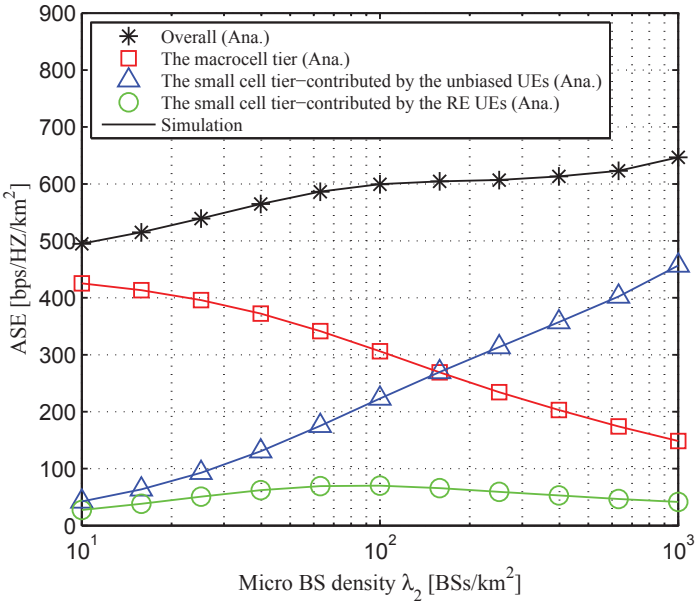

Figure 3.5: The results of ASE with respect to the small cell BS density λ_2

constant when the BS density is large enough (larger than the UE density), thanks to the IMC[2], while the signal power will continuously grow due to the closer proximity of the serving BSs, as well as the larger pool of BSs to select from.

3.4.3 Validation and Discussion on the ASE

In this subsection, I first validate the accuracy of Theorem 3.3.2, and then discuss the optimal ABS factor in different BS density regions.

In Fig. 3.5, I can observe that the analytical results on the per tier ASE match well with the simulation results. Moreover, the results show that with an increasing

[2]The interference power will become constant eventually when there are a large number of BSs. This is because of the IMC, which makes the number of active BSs at most equal to the number of UEs. Thus, from the viewpoint of the typical UE, the interference from other active BSs can be regarded as the aggregate interference generated by BSs on an HPPP plane with the same intensity as the UE intensity. Such aggregate interference is bounded and statistically stable [5].

number of BSs in the small cell tier, the ASE of $\mathcal{U}_1$ decreases, while ASE of $\mathcal{U}_2$ increases. The ASE performance decrease of $\mathcal{U}_1$ is because the interference power grows, as the BSs in the small cell tier get closer and transition to LoS, while the signal power remains constant. There is no densification in the macrocell tier. The ASE performance increase of $\mathcal{U}_2$ is because the signal power grows, as the UE is served by a stronger link in the small cell tier, while the interference power remains constant. This is because the BS density is larger than the UE density due to the IMC in the small cell tier. In contrast, the offloaded UE in $\mathcal{U}_3$ will first benefit from the network densification, but later they get a more severe interference from the increasing number of BSs in the small cell tier, whereas they do not have a large serving BS pool to select from.

In Fig. 3.6, the ASE is shown as a function of the BS density in the small cell tier for four different ABS fractions η. Note that $\lambda_u = 300$ UEs/km^2. I can draw the following conclusions from Fig. 3.6:

- The ASE almost monotonically grows as the network densifies. In more detail, the system throughput first increases quickly when λ_2 goes from 10 BSs/km^2 to 100 BSs/km^2. Then, the ASE suffers from a slow growth or even a decrease when $\lambda_2 \in [100, 900]$ BSs/km^2.

  Finally, the ASE monotonically grows again when $\lambda_2 > 900$ BSs/km^2.

- Different ABS factors should be applied in different BS density regions. In the region of $\lambda_2 < 900$ BSs/km^2, most users are associated with the MBSs and the less the number of ABSs, i.e., smaller η, the larger the ASE. However, when $\lambda_2 \geq 900$ BSs/km^2, the more the number of ABSs, i.e., lager η, the larger the ASE, since there are more users associated with the SBSs. The demarcation

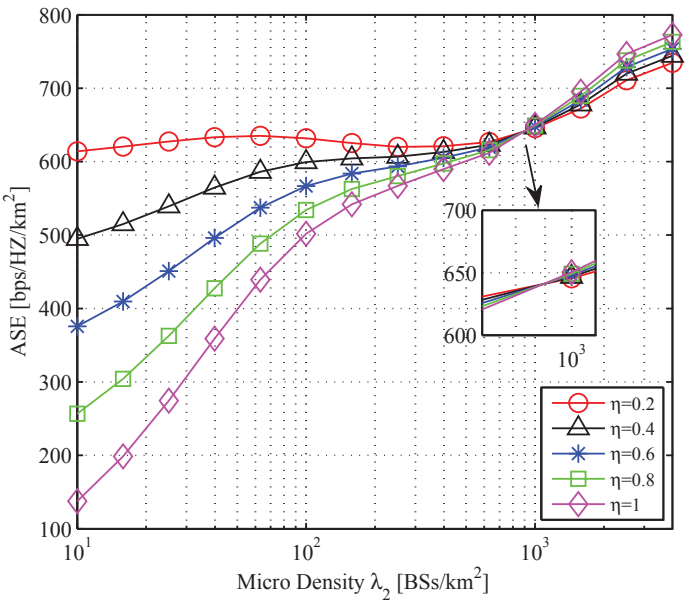

Figure 3.6: The system throughput with respect to the SBS density λ_2

point, 900 BSs/km^2, should be strongly related to the REB, which in this case is 5 dB.

In Fig. 3.7, I verify the observations from Fig. 3.7 by comparing the system throughput as a function of the ABS fraction for four different BS densities in the small cell tier λ_2. Note that $\lambda_u = 300$ UEs/km^2. Four SBS densities are considered in this figure to show the various trends of the ABS fraction. As can be found from the figure, more channel resource should be allocated to the BSs in the macrocell tier when the network is sparse, e.g., $\lambda_2 = 100$ BSs/km^2 and $\lambda_2 = 300$ BSs/km^2. When the network is denser, although the service to the macrocell UEs will get affected, for the benefit of the whole system, a larger η should be applied. It is important to note that MBSs should give up all resources and all subframes are ABSs, when the small cell networks go ultra-dense. The intuition is that most UEs are associated with

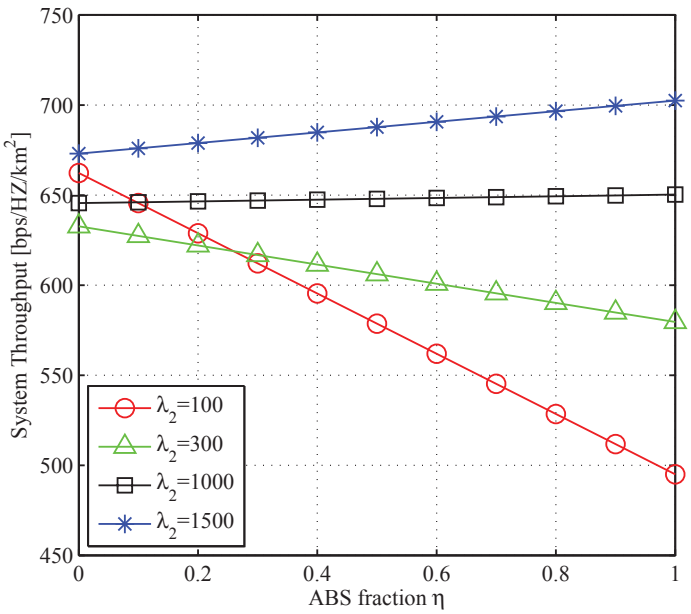

Figure 3.7: The system throughput with respect to the ABS factor η

small cell BSs at close proximity in UDNs, and the density of small cell BSs is very large. As a result, the cost of activating a MBS is high, since it will severely interfere with a large number of small cell BSs. Therefore, using a higher η, i.e., macrocell BSs giving up more subframe resources, is helpful to achieve a better overall system throughput. This reveals an important conclusion: to maximize network capacity, ultra-dense small cell networks should operate in a different frequency spectrum from the macrocell ones. In other words, the orthogonal deployment is superior to the co-channel deployment for ultra-dense small cell networks in future wireless networks. The intuition is that the additional spatial reuse of spectrum in the co-channel deployment is over-shadowed by the large interference emitted from the macrocell tier to the ultra-dense small cell tier.

In Fig. 3.8, I compare the current results with the bounded path loss model in

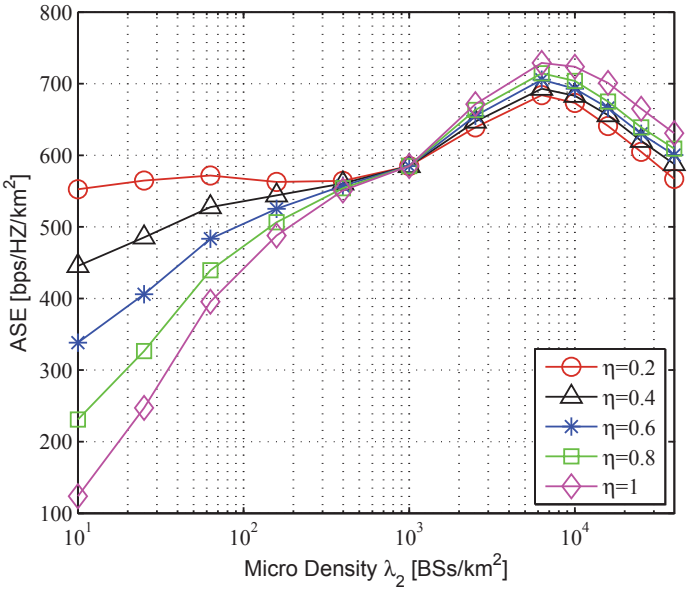

Figure 3.8: The system throughput with respect to the SBS density λ_2

[84] as follows,

$$\zeta_k'(r) = \begin{cases} \zeta_k^{\mathrm{L'}}(r) = A_k^{\mathrm{L}}(1+r)^{-\alpha_k^{\mathrm{L}}}, \\ \text{LoS: } \Pr_k^{\mathrm{L}}(r); \\ \zeta_k^{\mathrm{NL'}}(r) = A_k^{\mathrm{NL}}(1+r)^{-\alpha_k^{\mathrm{NL}}}, \\ \text{NLoS: } \Pr_k^{\mathrm{NL}}(r) = 1 - \Pr_k^{\mathrm{L}}(r). \end{cases} \tag{3.4.1}$$

From Fig. 3.8, I can find that there are two main differences from previous results. The first one is the crossing point, which is about 1000 BSs/km^2, is a little bigger than that in Fig. 3.6. This is because of the application of the bounded path loss model, which makes the receive power smaller than the previous one, especially for the SBS UEs. Thus, more resources should be allocated in the MBSs when the density of small cell BSs is not very large, and the crossing point shifts right. The second difference is that the ASE will first increase and then decrease with the density of the SBS, and should finally keep constant [85]. The intuition is that the received signal from BSs is

bounded while the interference power keeps increasing, so the ASE will decay for the denser BSs. When the network goes into ultra-dense, because of the limited number of UEs and the IMC of the BSs, the user signal power and the interference power are both bounded, so the ASE will keep constant in the end. Similarly, the same conclusion can be found from the results of the ASE performance: MBSs should give up all resources when the small cell networks go ultra-dense.

3.5 Summary

In this chapter, the impact of the IMC, caused by the finite number of UEs, on the network performance in a dense two-tier HCN with LoS and NLoS transmissions has been studied. Moreover, to address the under-utilization of SBSs, CRE and eICIC via ABSs are adopted in this work. The results show that as the BS density in the second tier surpasses the UE density, for the considered path loss model, the coverage probability and the ASE will continuously increase in this dense two-tier HCN, addressing the issue caused by the NLoS to LoS transition of interfering paths. Moreover, it is important to note that more ABSs are needed to enhance the performance of range expanded UEs as the small cell BS density grows, indicating that ultra-dense small cells should operate in a different frequency spectrum from the macrocell ones. This conclusion enlightens the new design and deployment of dense HCNs in 5G and beyond.

Chapter 4

Socially Aware Caching Strategy in Device to Device Communication Networks

In this chapter, the average performance of the D2D caching networks is studied, and an enhanced learning algorithm is proposed to solve the optimal caching placement problem in the socially aware D2D caching networks. To promote content dissemination in D2D communications, the concept of the social networks is introduced and implemented in the design of the caching strategy. Theoretical results of the average caching performance are derived using stochastic geometry theory and the system throughput gain is achieved by the proposed distribution caching algorithm.

4.1 System Model and Problem Formulation

4.1.1 Transmission Model

A content downloading scenario assisted by D2D overlaying communications is considered, where dedicated radio resources are allocated to D2D users by the BS as shown in Fig. 4.1, and thus there is no interference between the cellular and D2D links. There are a total of N users in the network. Denote by $\mathcal{N} = \{1, 2, \cdots, N\}$

Table 4.1: Parameter and Symbols Summary

Meaning	Symbol
Transmit power of IU m	P_m
Distance between IU m and user n	$r_{m,n}$
Request probability of file f	p^f
Social trust distance	A
The importance of IU m	$\mathcal{I}_m$
Probability of caching file i	p_i
Reward estimation of caching file i at time t	$o_i(t)$
Resolution parameter	δ
Physical influence of IU m and user n	$x_{m,n}$
Social influence of IU m and user n	$s_{m,n}$
The set of common neighbor of user m and n	$N_{m,n}$

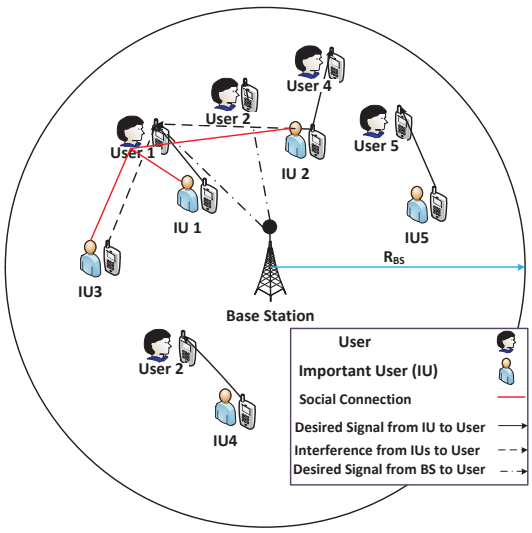

Figure 4.1: Illustration of the network deployment under consideration. Within the transmission distance of the BS (R_{BS}), User 1 can acquire content either from its adjacent IU 1 with social connection or from the BS. This connection will suffer from interference from other IUs.

the set of mobile users and it is assumed that each user carries a mobile device with D2D communication capability. Furthermore, denote by $\mathcal{M} = \{1, 2, \cdots, M\}$ the set of important users (IUs), which is a subset of mobile users in this network. I assume that the distribution of the IUs follows a homogeneous poisson point process[1] (HPPP) of density λ UEs/m^2. The BS caches files into the memories of the IUs during the off-peak time. Once the caching process is completed, the BS and IUs are ready to act upon the downloading requests of users.

I assume that a dedicated frequency band with a bandwidth of W Hz is allocated to the downlink channels for file-dissemination via D2D communications. Furthermore, I consider a "D2D-first" scheme, where each user will try to download data from its adjacent IUs first and only turn to the BS if no available D2D link exists or the requested file is not available from its adjacent IUs.

I assume that the channel between an IU and a mobile user is a Rayleigh fading channel. Furthermore, all downlink channels from the IUs to the users are assumed to be independent and identically distributed (i.i.d.). I consider the fully-loaded network scenario, where the IUs keep transmitting data to the users. This is because I intend to investigate the performance in the worst case that each user is subject to the interference imposed by all the other IUs in $\mathcal{M}$. The channel capacity between the mth IU and the nth user can be calculated based on the signal-to-interference-plus-noise ratio (SINR) as

$$C_{m,n} = W \log_2 \left(1 + \frac{P_m h_{m,n} r_{m,n}^{-\alpha}}{\sum\limits_{m' \neq m, m' \in \mathcal{M}} P_{m'} h_{m',n} r_{m',n}^{-\alpha} + \sigma^2} \right), \tag{4.1.1}$$

where $h_{m,n}$ is modeled as an exponential random variable (RV) with the mean of

[1] I assume the UE number is a Poisson distributed random variable, and the UEs are uniformly distributed on the plane. As the IUs are the subset of UEs, I thus have the distribution of the IUs as a thinned HPPP.

one due to Rayleigh fading, P_m is the transmit power of the mth IU, and σ^2 is the noise power. The path-loss between the mth IU and the nth user is modeled as $r_{m,n}^{-\alpha}$, where $r_{m,n}$ is the physical distance between the mth IU and the nth user and α is the path-loss exponent. Additionally, the channel capacity between the BS and the nth user is denoted by $C_{0,n}$.

The file library consists of F popular files, of which the popularity distribution is represented by $\mathcal{P} = \{p_1, p_2, \cdots, p_F\}$. Users make independent requests of the fth file, $f \in \{1, 2, \cdots, F\}$, with a probability of p^f. I use the Zipf distribution, which is commonly used in the caching literature, to model this probability. Specifically, for the fth file, its file request probability p_f can be written as

$$p^f = \frac{\frac{1}{f^\omega}}{\sum_{i=1}^{F} \frac{1}{i^\omega}}, \tag{4.1.2}$$

where F is the file library size and ω is the discounted rate in the Zipf distribution [19].

All these popular files are assumed to have the same size of L bits for simplicity. Also, I assume that the BS has a sufficiently large memory and hence can store the entire library of files, while the maximum storage of the IU is limited to $\mathcal{G}$ files, where $\mathcal{G} < F$. Denote by $\theta_{m,f} \in \{0, 1\}$ the event whether the mth IU has cached the fth file or not. Specifically, $\theta_{m,f} = 1$ if file f is cached by the mth IU; otherwise, $\theta_{m,f} = 0$. A D2D link can be established if the associated SINR of the link exceeds a predefined threshold γ and these two users have a social relationship, i.e., $\varsigma_{m,n} = 1$.

4.1.2 Social Relationship Model

In this work, I investigate two social relationship models, termed as the physically distance-dependent social model and the deterministic social model, respectively.

The physically distance-dependent social model

It is reported in [86] that only one-third of the social friendships are independent of geography. Experimental studies have verified this property in real social networks, and theoretical models have since been proposed to capture this fact that the probability of befriending with a particular person is inversely proportional to the physical distance between them [87], [88].

Considering the practical social relations among different users, I propose to model the probability of two users having a social relationship with respect to their physical distance r [86] as

$$\mathrm{P_S}(r) = \begin{cases} 1, & \text{when } 0 < r \leq A; \\ A^2/r^2, & \text{when } r > A. \end{cases} \tag{4.1.3}$$

Eq. (4.1.3) indicates that if the distance r between the receiver and the IU is smaller than a predefined distance A, the two users are surely to have a stable social relationship; otherwise, this probability is dependent on their physical distance.

Remark 4.1.1. The physically distance-dependent social model will be used to analyze the average performance of the D2D caching networks in Chapter 4.2.

The deterministic social model

The deterministic social model is widely adopted in open literature, e.g., [23], [89], and [90]. In this model, social characters (such as the social connections and the relationship closeness) are assumed to be known as a prior information. As such, the average successful transmission probability of the deterministic network scenario can be obtained by substituting known parameters into the analytical expression derived in Chapter 4.2.

Remark 4.1.2. The deterministic social model will be used to design a distributed caching algorithm in Chapter 4.3.

4.1.3 Problem Formulation

Given that the storage capacity of each IU is limited, it is imperative to design an effective caching strategy to optimize the QoE (defined as the average delay required to download a file) of all users in the networks.

First, given the channel coefficients, the specific location, and the nearby information of each user, the delay of downloading a file f in $\mathcal{F}$ by the nth user can be calculated as

$$D_{n,f} = \begin{cases} \min\{\frac{L}{C_{m,n}}\}, & \exists \varsigma_{m,n} \times \theta_{m,f} \neq 0 \text{ and } \mathrm{SINR}_{m,n} \geq \gamma, \\ \frac{L}{C_{0,n}}, & \text{otherwise.} \end{cases} \tag{4.1.4}$$

Mentioned here, the delay should be zero if the request file is cached locally by the user itself, which is not considered in the delay calculation.

To analyze the average downloading delay performance, I rewrite (4.1.4) as

$$D = p^{\text{trans}} \times \kappa \times \frac{L}{\overline{C}_{D2D}} + (1 - p^{\text{trans}} \times \kappa) \times \frac{L}{\overline{C_0}}, \tag{4.1.5}$$

where p^{trans} is the average transmission probability, κ is the average hitting rate used by the chosen caching strategy, $\overline{C}_{D2D}$ is the average transmission capacity of the D2D link, which is captured by the average of the $C_{m,n}$, and $\overline{C_0}$ is the average transmission capacity of the cellular link.

In order to reduce the downloading delay, it is important to analyze the baseline network performance first. Based on the average performance, the corresponding caching solutions can be evaluated. In the subsequent two sections, I first derive the successful transmission probability and the average downloading performance. Under the deterministic network scenario, I then focus on the cache placement optimization

at IUs by designing a socially aware distributed caching strategy, which decreases the downloading delay.

4.2 Stochastic Geometry Based Performance Analysis

In this section, I first adopt the physical distance-dependent social model in the D2D caching network and apply the stochastic geometry theory to derive the analytical expression for the average D2D transmission probability and the average downloading delay performance under different caching strategies.

4.2.1 Average D2D Transmission Probability

Recall that I use the following user association strategy (UAS). Each D2D receiver should be associated with the IU with the highest SINR. Also, each D2D link can be established under two conditions: (1) the IU and the receiver have a social relationship; (2) the SINR of this link is above the threshold γ. Using the property of the HPPP, I study the performance of the proposed socially aware D2D networks by considering the performance of a typical receiver located at the origin o. Under these assumptions, I first investigate the average transmission probability that a typical receiver can communicate with its associated IU. The average transmission probability is defined as

$$p^{\text{trans}}(\lambda, \gamma) = \Pr[\text{SINR} > \gamma], \tag{4.2.1}$$

where the SINR is computed by

$$\text{SINR} = \frac{Phr^{-\alpha}}{I_d + \sigma^2}, \tag{4.2.2}$$

where the path-loss of the channel from an IU to a receiver is simplified to $r^{-\alpha}$, and each IU is assumed to have the same transmission power P. Furthermore, I_d is the cumulative interference given by

$$I_d = \sum_{i:b_i \in \Phi \setminus b_0} P h_i r_i^{-\alpha}, \tag{4.2.3}$$

where b_0 denotes the IU serving the typical receiver and located at distance r from the typical receiver. Besides, for notation simplicity, I rewrite the rest parameters in Eq. (4.1.1): b_i and r_i denote the ith interfering IU and the distance between b_i and the receiver, respectively.

Given the definition of the average transmission probability presented in Eq. (4.2.1), in the following, I will analyze the performance measures for the considered UAS. Base on the proposed social relationship model in Eq. (4.1.3), I present the main result of $p^{\text{trans}}(\lambda, \gamma)$ in Theorem 4.2.1.

Theorem 4.2.1. *Considering the proposed social relationship model in Eq. (4.1.3), $p^{\text{trans}}(\lambda, \gamma)$ can be derived as*

$$\begin{aligned} p^{\text{trans}}(\lambda, \gamma) = &\int_0^A \Pr\left[\frac{Phr^{-\alpha}}{I_d + \sigma^2} > \gamma\right] f_{R1}(r) dr \\ &+ \int_A^\infty \Pr\left[\frac{Phr^{-\alpha}}{I_d + \sigma^2} > \gamma\right] f_{R2}(r) dr, \end{aligned} \tag{4.2.4}$$

where $f_{R1}(r)$ and $f_{R2}(r)$ are the piece-wise PDFs of the random variable (RV) R_1 and R_2, and R_1 and R_2 are the distance that the typical receiver has a nearest IU with a social relationship, and they represent different distance intervals. Moreover, $f_{R1}(r)$ and $f_{R2}(r)$ are represented by

$$f_{R1}(r) = \exp(-\pi\lambda r^2) 2\pi\lambda r, \quad (0 < r \leq A), \tag{4.2.5}$$

and

$$\begin{aligned} f_{R2}(r) = &\exp[-(\pi\lambda A^2 + 2\pi\lambda A^2(\ln r - \ln A)] \\ &\times 2\pi\lambda A^2 \frac{1}{r}, \quad (r > A). \end{aligned} \tag{4.2.6}$$

Furthermore, $\Pr\left[\frac{Phr^{-\alpha}}{I_d+\sigma^2} > \gamma\right]$ *is computed by*

$$\Pr\left[\frac{Phr^{-\alpha}}{I_d + \sigma^2} > \gamma\right] = \exp\left(-\frac{\gamma r^\alpha \sigma^2}{P}\right) \mathcal{L}_{I_d}\left(\frac{\gamma r^\alpha}{P}\right), \tag{4.2.7}$$

where $\mathcal{L}_{I_d}(s)$ is the Laplace transform of RV I_d evaluated at s.

Proof. See Appendix B.1. □

Because the physically distance-dependent social model in Eq. (4.1.3) takes the form of a piece-wise functions, I need to evaluate the interference $\mathcal{L}_{I_d}(s)$ for two regions of r, i.e., $0 < r \leq A$ and $r > A$.

To compute $\mathcal{L}_{I_{d1}}(s)$ in Eq. (4.2.4) for the range of $0 < r \leq A$, I attain Lemma 4.2.1.

Lemma 4.2.1. *$\mathcal{L}_{I_{d1}}(s)$ in the range of $0 < r \leq A$ can be calculated by*

$$\mathcal{L}_{I_{d1}}(s) = \exp\left(\frac{-2\pi\lambda r^2\gamma}{\alpha - 2} \times \nabla_1(\alpha, \gamma)\right), \ (0 < r \leq A), \tag{4.2.8}$$

where $\nabla_1(\alpha, \gamma) = {}_2F_1\left[1, 1 - \frac{2}{\alpha}; 2 - \frac{2}{\alpha}; -\gamma\right]$, ${}_2F_1[\cdot, \cdot; \cdot; \cdot]$ is the hyper-geometric function [91]*, and $\alpha > 2$.*

Proof. See Appendix B.2. □

Same as before, I have the following Lemma Eq. 4.2.2 to compute $\mathcal{L}_{I_{d2}}(s)$ in (4.2.4) for the range of $r > A$.

Lemma 4.2.2. *$\mathcal{L}_{I_{d2}}(s)$ in the range of $r > A$ can be calculated by*

$$\begin{aligned}\mathcal{L}_{I_{d2}}(s) = &\exp\left(-2\pi\lambda\gamma^2\frac{1}{\alpha}\left(\ln\left(1 + \frac{1}{\gamma}\right) - \ln\left(\frac{1}{\gamma}\right)\right)\right)\\ &\times \exp\left(\frac{-2\pi\lambda A^{2-\alpha}r^{\alpha}\gamma}{\alpha - 2} \times \nabla_2(\alpha, A, r, \gamma)\right)\\ &\times \exp\left(\frac{2\pi\lambda A^2}{\alpha}\left[\ln(1 + \frac{A^{\alpha}r^{-\alpha}}{\gamma}) - \ln(\frac{A^{\alpha}r^{-\alpha}}{\gamma})\right]\right),\\ &\qquad (r > A)\end{aligned} \tag{4.2.9}$$

where $\nabla_2(\alpha, A, r, \gamma) = {}_2F_1\left[1, 1 - \frac{2}{\alpha}; 2 - \frac{2}{\alpha}; -A^{-\alpha}r^{\alpha}\gamma\right]$, ${}_2F_1[\cdot, \cdot; \cdot; \cdot]$ is the hyper-geometric function [91]*, and $\alpha > 2$.*

Proof. See Appendix B.3. □

Substituting Eqs. (4.2.5)-(4.2.9) into Eq. (4.2.4), $p^{\text{trans}}(\lambda, \gamma)$ for the proposed model can be obtained.

Remark 4.2.1. The results shown in Theorem 4.2.1 reveal an interesting finding. Specifically, the successful transmission probability becomes stable when the density of users is large enough. More discussions are relegated to Sec. V-A. In order to reduce the downloading delay from Eq. (4.1.5), the following approach is to optimize the caching content in IU, which will increase the hitting rate.

4.2.2 Average Downloading Delay Performance

I first introduce two popular caching strategies to estimate the average downloading delay performance.

Random Caching (RC)

The random caching is realized by randomly picking files from the file library to cache into IUs, and I denote this hitting rate by κ_{ran}, and $\kappa_{ran} = \mathcal{G}/F$.

Deterministic Caching (DC)

The deterministic caching is realized by caching the most popular files according to the file request probability. Then I denote the hitting rate used in the deterministic caching strategy by κ_{det}, and $\kappa_{det} = \sum_1^{\mathcal{G}} p^f$, where p^f is the file request probability and defined in Eq. (4.1.2).

Substituting different hitting rates into Eq. (4.1.5), I can get the average downloading delay performances. Note that such an average delay performance can be achieved by simple caching schemes such as the RC and DC schemes, where every IU caches same files and it provides a theoretical understanding of the D2D caching network. With various numbers and locations of users, the trends regarding the user density or the file request probability are obtained. In practice, more sophisticated content caching algorithms can be devised and implemented when more information is available, such as social relationship and physical distance. In this case, each IU

may cache files according to its local feedback that in turn increases the hitting rate.

In the following section, I will explore new implementation algorithms based on the decentralized learning technique to optimize the caching content in IUs.

4.3 Socially Aware Distributed Caching Algorithm

In the previous section, I adopt the physically distance-dependent social model in the D2D caching network and study the performance under different caching strategies. Such analysis provides us a theoretical understanding of the network performance for the considered D2D caching network with various numbers and locations of users. As to be shown in the section on simulations and discussions, the analysis is useful to qualitatively predict the performance trend of D2D caching in 5G. However, it still remains unclear how to implement the 5G D2D caching in practice. And more importantly, can we even do better than the derived analytical results by means of more advanced algorithms? If yes, how much better? Note that in the theoretical analysis conducted in the previous section, only simple D2D caching strategies such as RC and DC, have been analyzed, where each IU caches the same files. In practice, it is desirable and might be feasible to optimize the D2D content placement on the fly, and popular content can be specifically placed in particular devices to achieve high performance gains in particular areas. Therefore, in this section, I consider a deterministic D2D caching scenario with fixed number and locations of users, and devise a distributed algorithm to enable each IU to optimize its content placement. To take fully advantage of the social characters as well as the content request probability, a class of reinforcement learning algorithm is proposed. In each iteration, the exact

content requested by the user is generated using simulation, and a reward/penalty will be imposed after this action. The IU will know which content should be exactly cached after the entire learning process.

To this end, I develop a distributed learning automation that enables each IU to optimize the cache placement according to its local demands. The proposed algorithm is inspired by the DGPA [92]. In the following, by adopting the deterministic social network model, in which the successful transmission probability among IUs and users is invariant, I first introduce a scheme to select the IUs in the considered network, then provide some preliminaries of DGPA before formally presenting the proposed algorithm. Furthermore, I also design a scheme to characterize the mutual impacts of content placement in different IUs, which enables the proposed algorithm to be implemented in large-scale networks.

4.3.1 Selection of The Important Users

The important users (IUs) in the proposed network will pre-cache files from the BS during the off-peak hours and transmit these files to other users. I first determine the number of the IUs in the network.

Throughout the paper, a user is called a neighbor of another user if there is a social relationship between them. According to [93], in social networks, the distribution of the node degree, i.e., the number of neighbors of a node, decays according to a power law distribution given by

$$p(k) = c_k \times k^{-\varphi}, \tag{4.3.1}$$

where $\sum_{k=0}^{\infty} c_k k^{-\varphi} = 1$, and $p(k)$ is the probability that a randomly chosen node has k neighbors, and φ is the decaying coefficient. Let M_k be the number of nodes that

have at least k neighbors in a network with total N nodes. Using the aforementioned power law degree distribution, M_k can be calculated as

$$M_k = \lfloor N \times \sum_{i=k}^{N-1} p(i) \rfloor, \tag{4.3.2}$$

where $\lfloor x \rfloor$ is the floor function, retrieving the largest integer that is equal or smaller than x. In the following, I ignore the subscript of M_k, and rewrite as M for notational convenience. I assume that these M users can download contents directly from BSs and they are regarded as the important users (IUs).

Next, I present a scheme to sort these M IUs. In the process of sorting the IUs, the betweenness centrality $\mathcal{B}$ and the available storage capacity $\mathcal{G}$ are used to characterize the importance, which is denoted by $\mathcal{I}$. For the mth IU, the importance is defined as

$$\mathcal{I}_m = \mu \times \mathcal{B}_m + \nu \times \mathcal{G}_m, \tag{4.3.3}$$

where μ and ν are tunable parameters satisfying $\mu + \nu = 1$ [94]. Betweenness centrality $\mathcal{B}$ measures the social importance of one user. According to [95], the betweenness centrality of the mth user can be calculated as

$$\mathcal{B}_m = \sum_{j=1}^{N} \sum_{j<k} \frac{g_{jk}(m)}{G_{jk}}, \tag{4.3.4}$$

where G_{jk} is the number of shortest links between user j and user k, and $g_{jk}(m)$ is the number of those shortest links between user j and user k that include or pass user m.

After collecting each user equipment's available storage capacity $\mathcal{G}_i$, the BS can get a list of the importance, which is denoted by $\mathfrak{I} = \{\mathcal{I}_1, \mathcal{I}_2, ..., \mathcal{I}_m\}$. Then these M IUs are sorted by the list $\mathfrak{I}$ in descending order.

4.3.2 Discrete Generalized Pursuit Algorithm

The goal of the DGPA is to determine an optimal action out of a set of allowable actions $\mathcal{F} = [1, 2, ..., F]$. The DGPA has a probability vector $\mathbf{P}(t) = [p_1(t), p_2(t), ..., p_F(t)]$, where $p_i(t)$ is the probability that the automaton will select the action i at iteration t with $\sum_{i=1}^{F} p_i(t) = 1$. The update of the probability vector is performed based on the reward estimation $\mathbf{o}(t) = [o_1(t), o_2(t), ..., o_F(t)]$ and each reward estimation is determined by the environment feedback [92]. In the considered D2D caching system, at each learning process, an action of each IU is to choose one file from the file library to cache. This action is performed according to the file request probability. A certain action will get a positive reward from the aggregate environment feedback if it is beneficial to the system.

The DGPA generalizes the concepts of the pursuit algorithm by "pursuing" all the actions that have higher reward estimates than the current chosen action. In the algorithm, the action probability vector $\mathbf{P}(t)$ is recursively updated by the following equation:

$$\mathbf{P}(t+1) = \mathbf{P}(t) + \frac{\Delta}{K(t)} \times \mathbf{e}(t) - \frac{\Delta}{F - K(t)} \times [\mathbf{u} - \mathbf{e}(t)], \tag{4.3.5}$$

where $\mathbf{u}$ is a vector in which $u_i = 1, i = 1, 2, ..., F$, and $\mathbf{e}$ is a direction vector given by:

$$\begin{aligned} e_i(t) &= \begin{cases} 1, & \text{if } o_i(t) = \max\{o_j(t)\}\ j \in 1, ...F; \\ 0, & \text{otherwise.} \end{cases} \\ e_j(t) &= \begin{cases} 0, & \text{if } o_j(t) \leq o_i(t); \\ 1, & \text{if } o_j(t) > o_i(t). \end{cases} \end{aligned} \tag{4.3.6}$$

According to Eq. (4.3.5), the probabilities of the chosen action i and other action j

are updated as following:

$$\begin{cases} p_j(t+1) = \min\{p_j(t) + \frac{\Delta}{K(t)}, 1\}, \text{if } o_j(t) > o_i(t); \\ p_j(t+1) = \max\{p_j(t) - \frac{\Delta}{F-K(t)}, 0\}, \text{if } o_j(t) < o_i(t); \\ p_i(t+1) = 1 - \sum\limits_{j \neq i} p_j(t+1). \end{cases} \tag{4.3.7}$$

At each iteration of the DGPA, the number of actions which has a higher reward estimation $o(t)$ than the current chosen one is counted, denoted by $K(t)$. At the end of an iteration, the probability of all actions with a higher reward estimation $o(t)$ will increase by an amount of $\Delta/K(t)$, and the probability of all the other actions except the chosen one will decrease by an amount of $\Delta/(F - K(t))$, where F is the action library size. Besides, $\Delta = 1/F\delta$ and it is a resolution step and δ is the resolution parameter.

In order to update the probability of each action, the reward estimation $o(t)$ should be estimated at first. The update equations of reward estimation $o(t)$ for the chosen action i are as follows:

$$\begin{cases} Z_i(t+1) = Z_i(t) + 1; \\ W_i(t+1) = W_i(t) + \beta(t); \\ o_i(t+1) = \frac{W_i(t+1)}{Z_i(t+1)}, \end{cases} \tag{4.3.8}$$

where $Z_i(t)$ represents the number of times that action i has been chosen, and $W_i(t)$ represents the number of times that action i has been rewarded. $\beta(t) \in \{0, 1\}$ is a binary factor reflecting the positive or negative feedback. If the feedback is positive (i.e., $\beta = 1$), then this action i is rewarded.

In the next subsection, based on the above preliminaries of DGPA, I will design the functions of the aggregate environment feedback in the proposed socially aware D2D networks.

4.3.3 Environment Feedback

In this model, the BS can acquire the position of every user, thus BSs will provide each IU with its relevant downloaders' information (e.g., the file request probability) and each IU can broadcast the cached files to its relevant downloaders. In this sense, different cached files (actions) at a certain IU would lead to different influences on its neighbors and other IUs. In the process of learning, when the mth IU caches the file f according to its downloading neighbor n's request, I define the aggregate environment reward $R^f_{m,n}$ as a weighted sum of the request probability (p^f_n) of file f, the physical influence ($x_{m,n}$) between IU m and its neighbor n, and the social influence ($s_{m,n}$) between them, which can be expressed by:

$$R^f_{m,n} = \tau_1 \times p^f_n + \tau_2 \times x_{m,n} + \tau_3 \times s_{m,n}, \tag{4.3.9}$$

where τ_1, τ_2, and τ_3 are tunable parameters and satisfy $\tau_1 + \tau_2 + \tau_3 = 1$. I provide detailed explanation of each term in Eq. (4.3.9) as follows.

The request probability p^f_n

The BS will record the request files of each user, and provide this probability to the IUs. According to Eq. (4.1.2), for the fth file, its file request probability p_f by user n can be written as

$$p^f_n = \frac{\frac{1}{f^\omega}}{\sum_{i=1}^{F_n} \frac{1}{i^\omega}}, \tag{4.3.10}$$

where F_n is the file library size of user n.

The physical influence $x_{m,n}$

Intuitively speaking, there will be significant influence if the distance between the mth IU and user n is small [96]. In order to provide the shortest download time, the

request file by the nearest user n, for example, should be cached by the IU m. In this sense, the physical influence is modeled as

$$x_{m,n} = \frac{1}{1 + r_{m,n}}, \tag{4.3.11}$$

where ${r_{m,n}}^2$ represents the distance between the mth IU and the user n.

The social influence $s_{m,n}$

The degree of similarity among users has an important effect in information dissemination [97]. Particularly, when the degree of similarity between two users is lower, more time would be needed for transmitting the same length of information because they may not have the required content. As a result, I use the degree of similarity to characterize the social influence $s_{m,n}$.

The degree of similarity can be measured by the ratio of common neighbors between individuals. According to [97], I assume that the mth IU is connected to user n. Let $V(m)$, $V(n)$ denote the set of neighbors of users m and n, respectively. Let z be one of the common neighbors of them and let $V(z)$ denote the number of user $z's$ neighbor. I can then define the similarity between IU m and its neighbor n as:

$$q_{m,n} = \sum_{z \in V(m) \cap V(n)} \frac{1}{V(z)}. \tag{4.3.12}$$

If m and n have no common neighbors, then $q_{m,n} = 0$. In order to make the three factors of the environment feedback comparable, I normalize the similarity $s_{m,n}$ as follows:

$$s_{m,n} = \frac{q_{m,n}}{\sum_{m \in M} q_{m,n}}. \tag{4.3.13}$$

Now, I am ready to calculate the environment feedback using the reward functions.

[2] $C_{m,n}$ can be the considered parameter instead of $r_{m,n}$ if the channel condition and other interference signals are known, and it will provide more sense than the distance between users.

Denote by N_m the neighbor set of the mth IU. At each learning iteration, IU m will choose a file f to cache, and its neighboring users will also ask a file to download according to their own file request probabilities. If the mth IU and one of its neighbors n choose the same file, such as the file f, I define this action as a positive one, which brings a positive reward (Ψ_P). If not, this action will be determined as a negative action (Ψ_N). Mathematically, the reward functions are defined as:

$$\begin{cases} \Psi_P = R^f_{m,n}, \text{ if } m \text{ and } n \text{ choose the same file;} \\ \Psi_N = -R^f_{m,n}, \text{ if } m \text{ and } n \text{ choose different files.} \end{cases} \tag{4.3.14}$$

Thus, for the mth IU, the aggregate environment feedback function of choosing the file f can be expressed as:

$$\digamma^f_m = \sum_{n=1}^{N_m} (\Psi_P + \Psi_N). \tag{4.3.15}$$

If $\digamma^f_m > 0$, then $\beta = 1$ and this action that the mth IU caches the file f will get a positive feedback from the environment. The estimation vector $o(t)$ is updated by Eq. (4.3.8).

According to the aggregate environment feedback, the mth IU will keep learning and acquiring the request files from BSs until its available storage is full.

Remark 4.3.1. From Eq. (4.3.9) I can see that the design of environment feedback is important and different feedback functions will lead to different learning results.

4.3.4 The Mutual Impact of Nearby IUs

The decision of content placement for the mth IU will affect its nearby IUs, which have common neighbors with the mth IU. If there are two IUs in the nearby area, the content placement of these two IUs should be made different as much as possible to serve different requests of their common neighbors. In this case, the BS should

update the file request probability of the common neighbors according to the former IUs who have already cached contents.

IUs start learning in the order determined by the list $\mathfrak{I}$. To update the file request probability of the common neighbors, all the IUs should report the cached files to the BS after learning. This update should consider both the cached files and the physical distance. For example, if two previous IUs m and m' have already cached files f and f', respectively, then for the next IU n, it should first estimate which IU has a larger physical influence (a shorter distance) to IU n. If IU m has a larger physical influence than IU m', i.e., $r_{n,m} < r_{n,m'}$, then file f cached by IU m should be considered when updating the file request probability of their common neighbors. Let $N_{m,n}$ denote the set of the common neighbor of the mth IU and the nth IU, then the request probability ($Y_f^{N_{m,n}}$) of file f for the common neighbor ($N_{m,n}$) can be updated as

$$Y_f^{N_{m,n}} = Y_f^{N_{m,n}} \times \frac{1}{1 + r_{n,m}}, \tag{4.3.16}$$

where $r_{n,m}$ represents the physical distance between the nth IU and the mth IU and α is the path loss exponent.

After updating the probability of every cached file by the mth IU, the file probabilities $Y^{N_{m,n}}$ of the common neighbors between the mth IU and the nth IU will be normalized, and the nth IU can start its learning process.

To sum up, the proposed algorithm has been formally presented in Algorithm **1** by using the variable definitions presented in the previous subsections.

4.3.5 Convergence

I now analyze the convergence of the proposed algorithm. If the algorithm converges, then the result would give the optimal cached file decided by the environment

Algorithm 1 Distributed and Socially Aware D2D Caching Algorithm for the mth IU

Start

Initialization for the mth IU.

1: Choose one IU m' in $\mathfrak{I}$, which has the biggest physical influence to m, and update the file request probability of m in (4.3.16).

2: Normalize the file request probability of m and set it as $P(0)$.

3: Randomly choose files according to $P(0)$, and record the aggregate environment feedback β, until each file is selected at least $Z(0)$ times.

4: Record the rewarded times of each file ($W_i(0)$).

5: Initializes $o_f(0)$, where $o_f(0) = \frac{W_f(0)}{Z_f(0)}$.

Learning Process for the mth IU. Do:

1: At time t choose file f according to $P(t)$. Let $\alpha(t) = \alpha_f$.

2: Update $P(t)$ according to Eq. (4.3.7).

3: Update $o(t)$ according to Eq. (4.3.8).

Until: $\max P_f(t) > \delta$, where δ is a convergence threshold.

Repeat Initialization and Learning until the storage of the mth IU is full.

Until: every IU finishes learning.

End

feedback. According to [92], if the algorithm possesses the moderation and monotonicity properties, the algorithm is ε-optimal in all random environments and it will converge. Therefore, I show the proof of convergence in the following lemma.

Lemma 4.3.1. *The proposed algorithm possesses the moderation and monotone properties.*

Proof. Please refer to Appendix B.4. □

Because the proposed algorithm possesses the moderation and monotony properties, the convergence is guaranteed [92]. Thus, after learning, each IU will cache the content according to the learning results. To calculate the hitting rate of the proposed algorithm, the learning result will be compared with the target in the algorithm, and subsequently, the downloading performance in the considered social model can be obtained from the hitting rate.

4.4 Performance Evaluation

In this section, I first focus on the proposed network with IUs distributed following an HPPP, where I investigate the average transmission probability and the average performance of the two caching strategies, i.e., DC[3] and RC. Then I consider the network with a fixed number of IUs. Using the average transmission probability, I investigate the delay performance of the proposed caching algorithm and compare it to the benchmarks, including DC and a simple reward function which also uses the DGPA learning algorithm proposed in [11]. Note that the physical layer parameters in the simulations, such as the path-loss exponent, the noise power, and the transmit power of the IUs and the BS, are chosen to be practical and in line with the values

[3]Before caching, the macro BS will broadcast the most request files of the past 24 hours to the IUs first. Then the IUs can cache the most popular files according to this information.

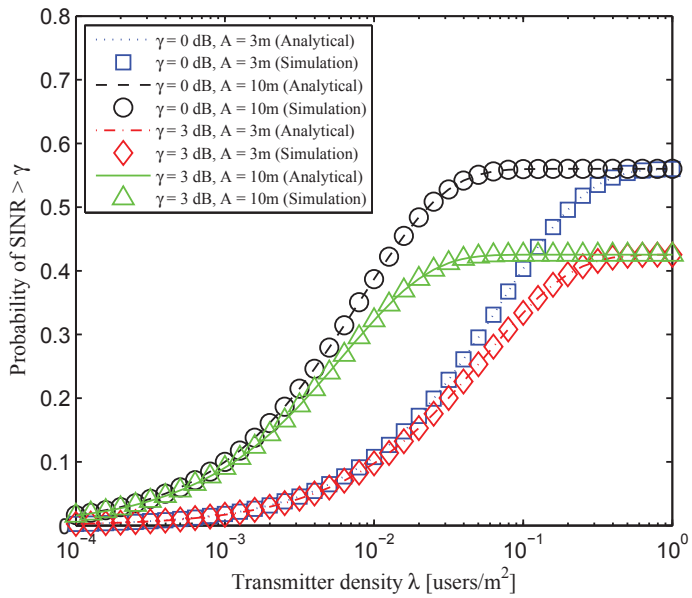

Figure 4.2: The transmission probability $p^{\text{trans}}(\lambda, \gamma)$ vs. density of the IU λ with various SINR thresholds γ and different social trust distance A

set by 3GPP standards. For instance, the coverage of the BS is 25 km^2, and the transmission power of IUs is 25 dBm. Unless specified otherwise, I set the path loss exponent $\alpha = 3$, and the noise to $\sigma^2 = -95$ dBm. All the simulations are executed using MATLAB.

4.4.1 Average Transmission Probability of D2D Link

I first compare the simulation and analytical results in the proposed network with different transmitter densities, different social trust distances, and various SINR thresholds. As can be observed from Fig. 4.2, the analytical results perfectly match the simulation results. Due to the significant accuracy of $p^{\text{trans}}(\lambda, \gamma)$, I will only use analytical results of $p^{\text{trans}}(\lambda, \gamma)$ in the discussion later. From Fig. 4.2 I can observe that the transmission probability first increases with the transmitters density because

more transmitters provide better coverage in noise-limited networks. Then, when λ is large enough ($\lambda > 10^{-1}$ users/m^2), the transmission probability becomes independent of λ because the network is pushed into the interference-limited region. From this finding, in order to reduce the downloading delay, I should optimize the caching content in each IU. Another two observations are that when the smallest social trust distance A is the same, the transmission probabilities of different SINR thresholds show similar trends as they converge at same λ, and when the SINR threshold γ is the same, the transmission probabilities of different small social trust distances saturate to the same level at different λ.

4.4.2 Average Delay of Downloading Performance for the Physical Distance-dependent Social Model

I evaluate the average delay of downloading performance for the RC and the DC strategy in Fig. 4.3. I also simulate the non-D2D caching scenario for comparison. For the simulation results of this subsection, I assume a SINR threshold of $\gamma = 0$ dB, a file size of $L = 10^9$ bits, an IU density of $\lambda = 10^{-2}$ users/m^2, and a smallest social trust distance of $A = 10$ m.

Fig. 4.3 illustrates the average downloading delay associated with different ω values. I can see that DC always outperforms RC, and the performance gap between these two strategies becomes larger with an increasing ω, while the non-D2D caching scheme behaves the worst.

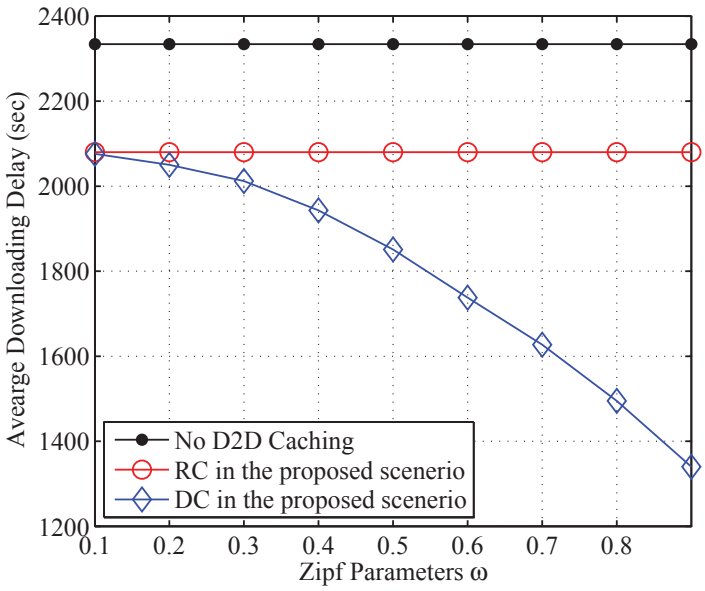

Figure 4.3: Average downloading delay D vs. the Zipf parameter ω under different scenarios

4.4.3 Convergence of the Socially Aware Distributed Caching Algorithm

After presenting the system performance of the physical distance-dependent social model, let us now focus on the socially aware distributed caching algorithm which applies the deterministic social model in the following subsections. I first test and verify the convergence of the proposed algorithm. A small-scale mobile network is considered, which consists of 3 IUs and each of them has 6 neighboring downloaders. The algorithm is considered to converge when the probability of taking one action (caching one file) is greater than 0.999. I recorded the number of the executed iterations, and each point in the figures is obtained by averaging the results over 50 independent run of the proposed algorithm.

Fig. 4.4.(a) shows the executed iterations of different δ, in which more complex

Table 4.2: Reward times after repeating 50 times of learning when the file library size is 10

	IU1	IU2	IU3	Reward probability
$\delta = 0.5$	20	17	16	0.353
$\delta = 0.5$ in [11]	15	16	15	0.307
$\delta = 1$	25	22	20	0.446
$\delta = 1$ in [11]	20	19	20	0.393
$\delta = 2$	29	26	25	0.514
$\delta = 2$ in [11]	23	23	22	0.453

algorithm will cost more iterations to converge, and more time to finish the learning process. As the file library size grows, the average number of iterations increases. Moreover, different resolution parameters δ show different increasing trends, and require different numbers of iterations to converge. For example, when $\delta = 0.5$, the average number of iterations is nearly half (49.2%) of that when $\delta = 1$. I also compare the proposed algorithm with the work [11]. As can be observed from Fig. 4.4.(a), the algorithm presented in the work [11] requires fewer iterations on average compared with the proposed algorithm in this paper. This is because the algorithm in [11] was based on a simple environment feedback function, in which the physical distance influences were not considered.

As can be observed from Table 4.2, I present the reward times of different δ when the file library size is 10. Using the reward times, the average reward probability can be calculated for different file library size. Fig. 4.4.(b) depicts the average reward probability of different resolution parameters δ. It is shown that with the increasing size of the file library, the average reward probability decreases. Also the proposed algorithm can get a higher reward probability than the algorithm in [11]. Considering both Fig. 4.4.(a) and Fig. 4.4.(b), although a larger resolution parameter δ implies more time to converge, it can achieve a higher reward probability. Moreover, for the

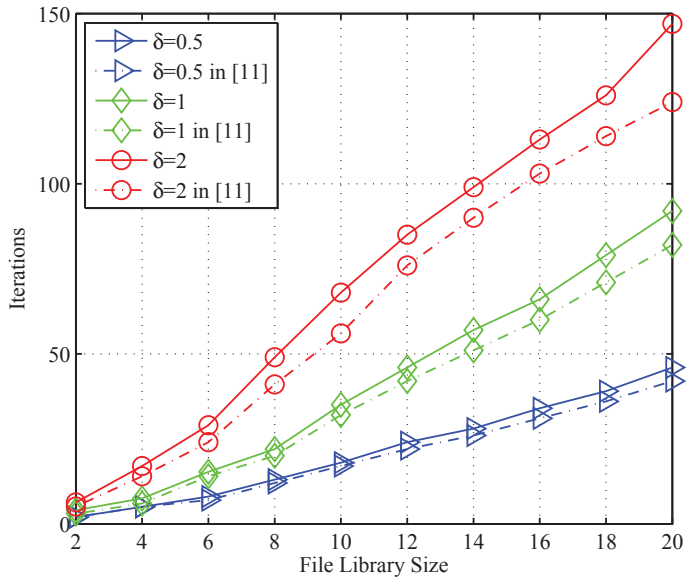

(a) The average number of iterations to converge of different resolution parameters δ

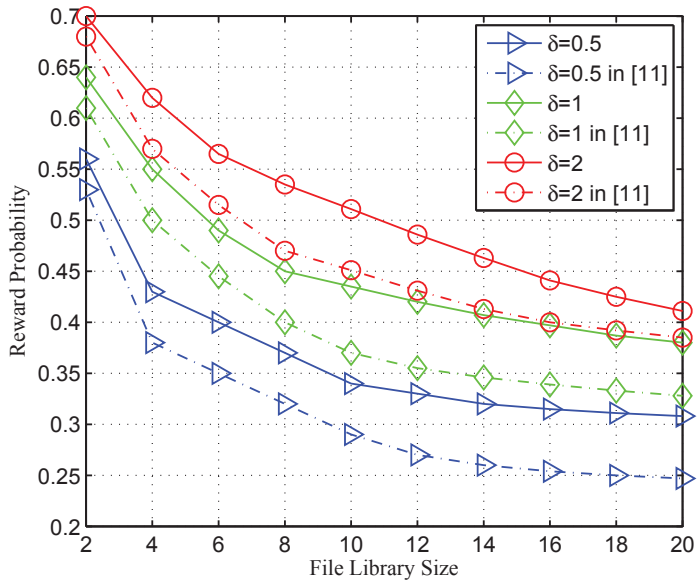

(b) The average reward probability of different resolution parameters δ

Figure 4.4: The performances of the proposed algorithm for different resolution parameters

proposed algorithm, although it takes more time to converge compared with [11] with the same δ, the reward probability is much better. Finally, it can be observed that the proposed algorithm strikes a fine balance between performance and complexity compared with the algorithm presented in [11]. This is because the proposed algorithm requires fewer iterations than the algorithm in [11] to achieve a similar reward probability performance. For example, the proposed algorithm only needs about 92 iterations to converge while the algorithm in [11] needs about 124 iterations to get a similar reward probability when there are totally 20 files.

4.4.4 Delay Performance of the Socially Aware Distributed Caching Algorithm

In this subsection, I first investigate the parameters in the environment feedback. Different combinations of the proportions of the request probability (p^f), the physical influence (x), and the social influence of (s) will lead to diverse optimized caching content.

As shown in the Fig. 4.5, different environment feedbacks are considered when the density of IU is 10^{-2} users/m^2. In this network scenario, the average transmission probability is around 0.56. I consider 3 cases in this figure: Case 1 gives the equal weights to all three components, while the physical influence is not considered in Case 2 and the social influence is not considered in Case 3.

I can see from Fig. 4.5 that the proposed algorithm can reduce the downloading delay when it allocates more weights on the physical influence, as shown by the comparison between Case 2 and Case 3. Moreover, with the increasing value of ω, the gap between these two cases is enlarged. This is because the physical influence shows a more important effect when I set a larger value of ω. In more detail, users tend

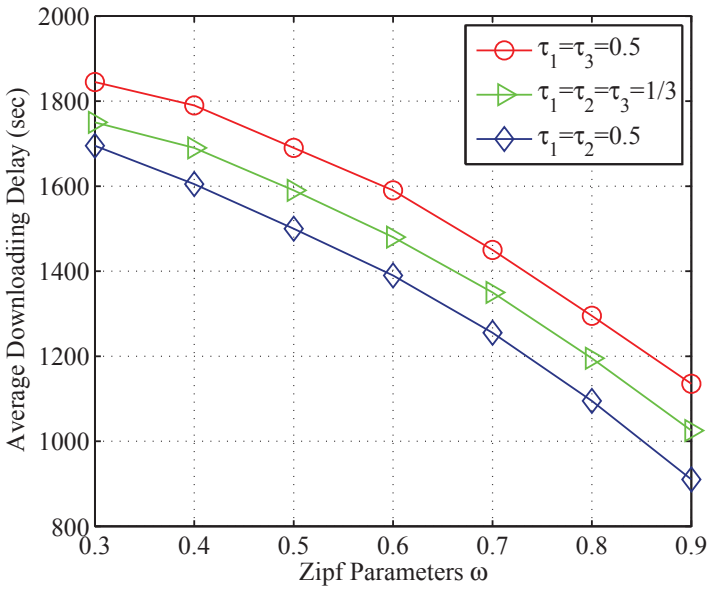

Figure 4.5: Average downloading delay D vs. the Zipf parameter ω under different environment feedbacks

to download the same files when I set a lager value of ω, then the delay among IUs and users mainly depends on the physical distance. So if I allocate more weights on the physical influence, the learning results will show a better downloading performance.

In the following, I study the delay performance of the socially aware distributed caching algorithm. The proposed algorithm is compared with the work in [11]. The DC scheme in the physically distance-dependent social model is used as the benchmark. Same with the previous subsection, I assume a file size of $L = 10^9$ bits, a IU which at least has 5 neighbors ($k = 5$), and equal environment feedback composition. In the process of sorting IUs, I collect each IU's social importance and available storage capacity, and treat them in descending order according to the importance list. As a result, the density of IU is around 10^{-2} users/m^2 and each IU can store 3 files at last. Fig. 4.6 shows the simulation results of the delay performance. From this

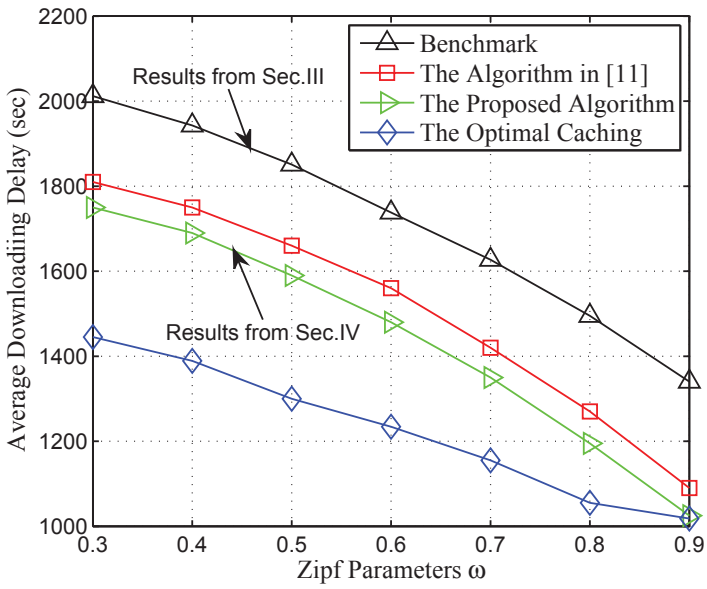

Figure 4.6: Average downloading delay D vs. the Zipf parameter ω under various caching schemes

figure, I can see that the average delay decreases as the value of ω increases, and the benchmark (i.e., DC scheme applied in the physically distance-dependent social model) shows the worst performance. This figure also demonstrates that the analytical results can qualitatively predict and assess the performance. However, using more advanced algorithms can achieve a better performance in the practical 5G settings. In addition, the proposed algorithm always performs better than the algorithm in [11]. For example, in comparison with the counterparts, the average delay of the proposed algorithm is reduced by 7.8%. Furthermore, the performance improvement between the proposed algorithm and the algorithm in [11] is obvious. This is because in [11] no mutual impact is considered, thus, nearby IUs may cache similar contents, and cannot provide downloading service for other popular contents. In contrast, the proposed algorithm encourages the IUs to cache different contents in order to achieve

caching diversity.

Moreover, I provide an average downloading delay performance using the optimal caching (OC) scheme in Fig. 4.6. The OC scheme is obtained by the non-causal algorithm [98], in which I remove the limit on the storage of each IU so that IUs have the knowledge of the entire network. From the figure, I can find that the gap between the proposed algorithm and the OC scheme is relatively large when ω is small, but it becomes small as ω increases. This is because the proposed algorithm considers a more practical situation than OC. In the OC scheme, it only sets the downloading delay as an optimization target regardless of other practical factors, such as the social relationship among users. In the proposed algorithm, a complex environment feedback consisting of multiple factors is incorporated, which not only considers the average delay performance, but also considers the feasibility in a practical situation. For example, when ω is small, the popular files are sparse and the proposed algorithm cannot satisfy all the demands. With the decreasing number of popular files, such as a large ω, the outcome of the proposed algorithm will gradually satisfy the demands. To make a fair comparison between these two schemes, I also record the average number of files cached in each IU for OC in Table 4.3, whereas the IUs can only cache 3 files in the proposed algorithm. In this sense, the proposed algorithm can achieve a performance close to that of OC, while economizing the storage space. For example, compared with the optimal caching scheme, the proposed algorithm has a similar delay (1025s v.s. 1018s), but requires less caching storage (3 v.s. 4.1) when $\omega = 0.9$.

Table 4.3: The average number of files cached in each IU

ω	0.3	0.4	0.5	0.6	0.7	0.8	0.9	average
OC	6.7	6.2	5.6	4.8	4.5	4.2	4.1	5.08

4.5 Summary

In this chapter, I conducted performance analysis using stochastic geometry to have a basic understanding of the average network performance under varying numbers and locations of the users. Specifically, I adopted a social relationship model considering the physical distance between users, and developed an analytical result of downloading delay. To achieve a better performance under practical 5G settings, I developed a distributed and socially aware framework based on a learning automaton to solve the optimum cache placement problem in D2D overlaying networks. Specifically, in order to promote content dissemination in D2D communications, I updated the algorithm with the aggregate environment feedback including the social relationship between users. Also the mutual user impacts were considered in this scheme to enable its application in the large-scale networks. The average performance obtained by stochastic geometry analysis agreed well with the simulations results. Furthermore, the proposed algorithm has a fast convergence speed and can achieve significant system throughput gains when compared with the existing caching strategies.

Chapter 5

Performance Analysis for Practical Unmanned Aerial Vehicle Networks with LoS/NLoS Transmissions

In this chapter, a performance analysis for practical unmanned aerial vehicle (UAV)-enabled networks is provided. By considering both line-of-sight (LoS) and non-line-of-sight (NLoS) transmissions between aerial base stations (BSs) and ground users, the coverage probability and the area spectral efficiency (ASE) are derived. Considering that there is no consensus on the path loss model for studying UAVs in the literature, in this chapter, three path loss models, i.e., high-altitude model, low-altitude model, and ultra-low-altitude model, are investigated and compared. From the analytical and simulation results for a practical UAV height of 50 meters, the network performances of the high-altitude model and the low-altitude model exhibit similar trends, while that of the ultra-low-altitude model deviates significantly from the above two models. In addition, the optimal density of UAVs to maximize the coverage probability performance is also investigated.

5.1 System Model

A UAV network, where UAV aerial base stations follow a 3D-PPP distribution with a density λ in an infinite 3D space $\mathbb{V}$ and the UAV height is set to h, that is $\mathbb{V} = \{(x, y, z) : x, y \in \mathbb{R}, z = h\}$, is considered. Here, I consider practical values for h around 50∼100 meters. Such a medium-altitude deployment of UAVs is because UAVs should not fly too high (e.g., higher than 100 meters) due to the recently discovered network capacity crash [27], and UAVs should not fly too low (e.g., lower than 10 meters) due to obvious safety reasons. User equipments (UEs) are Poisson distributed in the considered network with a density of λ_{UE}. Here, λ_{UE} is assumed to be sufficiently larger than λ so that each UAV has at least one associated UE in its coverage area. The 3D distance between an arbitrary UAV and an arbitrary UE is denoted by r in km.

Considering practical LoS and NLoS transmissions, I propose to model the path loss associated with distance r as a path loss function $\zeta(r)$. Such $\zeta(r)$ is segmented into 2 pieces, where $\zeta^{\mathrm{L}}(r)$ is the path loss function for LoS transmission, $\zeta^{\mathrm{NL}}(r)$ is the path loss function for NLoS transmission, and $\mathrm{Pr}^{\mathrm{L}}(r)$ is the LoS probability function. In more detail,

- $\zeta(r)$ is modeled as
$$\zeta(r) = \begin{cases} \zeta^{\mathrm{L}}(r) = A^{\mathrm{L}} r^{-\alpha^{\mathrm{L}}}, & \text{for LoS} \\ \zeta^{\mathrm{NL}}(r) = A^{\mathrm{NL}} r^{-\alpha^{\mathrm{NL}}}, & \text{for NLoS} \end{cases}, \tag{5.1.1}$$
with A^{L} and A^{NL} being the path losses at a reference distance $r = 1$, and α^{L} and α^{NL} being the path loss exponents for the LoS and the NLoS cases in $\zeta(r)$, respectively. In practice, A^{L}, A^{NL}, α^{L}, and α^{NL} are constants obtained from field tests [52].

- $\Pr^{\mathrm{L}}(r)$ is the probability function that a transmitter and a receiver have LoS connections. Also, the probability of NLoS is $\Pr^{\mathrm{NL}}(r) = 1 - \Pr^{\mathrm{L}}(r)$.

As a common practice in the field, each UE is assumed to be associated with the UAV that provides the strongest signal strength, and the multi-path fading between an arbitrary UAV-BS and an arbitrary UE is modeled as independently identical distributed (i.i.d.) Rayleigh fading. Thus, the channel gain denoted by g can be modeled as an i.i.d. exponential random variable (RV). The transmit power of each UAV and the additive white Gaussian noise (AWGN) power at each UE are denoted by P and σ^2, respectively.

5.2 Discussion and Analysis of path loss models

Because there is no consensus on proper path loss model for UAV-enabled networks, I choose three widely adopted path loss models and apply them to the considered UAV networks.

5.2.1 High-altitude model

The high-altitude model based on the elevation angle has been widely used in the satellite communication model, e.g., thousands of meters. The probability function that a transmitter and a receiver have a LoS connection at an elevation angle of θ can be expressed as $\Pr^{\mathrm{L}}(\theta)$ [69]:

$$\Pr^{\mathrm{L}}(\theta) = \frac{1}{1 + C\exp\left(-B[\theta - C]\right)}, \tag{5.2.1}$$

where B and C are constant values that depend on the environment (rural, urban, dense urban, etc.). Furthermore, the elevation angle θ can be written as $\theta = \frac{180}{\pi}\arcsin\left(\frac{h}{r}\right)$, so the LoS probability function for this high-altitude model can be reformulated as a

new function with respect to r:

$$\Pr_{\text{high}}^{\text{L}}(r) = \frac{1}{1 + C\exp\left(-B[\frac{180}{\pi}\arcsin\left(\frac{h}{r}\right) - C]\right)}. \tag{5.2.2}$$

5.2.2 Low-altitude model

Provided that the practical height of UAV-BSs is usually limited to a medium altitude, like 50m and 100m and such height is comparable to the antenna height of terrestrial base stations, I further analyze the path loss model proposed for 3GPP terrestrial communications and apply it to the considered UAV networks.

In particular, the 3GPP macrocell-to-UE path loss model has been proposed for connection between a UE and its associated macrocell BS. Considering that the height of a macrocell base station is usually around 32m, which is slightly lower than the considered altitude of UAV around 50∼100m, it is reasonable to use this model to study the UAV network. In this case, the LoS probability function for this low-altitude model can be expressed as [99]

$$\begin{aligned}\Pr_{\text{low}}^{\text{L}}(r) =& \min\left(0.018/r, 1\right) \times \left(1 - \exp\left(-r/0.063\right)\right) \\ &+ \exp\left(-r/0.063\right).\end{aligned} \tag{5.2.3}$$

5.2.3 Ultra-low-altitude model

To obtain a comprehensive insight of the proper path loss model for UAVs, I also introduce the 3GPP picocell-to-UE model as the ultra-low-altitude model, because the typical height of a picocell base station is about 10m. In this case, the LoS probability function is defined as [99]

$$\begin{aligned}\Pr_{\text{ultra}}^{\text{L}}(r) =& 0.5 - \min\left(0.5, 5\exp\left(-0.156/r\right)\right) \\ &+ \min\left(0.5, 5\exp\left(-r/0.03\right)\right).\end{aligned} \tag{5.2.4}$$

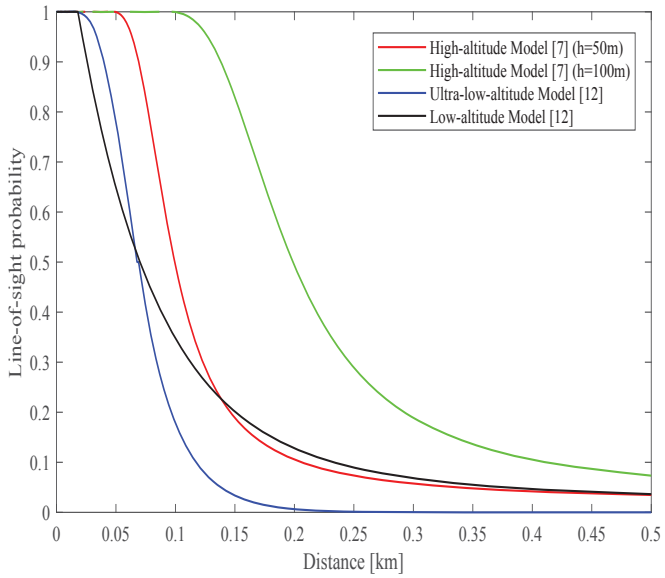

Figure 5.1: Comparison of LoS probability function

5.2.4 The Comparison of the Three Path Loss Models

Fig. 5.1 compares the LoS probability functions for different path loss models. It can be seen from this figure that the LoS probability for the ultra-low-altitude model drops very quickly with respect to the distance, followed by the low-altitude model. Moreover, it should be noted that the high-altitude model generates different LoS probability functions for different altitudes.

5.3 Analysis for the Proposed UAV Networks

To analyze the performance of UAV-BSs based on the interested path loss models, I investigate the coverage probability and the ASE of the network in this section. The coverage probability represents the probability that the typical user is covered

by the associated UAV-BS and is defined as the probability that the received signal-to-interference-noise-ratio (SINR) is larger than a pre-set threshold γ, which can be expressed as

$$p^{cov} = \Pr(\text{SINR} > \gamma), \tag{5.3.1}$$

where SINR is expressed as

$$\text{SINR} = \frac{Pg\zeta(r)}{I_r + N_0}, \tag{5.3.2}$$

where P and N_0 denote the transmission power of the UAV-BS and the AWGN power, respectively. Moreover, I_r is the sum of interference from other UAV-BSs, and g is the channel gain of Rayleigh fading and can be modeled as a RV which follows an exponential distribution with the mean value of one. It can be further written as

$$I_r = \sum_{i:b_i \in \Phi \setminus b_o} P\beta_i g_i. \tag{5.3.3}$$

Obviously, when UAV-BSs are HPPP distributed and randomly hovering in the network, the network performance reaches a lower bound because the mobility of UAVs is completed ignored. Such lower-bound performance is characterized in the following Theorem 5.3.1.

Theorem 5.3.1. *Considering the path loss of the LoS and the NLoS connections, the lower bound of the coverage probability $p^{cov}(\lambda, \gamma)$ can be expressed as*

$$p^{cov}_{lower}(\lambda, \gamma) = T^{\mathrm{L}} + T^{\mathrm{NL}}, \tag{5.3.4}$$

where $T^L = \int_h^\infty \Pr\left[\frac{P\zeta^L(r)g}{I_r+N_0} > \gamma\right] f^L(r)dr$ and $T^{NL} = \int_h^\infty \Pr\left[\frac{P\zeta^{NL}(r)g}{I_r+N_0} > \gamma\right] f^{NL}(r)dr$. The $f^{\mathrm{L}}(r)$ and $f^{\mathrm{NL}}(r)$ are expressed as

$$\begin{aligned} f^{\mathrm{L}}(r) = &\exp\left(-\int_h^{r_1} \left(1 - \Pr^{\mathrm{L}}(u)\right) 2\pi u\lambda du\right) \\ &\times \exp\left(-\int_h^{r} \Pr^{\mathrm{L}}(u)\, 2\pi u\lambda du\right) \times \Pr^{\mathrm{L}}(r) \times 2\pi r\lambda, \end{aligned} \tag{5.3.5}$$

and

$$f^{\mathrm{NL}}(r) = \exp\left(-\int_h^{r_2} \Pr^{\mathrm{L}}(u)\, 2\pi u\lambda du\right) \times \exp\left(-\int_h^{r} \left(1-\Pr^{\mathrm{L}}(u)\right) 2\pi u\lambda du\right) \times \left(1-\Pr^{\mathrm{L}}(r)\right) \times 2\pi r\lambda, \tag{5.3.6}$$

where r_1 and r_2 are the solutions of $\zeta^{\mathrm{NL}}(r_1) = \zeta^{\mathrm{L}}(r)$ and $\zeta^{\mathrm{L}}(r_2) = \zeta^{\mathrm{NL}}(r)$, respectively. Moreover, $\Pr\left[\frac{P\zeta^{\mathrm{L}}(r)g}{I_r+N_0} > \gamma\right]$ *and* $\Pr\left[\frac{P\zeta^{\mathrm{NL}}(r)g}{I_r+N_0} > \gamma\right]$ *are expressed by*

$$\Pr\left[\frac{P\zeta^{\mathrm{L}}(r)g}{I_r+N_0} > \gamma\right] = \exp\left(-\frac{\gamma N_0}{P\zeta^{\mathrm{L}}(r)}\right)\mathcal{L}_{I_r}\left(\frac{\gamma}{P\zeta^{\mathrm{L}}(r)}\right), \tag{5.3.7}$$

and

$$\Pr\left[\frac{P\zeta^{\mathrm{NL}}(r)g}{I_r+N_0} > \gamma\right] = \exp\left(-\frac{\gamma N_0}{P\zeta^{\mathrm{NL}}(r)}\right)\mathcal{L}_{I_r}\left(\frac{\gamma}{P\zeta^{\mathrm{NL}}(r)}\right), \tag{5.3.8}$$

where $\mathcal{L}_{I_r}$ is the Laplace transform of I_r in the computation of interference.

Proof. See Appendix C.1. □

In Theorem 5.3.1, I assume that UAVs are randomly hovering in the network. On the other hand, if the mobility of UAVs is considered, the system performance can surely be improved. However, the analysis of such mobile UAVs is difficult because I need to further consider UAV mobility control management. Fortunately, I can instead consider a UAV teleportation model, where UAVs can instantaneously move to the positions directly overhead the users to show the upper-bound performance of a UAV network. In this case, each user will be associated with its UAV-BS overhead. Such upper-bound performance is characterized in the following lemma, which is derived from Theorem 5.3.1.

Lemma 5.3.1. *The coverage probability of teleporting UAVs can be expressed as*

$$\begin{aligned} p_{upper}^{cov}(\lambda,\gamma) &= \Pr\left[\frac{P\zeta^{L}(h)g}{I_r+N_0} > \gamma\right] + \Pr\left[\frac{P\zeta^{NL}(h)g}{I_r+N_0} > \gamma\right] \\ &= \exp\left(-\frac{\gamma N_0}{P\zeta^{\mathrm{L}}(h)}\right)\mathcal{L}_{I_r}\left(\frac{\gamma}{P\zeta^{\mathrm{L}}(h)}\right) \\ &\quad + \exp\left(-\frac{\gamma N_0}{P\zeta^{\mathrm{NL}}(h)}\right)\mathcal{L}_{I_r}\left(\frac{\gamma}{P\zeta^{\mathrm{NL}}(h)}\right). \end{aligned} \tag{5.3.9}$$

In this case, the associated UAV is set at the positions overhead the users, so the space distance from users to their associated UAVs is h rather than r. In comparison with the case of HPPP distributed UAVs, the case of teleporting UAVs can provide the user with the strongest received signal power due to the minimized distance between them and the highest probability of having a LoS connection. As a result, this teleporting model gives the upper bound of network performance.

According to [100], the ASE can be expressed as

$$\begin{aligned} A^{\mathrm{ASE}}(\lambda, \gamma_0) = & \frac{\lambda}{\ln 2} \int_{\gamma_0}^{+\infty} \frac{p^{\mathrm{cov}}(\lambda, \gamma)}{1+\gamma} d\gamma \\ & + \lambda \log_2 (1+\gamma_0)\, p^{\mathrm{cov}}(\lambda, \gamma_0), \end{aligned} \tag{5.3.10}$$

where γ_0 is the minimum SINR threshold for UE to work normally.

5.4 Simulation Results

To find the appropriate path loss model when UAVs fly at a medium altitude, I use simulation results to demonstrate the coverage probability and the ASE of three LoS probability models and make a comparison. Parameters adopted in simulation are: $P = 24$ dBm, $N_0 = -95$ dBm [99], $\gamma_0 = 0$ dB, $C = 11.95$, $B = 0.136$ [69]. To obtain the numerical results at the medium height, I choose to analyze UAVs at the height of 50m and 100m, which are the most practical cases in reality. For the high-altitude model, the relative parameters are: $A^{\mathrm{L}} = 10.38$, $A^{\mathrm{NL}} = 14.54$, $\alpha^{\mathrm{L}} = 2.09$, $\alpha^{\mathrm{NL}} = 3.75$ [25] [101]. For the low-altitude model, path loss parameters are: $A^{\mathrm{L}} = 10.34$, $A^{\mathrm{NL}} = 13.11$, $\alpha^{\mathrm{L}} = 2.42$, $\alpha^{\mathrm{NL}} = 4.28$ [99]. For the ultra-low-altitude model, path loss parameters are: $A^{\mathrm{L}} = 10.38$, $A^{\mathrm{NL}} = 14.54$, $\alpha^{\mathrm{L}} = 2.09$, $\alpha^{\mathrm{NL}} = 3.75$ [99].

Table 5.1: Simulation Parameters

Parameters	Value
P	24 dBm [99]
N_0	-95 dBm [99]
γ_0	0 dB
C	11.95 [69]
B	0.136 [69]
h	50m, 100m
High-altitude model [101] and ultra-low-altitude model [99]	
A^{L}	10.38
A^{NL}	14.54
α^{L}	2.09
α^{NL}	3.75
Low-altitude model [99]	
A^{L}	10.34
A^{NL}	13.11
α^{L}	2.42
α^{NL}	4.28

5.4.1 The coverage probability for hovering UAVs

Fig. 5.2 and Fig. 5.3 show the comparison of the coverage probability for UAVs hovering at 50m and 100m based on the investigated three models of path loss, i.e., the high-altitude model, the low-altitude model, and the ultra-low-altitude model.

It can be seen from Fig. 5.2 that with the increase of the UAV density, the coverage probability of the high-altitude model first rises to the peak and then decreases. The optimal UAV density for this model is about 10 BSs/km^2. As for the low-altitude model, the performance trend is similar to that of the high-altitude one, with a slightly different optimal density around 6 BSs/km^2. The explanations of these phenomena are:

- For a sparse UAV-BSs density, the distance from associated UAV-BS to UE decreases with the increasing UAV-BS density and the associated UAV-BS is

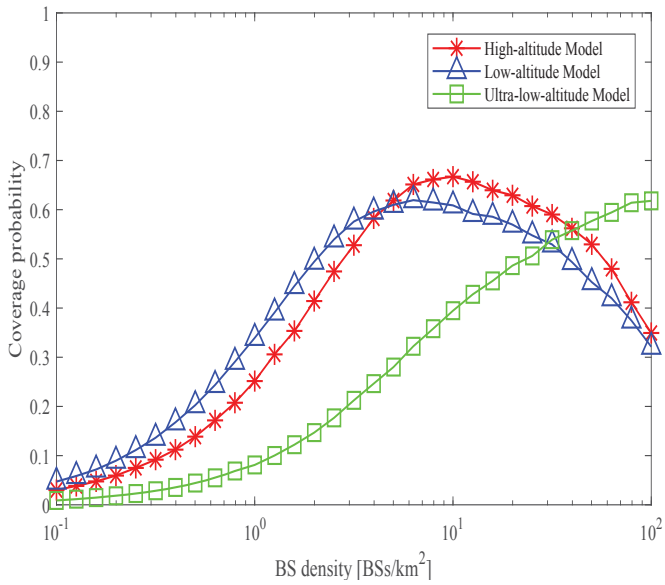

Figure 5.2: Comparison of the coverage probability for hovering UAVs (h=50m)

more likely to have a LoS transmission with UE, so the coverage probability grows as the UAV-BS density increases.

- For a dense UAV-BSs density, although the associated UAV has a higher probability to transmit data via a LoS channel, other UAVs also produce strong interference through LoS paths, thus, the coverage probability decreases after reaching the highest point.

For the ultra-low-altitude model, the performance is significantly different from the other two models. The reason is that the ultra-low-altitude model is designed for a scenario where UAVs fly at a relatively low altitude and the transmission distance is quite limited. Furthermore, even when the UAV is hovering over user's location, the probability of having a LoS connection is still low because the minimum distance from UAV-BS to UE is the height of UAV. As a result, the ultra-low-altitude model

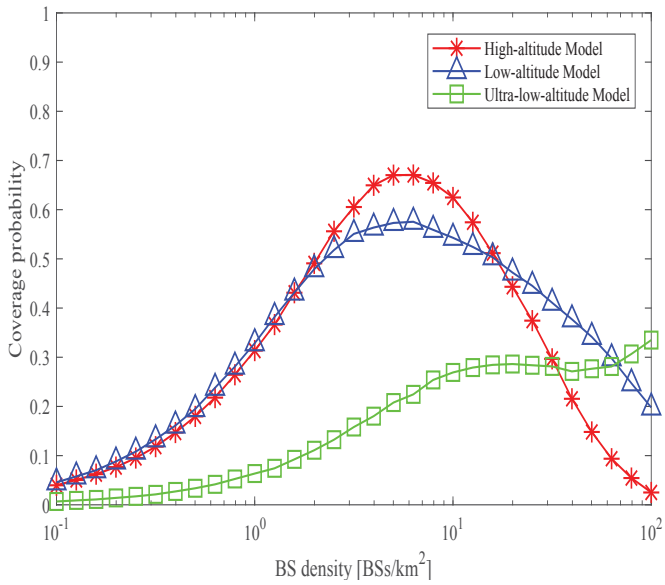

Figure 5.3: Comparison of the coverage probability for hovering UAVs (h=100m)

is not suitable for the practical UAV scenario with a height around 50∼100 meters.

In Fig. 5.3, I can see that the performance of the low-altitude model and high-altitude model is very similar when the UAV-BS density is less than 2 BSs/km^2. When the density is between 2 BSs/km^2 and 20 BSs/km^2, the coverage probability of the high-altitude model is higher than that of the low-altitude model, but the low-altitude model performs better than the high-altitude model when the density is beyond 20 BSs/km^2.

5.4.2 The ASE for hovering UAVs

Fig. 5.4 shows the ASE performance of different path loss models for a height of 50m. As can be seen from this figure, the ASE of the high-altitude model and the low-altitude model keeps growing due to the increasing coverage probability, but the growing rate slows down when the density of UAVs is more than 10 BSs/km^2. This

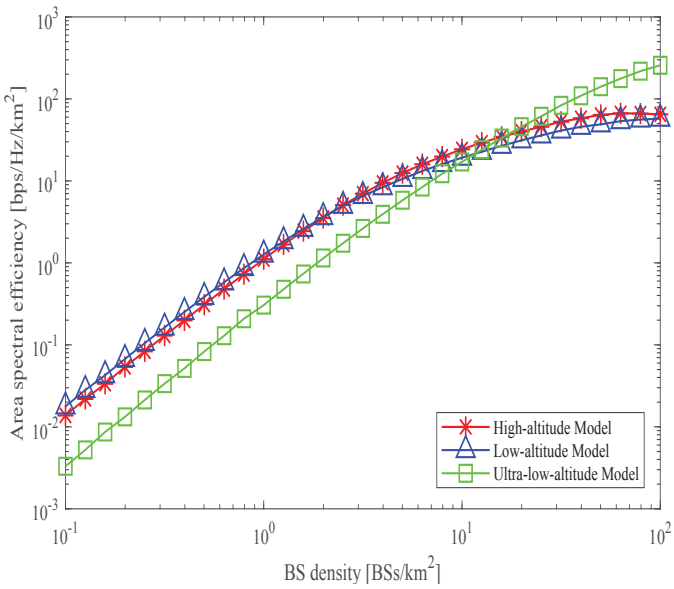

Figure 5.4: Comparison of the ASE for hovering UAVs (h=50m)

is because the declining coverage probability shown in Fig. 5.2 and Fig. 5.3 outweighs the increase of the UAV density. In Fig. 5.4 I can also find that the ASE for the ultra-low-altitude model differs from the other two. As a result, when the height of UAV is around 50m, the high-altitude model and the low-altitude model are equally good for the performance analysis of the UAV-based network. Fig. 5.5 shows the comparison of the ASE in different models when the height of UAV is 100m. When the UAV-BS density is lower than 20 BSs/km^2, the ASE of the high-altitude model and that of the low-altitude model leave the similar trail. However, after reaching the density of 10 BSs/km^2, their ASE performance diverges. The drop of the ASE for the high-altitude model indicates that the deceasing coverage dominates the ASE performance compared with the growing UAV density. Considering that the low-altitude model was developed for a height around 32 meters, it might not be suitable for the UAVs flying at 100 meters studied here. Hence, the high-altitude model might be more

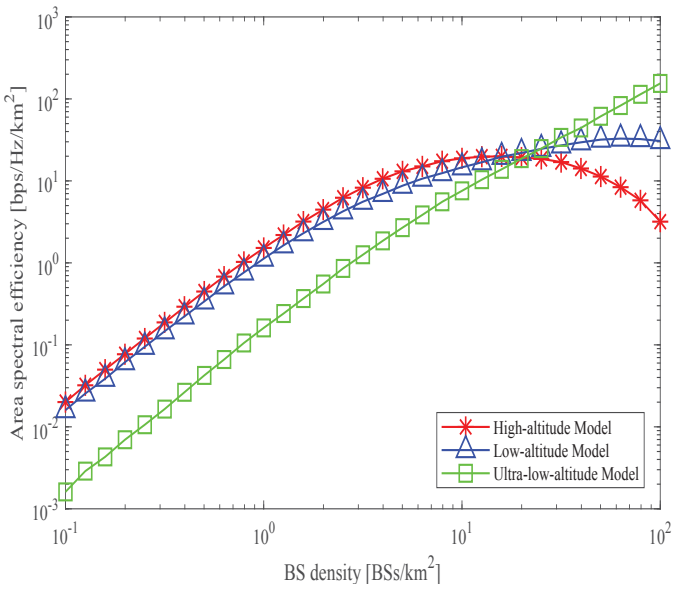

Figure 5.5: Comparison of the ASE for hovering UAVs (h=100m)

appropriate here. However, it may need to conduct real-life channel measurement to confirm this conjecture.

5.4.3 The performance for Teleporting UAVs

It can be seen from the previous simulation that when UAVs fly at the height of 50m, the coverage probability and the ASE performance of the high-altitude model and the low-altitude model are very similar. However, when the height of UAV is at 100m, the performance of these two models deviates in dense networks. To verify whether these two models are still equally good for teleporting UAVs at 50m, I investigate and compare their coverage probability and ASE performance in this subsection.

From Fig. 5.6 and Fig. 5.7, it can be seen that the high-altitude model and the low-altitude model generate similar results. In Fig. 5.6, It can be found that the optimal

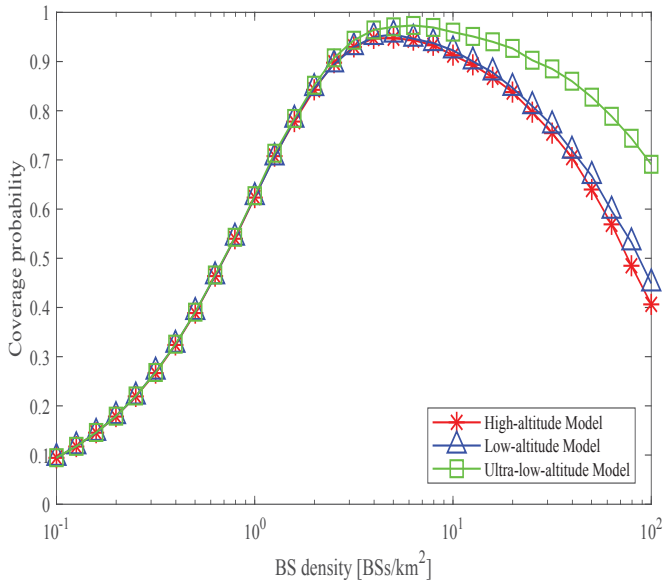

Figure 5.6: Comparison of the coverage probability for teleporting UAVs (h=50m)

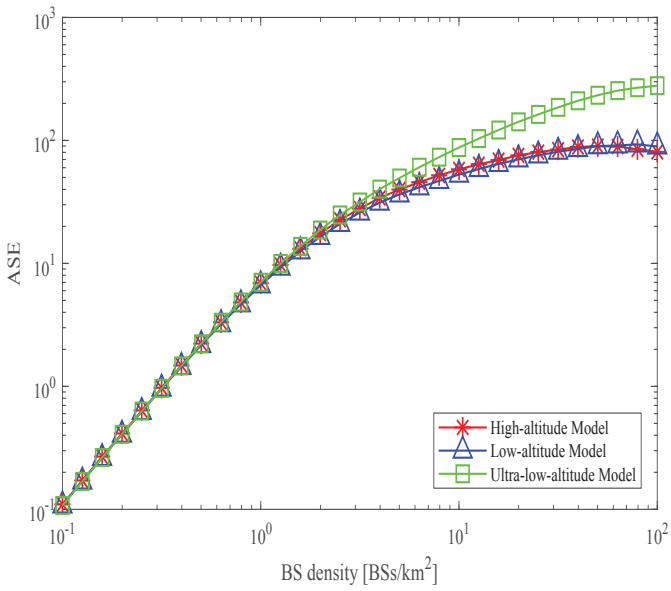

Figure 5.7: Comparison of the ASE for teleporting UAVs (h=50m)

UAV density for these two models can be found at around 6 BSs/km^2. Fig. 5.7 shows that the ASE of both models increases linearly at first, and then grows slowly.

5.4.4 Comparison of the Upper and Lower bounds of Performance

From Fig. 5.2 and Fig. 5.4, it can found that the high-altitude model and the low-altitude model are equally good for network performance analysis. Hence, I choose the high-altitude model to show the difference between the upper bound of ASE and the lower bound of ASE when the UAVs fly at the height of 50m. Such comparison is displayed in Fig. 5.8. It can be seen that when the density is lower than 10 BSs/km^2, the gap between the upper bound and the lower bound is large, which shows great promise for optimization of UAV mobility in UAV-enabled networks. However, as the UAV density increases, the ASE gain due to the UAV mobility becomes marginal, e.g., at a UAV density of 100 UAV-BSs/km^2.

5.5 Summary

In this chapter, I studied the performance of UAV-enabled wireless networks. In order to identify the proper path loss models for UAVs flying at practical heights, such as 50m and 100m, I first analyzed the performance when adopting the conventional high-altitude model based on the elevation angle. Then I further investigated the coverage probability and the ASE by using path loss models which have been widely applied to terrestrial communications, including the low-altitude model and the ultra-low-altitude model. From simulation results, it can be found that performance for networks with the high-altitude model and the low-altitude model are equally good

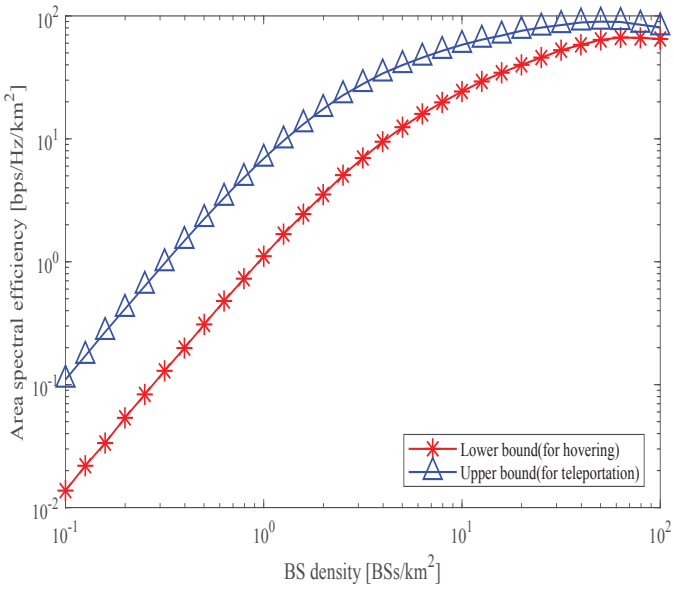

Figure 5.8: Upper bound and lower bound of the ASE for the high-altitude model when h=50m

when UAVs fly at the height of 50m, while the performance trend of the ultra-low-altitude model is quite different. I also found that the number of the UAVs should be optimized for the benefits of the networks, which sheds new light on the design of the future UAV-enabled networks.

Chapter 6

Conclusions and Future Works

This thesis focuses on the performance analysis and resource allocation in the 5G wireless network. Specifically, the performance of the dense HetNets, D2D caching, and UAV-enabled networks are investigated and discussed. In this chapter, I conclude the thesis by summarizing the contributions and listing some interesting directions for future work.

6.1 Conclusions

In Chapter 3, to consider a more practical system model, the impact of the IMC, caused by the finite number of UEs, was introduced in a dense two-tier HetNets. By applying the stochastic geometry, the performance of this network was studied with the LoS/NLoS transmission. Moreover, to address the under-utilization of SBSs, CRE and eICIC via ABSs were adopted in this work. The results show that the coverage probability and the ASE will continuously increase in the dense network, when the density of BS is larger than the UE one. Additional, it is important to note that more bandwidth or frequency resources should be allocated to the small cell BSs, which implies that the ultra-dense small cells should operate in a different frequency

spectrum from the macrocell ones.

In Chapter 4, to investigate the performance of the D2D caching networks, I conducted the analysis using stochastic geometry. Specifically, a social relationship model considering the physical distance between users was provided to develop the basic downloading performance. To achieve a better performance under practical 5G settings, I proposed a distributed and socially aware caching algorithm based on the reinforce learning to solve the optimum caching resources, i.e., contents, in D2D overlaying networks. Moreover, the mutual user impacts were considered to enable its application in the large scale networks. The analysis results provided a basic understanding of the D2D caching networks, and the proposed algorithm were proven to have a faster convergence speed than other conventional algorithms, and can achieve significant system throughput gains.

In Chapter 5, to understand the performance of the UAV-enabled networks in terms of the LoS/NLoS transmissions, I studied the analysis when the UAVs are flying at practical heights. Three path loss models are provided in this chapter, which depend on the altitudes on the UAVs. Moreover, I derived the analytical results for the upper and lower bound of the network performance, in which UAVs can instantaneously move to positions directly overhead ground users or hovering randomly. From the results it can be found that the performance for high and low altitudes are equally good when the height of UAVs is around 50m, while the performance of the ultra-low-altitude model is relatively different. Moreover, the number of the UAVs should also be optimized in the network to achieve a better performance, which sheds new light on the design of future UAV-enabled networks.

6.2 Future Work

In this section, several interesting research directions are listed.

- With the dense and dense deployment of SBSs available in 5G HetNets, it is interesting and challenging to conduct a more practical system analysis. Compared with the current analysis works, the impact of the shadow fading lacks in most of the system models, which will be a key issue in the ultra-dense networks. This new direction can bring a deeper understanding of 5G dense networks.

- The D2D caching analysis in Chapter 4 considers Zipf-based file popularity. Compared with this basic file popularity model, the time-varying file popularity may bring a brand new view. Besides, by analysing the big data, the content popularity may be estimated by the machine learning algorithm, which can provide an accurate file popularity model. These topics can shed new light on the design of the future caching networks.

- With the development of the UAV-enabled networks, the mobility control of these UAVs are increasingly important. As of the analysis in Chapter 5, it is not that useful in improving the system performance if the number of UAVs keeps increasing. So, how to design the optimal positions and the movement track for the UAV-enabled network is a very challenging issue. In addition, in the 3GPP study, the accurate path loss model of UAV uplink channel has been proposed, and some relevant research can be conducted.

Appendix A

Proofs of Chapter 3

A.1 Proof of Lemma 3.2.1

In this proof I first derive the conditions that the UE is associated with a LoS MBS, which the LoS MBS provides stronger power than other BSs.

- UE is associated with a LoS MBS with no NLoS MBS inside:

$$\begin{aligned} p_{11}^{\mathrm{L}}(r) &= \Pr\left(P_1 \times A_1^{\mathrm{L}} r^{-\alpha_1^{\mathrm{L}}} > P_1 \times A_1^{\mathrm{NL}} r_1^{-\alpha_1^{\mathrm{NL}}}\right) \\ &= \Pr\left(r_1 > \left(\frac{A_1^{\mathrm{NL}}}{A_1^{\mathrm{L}}}\right)^{\frac{1}{\alpha_1^{\mathrm{NL}}}} \times r^{\frac{\alpha_1^{\mathrm{L}}}{\alpha_1^{\mathrm{NL}}}}\right) \\ &\overset{(a)}{=} \Pr(\text{No NLoS MBS closer than } \Delta_{11}^{\mathrm{L}}) \\ &= \exp\left(-\int_0^{\Delta_{11}^{\mathrm{L}}(r)} (1 - \Pr_1^{\mathrm{L}}(u)) \times 2\pi u \lambda_1 du\right), \end{aligned} \tag{A.1.1}$$

where step (a) is given by $\Delta_{11}^{\mathrm{L}}(r) = (\frac{A_1^{\mathrm{NL}}}{A_1^{\mathrm{L}}})^{\frac{1}{\alpha_1^{\mathrm{NL}}}} \times r^{\frac{\alpha_1^{\mathrm{L}}}{\alpha_1^{\mathrm{NL}}}}$.

- UE is associated with a LoS MBS with no LoS SBS inside:

$$\begin{aligned} p_{12}^{\mathrm{L}}(r) &= \Pr\left(P_1 \times A_1^{\mathrm{L}} r^{-\alpha_1^{\mathrm{L}}} > P_2 \times A_2^{\mathrm{L}} r_2^{-\alpha_2^{\mathrm{L}}} \times D\right) \\ &= \Pr\left(r_2 > \left(\frac{A_2^{\mathrm{L}}}{A_1^{\mathrm{L}}}\right)^{\frac{1}{\alpha_2^{\mathrm{L}}}} \times D^{\frac{1}{\alpha_2^{\mathrm{L}}}} \times \left(\frac{P_2}{P_1}\right)^{\frac{1}{\alpha_2^{\mathrm{L}}}} \times r^{\frac{\alpha_1^{\mathrm{L}}}{\alpha_2^{\mathrm{L}}}}\right) \\ &\overset{(b)}{=} \Pr(\text{No LoS SBS closer than } \Delta_{12}^{\mathrm{L}}) \\ &= \exp\left(-\int_0^{\Delta_{12}^{\mathrm{L}}(r)} \mathrm{Pr}_2^{\mathrm{L}}(u) \times 2\pi u \lambda_2 du\right), \end{aligned} \tag{A.1.2}$$

where step (b) is given by $\Delta_{12}^{\mathrm{L}}(r) = \left(\frac{A_2^{\mathrm{L}}}{A_1^{\mathrm{L}}}\right)^{\frac{1}{\alpha_2^{\mathrm{L}}}} \times D^{\frac{1}{\alpha_2^{\mathrm{L}}}} \times \left(\frac{P_2}{P_1}\right)^{\frac{1}{\alpha_2^{\mathrm{L}}}} \times r^{\frac{\alpha_1^{\mathrm{L}}}{\alpha_2^{\mathrm{L}}}}$.

- UE is associated with a LoS MBS with no NLoS SBS inside:

$$\begin{aligned} p_{13}^{\mathrm{L}}(r) &= \Pr\left(P_1 \times A_1^{\mathrm{L}} r^{-\alpha_1^{\mathrm{L}}} > P_2 \times A_2^{\mathrm{NL}} r_2^{-\alpha_2^{\mathrm{NL}}} \times D\right) \\ &= \Pr\left(r_2 > \left(\frac{A_2^{\mathrm{NL}}}{A_1^{\mathrm{L}}}\right)^{\frac{1}{\alpha_2^{\mathrm{NL}}}} \times D^{\frac{1}{\alpha_2^{\mathrm{NL}}}} \times \left(\frac{P_2}{P_1}\right)^{\frac{1}{\alpha_2^{\mathrm{NL}}}} \times r^{\frac{\alpha_1^{\mathrm{L}}}{\alpha_2^{\mathrm{NL}}}}\right) \\ &\overset{(c)}{=} \Pr(\text{No NLoS SBS closer than } \Delta_{13}^{\mathrm{L}}) \\ &= \exp\left(-\int_0^{\Delta_{13}^{\mathrm{L}}(r)} \left(1 - \mathrm{Pr}_2^{\mathrm{L}}(u)\right) \times 2\pi u \lambda_2 du\right), \end{aligned} \tag{A.1.3}$$

where step (c) is given by $\Delta_{13}^{\mathrm{L}}(r) = \left(\frac{A_2^{\mathrm{NL}}}{A_1^{\mathrm{L}}}\right)^{\frac{1}{\alpha_2^{\mathrm{NL}}}} \times D^{\frac{1}{\alpha_2^{\mathrm{NL}}}} \times \left(\frac{P_2}{P_1}\right)^{\frac{1}{\alpha_2^{\mathrm{NL}}}} \times r^{\frac{\alpha_1^{\mathrm{L}}}{\alpha_2^{\mathrm{NL}}}}$.

According to [5], the CCDF of r (the distance that the nearest BS with a LoS path to the UE) is written as $\bar{F}_R^{\mathrm{L}}(r) = \exp(-\int_0^r \mathrm{Pr}^{\mathrm{L}}(u) 2\pi u \lambda du)$. Taking the derivative of (1-$\bar{F}_R^{\mathrm{L}}(r)$) with regard to r, I can get the PDF of r as:

$$f_1^{\mathrm{L}}(r) = \exp\left\{-\int_0^r \mathrm{Pr}_1^{\mathrm{L}}(u) 2\pi \lambda_1 u du\right\} \times \mathrm{Pr}_1^{\mathrm{L}}(r) 2\pi \lambda_1 r. \tag{A.1.4}$$

So the probability that the UE is associated with a LoS MBS can be written as

$$\mathbb{P}_1^{\mathrm{L}} = \int_0^{\infty} p_{11}^{\mathrm{L}}(r) \times p_{12}^{\mathrm{L}}(r) \times p_{13}^{\mathrm{L}}(r) \times f_1^{\mathrm{L}}(r) dr. \tag{A.1.5}$$

A.2 Proof of Lemma 3.2.2

Following the same logic as Lemma 1, the conditions that the UE is associated with a MBS with the NLoS path can be derived as:

- UE is associated with a NLoS MBS with no LoS MBS inside:

$$p_{11}^{\mathrm{NL}}(r) = \exp\left(-\int_0^{\Delta_{11}^{\mathrm{NL}}(r)} \mathrm{Pr}_1^{\mathrm{L}}(u) \times 2\pi u \lambda_1 du\right), \tag{A.2.1}$$

  where $\Delta_{11}^{\mathrm{NL}}(r) = (\frac{A_1^{\mathrm{L}}}{A_1^{\mathrm{NL}}})^{\frac{1}{\alpha_1^{\mathrm{L}}}} \times r^{\frac{\alpha_1^{\mathrm{NL}}}{\alpha_1^{\mathrm{L}}}}$.

- UE is associated with a NLoS MBS with no LoS SBS inside:

$$p_{12}^{\mathrm{NL}}(r) = \exp\left(-\int_0^{\Delta_{12}^{\mathrm{NL}}(r)} \mathrm{Pr}_2^{\mathrm{L}}(u) \times 2\pi u \lambda_2 du\right), \tag{A.2.2}$$

  where $\Delta_{12}^{\mathrm{NL}}(r) = \left(\frac{A_2^{\mathrm{L}}}{A_1^{\mathrm{NL}}}\right)^{\frac{1}{\alpha_2^{\mathrm{L}}}} \times D^{\frac{1}{\alpha_2^{\mathrm{L}}}} \times \left(\frac{P_2}{P_1}\right)^{\frac{1}{\alpha_2^{\mathrm{L}}}} \times r^{\frac{\alpha_1^{\mathrm{NL}}}{\alpha_2^{\mathrm{L}}}}$.

- UE is associated with a NLoS MBS with no NLoS SBS inside:

$$p_{13}^{\mathrm{NL}}(r) = \exp\left(-\int_0^{\Delta_{13}^{\mathrm{NL}}(r)} \left(1 - \mathrm{Pr}_2^{\mathrm{NL}}(u)\right) \times 2\pi u \lambda_2 du\right), \tag{A.2.3}$$

  where $\Delta_{13}^{\mathrm{NL}}(r) = \left(\frac{A_2^{\mathrm{NL}}}{A_1^{\mathrm{NL}}}\right)^{\frac{1}{\alpha_2^{\mathrm{NL}}}} \times D^{\frac{1}{\alpha_2^{\mathrm{NL}}}} \times \left(\frac{P_2}{P_1}\right)^{\frac{1}{\alpha_2^{\mathrm{NL}}}} \times r^{\frac{\alpha_1^{\mathrm{NL}}}{\alpha_2^{\mathrm{NL}}}}$.

So the probability that the UE is associated with a NLoS MBS can be written as

$$\mathbb{P}_1^{\mathrm{NL}} = \int_0^{\infty} p_{11}^{\mathrm{NL}}(r) \times p_{12}^{\mathrm{NL}}(r) \times p_{13}^{\mathrm{NL}}(r) \times f_1^{\mathrm{NL}}(r) dr, \tag{A.2.4}$$

where $f_1^{\mathrm{NL}}(r)$ is the PDF that the UE is associated with the NLoS MBS and can be written as

$$\begin{aligned} f_1^{\mathrm{NL}}(r) = &\exp\left\{-\int_0^{r} \left(1 - \mathrm{Pr}_1^{\mathrm{L}}(u)\right) 2\pi\lambda_1 u du\right\} \\ &\times \left(1 - \mathrm{Pr}_1^{\mathrm{L}}(r)\right) 2\pi\lambda_1 r. \end{aligned} \tag{A.2.5}$$

A.3 Proof of Theorem 3.3.1

In this proof I first analyze the case that $u \in \{\mathcal{U}_1, \mathcal{U}_2\}$, where the derivation process follows the same approach. I first derive the distribution of the distance between the typical user u and the tagged BS. Let X_l denote this distance, then

$$\mathbb{P}(X_l > x) = \mathbb{P}(X_l > x | u \in \mathcal{U}_l) = \frac{\Pr(X_l > x | u \in \mathcal{U}_l)}{\Pr(u \in \mathcal{U}_l)}. \tag{A.3.1}$$

Based on Sec. II-B and [77], the corresponding PDFs are

$$\begin{aligned}
\mathcal{F}_1^{\mathrm{L}}(x) &= p_{11}^{\mathrm{L}}(x) \times p_{12}^{\mathrm{L}}(x) \times p_{13}^{\mathrm{L}}(x) \times f_1^{\mathrm{L}}(x);\\
\mathcal{F}_1^{\mathrm{NL}}(x) &= p_{11}^{\mathrm{NL}}(x) \times p_{12}^{\mathrm{NL}}(x) \times p_{13}^{\mathrm{NL}}(x) \times f_1^{\mathrm{NL}}(x);\\
\mathcal{F}_2^{\mathrm{L}}(x) &= p_{21}^{\mathrm{L'}}(x) \times p_{22}^{\mathrm{L'}}(x) \times p_{23}^{\mathrm{L}}(x) \times f_2^{\mathrm{L}}(x);\\
\mathcal{F}_2^{\mathrm{NL}}(x) &= p_{21}^{\mathrm{NL'}}(x) \times p_{22}^{\mathrm{NL'}}(x) \times p_{23}^{\mathrm{NL}}(x) \times f_2^{\mathrm{NL}}(x),
\end{aligned} \tag{A.3.2}$$

where

$$\begin{cases}
p_{21}^{\mathrm{L'}}(x) = \exp(-\int_0^{\Delta_{21}^{\mathrm{L'}}(x)} \Pr_1^{\mathrm{L}}(u) 2\pi u \lambda_1 du),\\
\Delta_{21}^{\mathrm{L'}}(x) = (\frac{P_1}{P_2})^{\frac{1}{\alpha_1^{\mathrm{L}}}} \times (\frac{A_1^{\mathrm{L}}}{A_2^{\mathrm{L}}})^{\frac{1}{\alpha_1^{\mathrm{L}}}} \times x^{\frac{\alpha_2^{\mathrm{L}}}{\alpha_1^{\mathrm{L}}}};\\
p_{22}^{\mathrm{L'}}(x) = \exp(-\int_0^{\Delta_{22}^{\mathrm{L'}}(x)} \Pr_1^{\mathrm{NL}}(u) 2\pi u \lambda_1 du),\\
\Delta_{22}^{\mathrm{L'}}(x) = (\frac{P_1}{P_2})^{\frac{1}{\alpha_1^{\mathrm{NL}}}} \times (\frac{A_1^{\mathrm{NL}}}{A_2^{\mathrm{L}}})^{\frac{1}{\alpha_1^{\mathrm{NL}}}} \times x^{\frac{\alpha_2^{\mathrm{L}}}{\alpha_1^{\mathrm{NL}}}},
\end{cases} \tag{A.3.3}$$

and

$$\begin{cases}
p_{21}^{\mathrm{NL'}}(x) = \exp(-\int_0^{\Delta_{21}^{\mathrm{NL'}}(x)} \Pr_1^{\mathrm{L}}(u) 2\pi u \lambda_1 du),\\
\Delta_{21}^{\mathrm{NL'}}(x) = (\frac{P_1}{P_2})^{\frac{1}{\alpha_1^{\mathrm{L}}}} \times (\frac{A_1^{\mathrm{L}}}{A_2^{\mathrm{NL}}})^{\frac{1}{\alpha_1^{\mathrm{L}}}} \times x^{\frac{\alpha_2^{\mathrm{NL}}}{\alpha_1^{\mathrm{L}}}};\\
p_{22}^{\mathrm{NL'}}(x) = \exp(-\int_0^{\Delta_{22}^{\mathrm{NL'}}(x)} \Pr_1^{\mathrm{NL}}(u) 2\pi u \lambda_1 du),\\
\Delta_{22}^{\mathrm{NL'}}(x) = (\frac{P_1}{P_2})^{\frac{1}{\alpha_1^{\mathrm{NL}}}} \times (\frac{A_1^{\mathrm{NL}}}{A_2^{\mathrm{NL}}})^{\frac{1}{\alpha_1^{\mathrm{NL}}}} \times x^{\frac{\alpha_2^{\mathrm{NL}}}{\alpha_1^{\mathrm{NL}}}},
\end{cases} \tag{A.3.4}$$

respectively.

Then I focus on the derivation of the SINR. Take the case of $u \in \mathcal{U}_1^{\mathrm{L}}$ for example,

for the typical user u, the coverage probability of the LoS MBS is given as

$$\begin{aligned}\mathcal{S}_1^{\mathrm{L}}(\tau) &= \mathbb{E}_x\left\{\mathbb{P}[\mathrm{SINR}_1^{\mathrm{L}}(x) > \tau]\right\} \\ &= \int_0^\infty \mathbb{P}[\mathrm{SINR}_1^{\mathrm{L}}(x) > \tau]\mathcal{F}_1^{\mathrm{L}}(x)dx.\end{aligned} \tag{A.3.5}$$

The SINR of UE in Eq. (A.3.5) is rewritten as $\gamma(x) = \frac{S_1^{\mathrm{L}}(x)h_{1,0}}{I_{agg}+\sigma^2}$, where $S_1^{\mathrm{L}}(x) = P_1 A_1^{\mathrm{L}} x^{-\alpha_1^{\mathrm{L}}}$ and I_{agg} denotes the aggregative interference, which comes from the other active MBSs and SBSs. So the CCDF of the typical user SINR at distance x from its associated LoS MBS is given as

$$\begin{aligned}\mathbb{P}[\gamma(x) > \tau] =& \mathbb{P}\left\{h_{1,0} > \frac{(I_x+\sigma^2)\tau}{S_1^{\mathrm{L}}(x)}\right\} \\ =& \exp(\frac{-\sigma^2\tau}{S_1^{\mathrm{L}}(x)})\mathcal{L}_{I_1^{\mathrm{L}}}(\frac{\tau}{S_1^{\mathrm{L}}(x)}),\end{aligned} \tag{A.3.6}$$

and the Laplace transform of I_x is shown as follows:

$$\begin{aligned}&\mathcal{L}_{I_1^{\mathrm{L}}}(\frac{\tau}{S_1^{\mathrm{L}}(x)}) \overset{(a)}{=} \\ &\exp\left\{-2\pi\tilde{\lambda}_1\int_x^\infty \mathrm{Pr}_1^{\mathrm{L}}(u)\left[1-E_{[g]}\left(\exp\left(-\frac{g\tau S_1^{\mathrm{L}}(u)}{S_1^{\mathrm{L}}(x)}\right)\right)\right]udu\right\} \\ &\times\exp\left\{-2\pi\tilde{\lambda}_1\int_{\Delta_{11}^{\mathrm{L}}(x)}^\infty \left(1-\mathrm{Pr}_1^{\mathrm{L}}(u)\right)\left[1-E_{[g]}\left(\exp\left(-\frac{g\tau S_1^{\mathrm{NL}}(u)}{S_1^{\mathrm{L}}(x)}\right)\right)\right]udu\right\} \\ &\times\exp\left\{-2\pi\tilde{\lambda}_2\int_{\Delta_{12}^{\mathrm{L}\prime}(x)}^\infty \mathrm{Pr}_2^{\mathrm{L}}(u)\left[1-E_{[g]}\left(\exp\left(-\frac{g\tau S_2^{\mathrm{L}}(u)}{S_1^{\mathrm{L}}(x)}\right)\right)\right]udu\right\} \\ &\times\exp\left\{-2\pi\tilde{\lambda}_2\int_{\Delta_{13}^{\mathrm{L}\prime}(x)}^\infty \left(1-\mathrm{Pr}_2^{\mathrm{L}}(u)\right)\left[1-E_{[g]}\left(\exp\left(-\frac{g\tau S_2^{\mathrm{NL}}(u)}{S_1^{\mathrm{L}}(x)}\right)\right)\right]udu\right\} \\ &=\exp\left(-2\pi\tilde{\lambda}_1\left(\int_x^\infty \mathrm{Pr}_1^L(u)\frac{u}{1+\frac{S_1^L(x)}{\tau S_1^L(u)}}du+\int_{\Delta_{11}^L(x)}^\infty \mathrm{Pr}_1^{NL}(u)\frac{u}{1+\frac{S_1^L(x)}{\tau S_1^{NL}(u)}}du\right)\right)\times \\ &\exp\left(-2\pi\tilde{\lambda}_2\left(\int_{\Delta_{12}^L(x)}^\infty \mathrm{Pr}_2^L(u)\frac{u}{1+\frac{S_1^L(x)}{\tau S_2^L(u)}}du+\int_{\Delta_{13}^L(x)}^\infty \mathrm{Pr}_2^{NL}(u)\frac{u}{1+\frac{S_1^L(x)}{\tau S_2^{NL}(u)}}du\right)\right),\end{aligned} \tag{A.3.7}$$

where step (a) states that the closest interferer from each type of BSs.

The results from other cases that $u \in \{\mathcal{U}_1^{\mathrm{NL}}\}$ can be obtained by a similar approach. For the case that $u \in \{\mathcal{U}_2^{\mathrm{L}}, \mathcal{U}_2^{\mathrm{NL}}\}$, the SINR constitutes 2 parts. The first part follows the same logic with that $u \in \{\mathcal{U}_1\}$ and constitutes a θ proportion of the whole unit, while the second part does not consider the mutual interference from the MBSs.

In the following, I turn to the case that $u \in \mathcal{U}_3$. Following the same approach, I first show how to compute the PDF $F_3^{\mathrm{L}}(x)$ in Eq. (3.3.5). To this end, I define two events as follow.

- Event Biased-SB^{L}: The nearest biased small BS with a LoS path to the UE is located at distance X^{L} with no other BSs outperforming the associated BS. According to the proof of Lemma 1, the PDF of X^{L} is written as

$$f_X^{\mathrm{L}}(x) = p_{21}^{\mathrm{L}}(x) \times p_{22}^{\mathrm{L}}(x) \times p_{23}^{\mathrm{L}}(x) \times f_2^{\mathrm{L}}(x). \tag{A.3.8}$$

- Event MB conditioned on the value of X^{L}: Given that $\mathrm{X}^{\mathrm{L}} = x$, the UE is associated with a biased LoS small BS with distance X^{L}, which is offloaded from a macro BS with a LoS path at distance $\mathrm{y}_1^{\mathrm{L}}$ (Event MB^{L}) or a macro BS with a NLoS path at distance $\mathrm{y}_1^{\mathrm{NL}}$ (Event MB^{NL}).

  - Event MB^{L} conditioned on the value of X^{L}: To make sure that the UE was associated with the LoS MB with distance $\mathrm{y}_1^{\mathrm{L}}$ before the power biasing process, there should be no other BSs having stronger signals than the associated one. Such a conditional probability of MB^{L} on condition of $\mathrm{X}^{\mathrm{L}} = x$ is

$$\mathfrak{p}_1^{\mathrm{L}}(x) = \int_0^{y_1^{\mathrm{L}}} p_{11}^{\mathrm{L}}(y_1^{\mathrm{L}}) \times p_{12}^{\mathrm{L}}(y_1^{\mathrm{L}}) \times p_{13}^{\mathrm{L}}(y_1^{\mathrm{L}}) \times f_1^{\mathrm{L}}(y_1^{\mathrm{L}}) dx, \tag{A.3.9}$$

    where y_1^{L} satisfies $y_1^{\mathrm{L}} = \arg\{S_2^{\mathrm{L}}(y_1^{\mathrm{L}}) \times D = S_1^{\mathrm{L}}(x)\}$.

– Event MB ^{NL} conditioned on the value of X^{L}: Similar to the event MB^{L}, the conditional probability is

$$\mathfrak{p}_1^{\mathrm{NL}}(x) = \int_0^{y_1^{\mathrm{NL}}} p_{11}^{\mathrm{NL}}(y_1^{\mathrm{NL}}) \times p_{12}^{\mathrm{NL}}(y_1^{\mathrm{NL}}) \times p_{13}^{\mathrm{NL}}(y_1^{\mathrm{NL}}) \times f_1^{\mathrm{NL}}(y_1^{\mathrm{NL}})dx, \tag{A.3.10}$$

where y_1^{NL} satisfies $y_1^{\mathrm{NL}} = \arg\{S_2^{\mathrm{L}}(y_1^{\mathrm{NL}}) \times D = S_1^{\mathrm{NL}}(x)\}$.

Thus, the expression of $\mathcal{F}_3^L(x)$ can be written as

$$\mathcal{F}_3^{\mathrm{L}}(x) = p_{21}^{\mathrm{L}}(x) \times p_{22}^{\mathrm{L}}(x) \times p_{23}^{\mathrm{L}}(x) \times \left(\mathfrak{p}_1^{\mathrm{L}}(x) + \mathfrak{p}_1^{\mathrm{NL}}(x)\right) \times f_2^{\mathrm{L}}(x). \tag{A.3.11}$$

Similarly, the expression of $\mathcal{F}_3^{NL}(x)$ is written as

$$\mathcal{F}_3^{\mathrm{NL}}(x) = p_{21}^{\mathrm{NL}}(x) \times p_{22}^{\mathrm{NL}}(x) \times p_{23}^{\mathrm{NL}}(x) \times \left(\mathfrak{p}_2^{\mathrm{L}}(x) + \mathfrak{p}_2^{\mathrm{NL}}(x)\right) \times f_2^{\mathrm{NL}}(x), \tag{A.3.12}$$

where $\mathfrak{p}_2^{\mathrm{L}}(x) = \int_0^{y_2^{\mathrm{L}}} p_{11}^{\mathrm{L}}(y_2^{\mathrm{L}}) \times p_{12}^{\mathrm{L}}(y_2^{\mathrm{L}}) \times p_{13}^{\mathrm{L}}(y_2^{\mathrm{L}}) \times f_1^{\mathrm{L}}(y_2^{\mathrm{L}})dx$, and y_2^{L} satisfies $y_2^{\mathrm{L}} = \arg\{S_2^{\mathrm{NL}}(y_2^{\mathrm{L}}) \times D = S_1^{\mathrm{L}}(x)\}$, and $\mathfrak{p}_2^{\mathrm{NL}}(x) = \int_0^{y_2^{\mathrm{NL}}} p_{11}^{\mathrm{NL}}(y_2^{\mathrm{NL}}) \times p_{12}^{\mathrm{NL}}(y_2^{\mathrm{NL}}) \times p_{13}^{\mathrm{NL}}(y_2^{\mathrm{NL}}) \times f_1^{\mathrm{NL}}(y_2^{\mathrm{NL}})dx$, and y_2^{NL} satisfies $y_2^{\mathrm{NL}} = \arg\{S_2^{\mathrm{NL}}(y_2^{\mathrm{NL}}) \times D = S_1^{\mathrm{NL}}(x)\}$.

The calculation of SINR for $u \in \mathcal{U}_3$ is similar to other cases and it only considers the interference from the SBSs, thus the rest proof is omitted. Therefore, the overall SINR coverage of a typical user can then be obtained using the law of total probability to get $\mathcal{S}(\tau) = \sum_l \mathcal{S}_l(\tau)$.

A.4 Proof of Theorem 3.3.2

From Eq. (3.3.16), the ASE of the k-th tier is

$$\mathcal{R}_k = \int_0^{\infty} \left\{\mathbb{E}_{\mathrm{SINR}_k}[\log_2(1 + \mathrm{SINR}_k(x))]\right\} \mathcal{F}_k(x)dx, \tag{A.4.1}$$

where $\mathcal{F}_k(x)$ is given in Theorem 1. Because $\mathbb{E}[R] = \int_0^\infty \mathbb{P}[X > x]dx$ for $X > 0$, I can obtain

$$\begin{aligned} &\mathbb{E}_{\mathrm{SINR}_k}[\log_2(1 + \mathrm{SINR}_k(x))] \\ &= \int_0^\infty \mathbb{P}\left\{\log_2[1 + \mathrm{SINR}_k(x)] > \rho\right\} d\rho \\ &= \int_{\log_2(\tau+1)}^\infty \mathbb{P}\left(\mathrm{SINR}_k(x) > 2^\rho - 1\right) d\rho. \end{aligned} \tag{A.4.2}$$

The rest proof is similar to Appendix A.3, and the result is obtained from plugging $\tau = 2^\rho - 1$, conditioned on the $\mathrm{SINR}_k(x) > \tau$.

For the users belonging to $\mathcal{U}_2$, because of the resource partitioning, they can be served in all time-slots. Thus, the calculation of their ergodic rate is composed of two parts. When the macro BS schedules ABSs, the users in $\mathcal{U}_2$ would not get interference from tier 1 BSs and they share the η fraction of channel resource with range expanded UEs, whereas the mutual interference would be considered when the macro BSs are working, in which the $1 - \eta$ fraction of resource is allocated to the users in $\mathcal{U}_1$ and $\mathcal{U}_2$.

A.5 Proof of Lemma 3.3.5

As $\lambda_2 \to +\infty$, all the UEs are assumed to be connected to BSs with a LoS channel, so the path loss $\zeta(r)$ can be rewritten as

$$\zeta_k(r) = \zeta_k^{\mathrm{L}}(r) = A_k^{\mathrm{L}} r^{-\alpha_k^{\mathrm{L}}}, \text{LoS: } \mathrm{Pr}_k^{\mathrm{L}}(r)\text{=1}. \tag{A.5.1}$$

Thus, the components of the NLoS part in R, which are $\mathcal{R}_1^{NL}$, $\mathcal{R}_2^{NL}$, and $\mathcal{R}_3^{NL}$, can be neglected. Furthermore, the interference power $\mathcal{L}_{I_1^L}(\frac{t(\rho)}{S_1^L(x)})$ can be written as

$$\begin{aligned}
\mathcal{L}_{I_1^L}(s) &= \exp\left(-2\pi\tilde{\lambda}_1\left(\int_x^\infty 1\times\frac{u}{1+\frac{S_1^L(x)}{\tau S_1^L(u)}}du\right)\right)\\
&\times\exp\left(-2\pi\tilde{\lambda}_2\left(\int_{\Delta_{12}^L(x)}^\infty 1\times\frac{u}{1+\frac{S_1^L(x)}{\tau S_2^L(u)}}du\right)\right)\\
&= \exp\left(-2\pi\tilde{\lambda}_1\left(\int_x^\infty 1\times\frac{u}{1+\left(\tau^{-1}x^{-\alpha_1^L}\right)u^{\alpha_1^L}}du\right)\right)\\
&\times\exp\left(-2\pi\tilde{\lambda}_2\left(\int_x^\infty 1\times\frac{u}{1+\left(\frac{P_1A_1^L}{P_2A_2^L\tau x^{\alpha_1^L}}\right)u^{\alpha_2^L}}du\right)\right).
\end{aligned} \tag{A.5.2}$$

In order to evaluate Eq. (A.5.2), I define the following integral functions according to [82]:

$$\begin{aligned}
\rho(\alpha,\beta,t,d) &= \int_d^\infty \frac{u^\beta}{1+tu^\alpha}du\\
&= \left[\frac{d^{-(\alpha-\beta-1)}}{t(\alpha-\beta-1)}\right]F_1\left[1,1-\frac{\beta+1}{\alpha};2-\frac{\beta+1}{\alpha};-\frac{1}{td^\alpha}\right],\\
&\qquad\qquad (\alpha>\beta+1),
\end{aligned} \tag{A.5.3}$$

where ${}_2F_1[\cdot,\cdot;\cdot;\cdot]$ is the hyper-geometric function [82]. The proof is completed by plugging Eq. (A.5.3) into Eq. (A.5.2), and the calculations of $\mathcal{L}_{I_{21}^L}(\frac{t(\rho)}{S_2^L(x)})$, $\mathcal{L}_{I_{22}^L}(\frac{t(\rho)}{S_2^L(x)})$, and $\mathcal{L}_{I_3^L}(\frac{t(\rho)}{S_2^L(x)})$ are following a similar procedure, which is omitted here.

Appendix B

Proofs of Chapter 4

B.1 Proof of Theorem 4.2.1

For clarity, I first summarize the ideas to prove Theorem 4.2.1. In order to evaluate $p^{\text{trans}}(\lambda, \gamma)$, the first key step is to calculate the distance probability density function (PDF) for the event that the typical receiver is associated with a nearest transmitter which also have a social relationship with it, so that the integral of $\Pr[\text{SINR} > \gamma]$ can be performed over the distance r. The second key step is to calculate $\Pr[\text{SINR} > \gamma]$ for the typical case conditioned on the distance r.

From Eq. (4.1.3) and Eq. (4.2.1), I can derive $p^{\text{trans}}(\lambda, \gamma)$ in a straightforward way

as

$$\begin{aligned} p^{\text{trans}}(\lambda,\gamma) &= \int_{r>0} \Pr\left[\text{SINR} > \gamma | r\right] f_R(r) dr \\ &= \int_{r>0} \Pr\left[\frac{Phr^{-\alpha}}{I_d+\sigma^2} > \gamma\right] f_R(r) dr \\ &= \int_0^A \Pr\left[\frac{Phr^{-\alpha}}{I_d+\sigma^2} > \gamma\right] f_{R1}(r) dr \\ &+ \int_A^\infty \Pr\left[\frac{Phr^{-\alpha}}{I_d+\sigma^2} > \gamma\right] f_{R2}(r) dr, \end{aligned} \tag{B.1.1}$$

where $f_{R1}(r)$ and $f_{R2}(r)$ are the different PDFs of the RV $R1$ and $R2$, and $R1$ and $R2$ are in the different intervals with respect to r.

According to the offline social relation model, when $0 < R_1 \leq A$, the PDF of R_1 can be represented as following. According to [102] and [5], the complementary cumulative distribution function (CCDF) of R_1 can be written as

$$F_{\text{R1}}^{\text{S}}(r) = \exp\left(-\int_0^r \text{P}_{\text{S}}(\mu) 2\pi\mu\lambda d\mu\right) = \exp\left(-\pi\lambda r^2\right). \tag{B.1.2}$$

Taking the derivative of $(1 - F_{\text{R1}}^{\text{S}}(r))$ with regard to r, I can get the PDF of R_1 as

$$f_{R1}(r) = \exp(-\pi\lambda r^2) \times 2\pi\lambda r. \tag{B.1.3}$$

When $R_2 > A$, the PDF of R_2 can be expressed as following. Same as Eq. (B.1.2), the CCDF of R_2 can be written as

$$\begin{aligned} F_{\text{R2}}^{\text{S}}(r) &= \exp\left(-\int_0^r \text{P}_{\text{S}}(\mu) \times 2\pi\mu\lambda d\mu\right) \\ &= \exp\left(-\left(\pi\lambda A^2 + 2\pi\lambda A^2(\ln r - \ln A)\right)\right). \end{aligned} \tag{B.1.4}$$

So taking the derivative of $(1 - F_{R2}^{S}(r))$ with regard to r, I can get the PDF as

$$f_{\text{R2}}(r) = \exp[-(\pi\lambda A^2 + 2\pi\lambda A^2(\ln r - \ln A)] \times 2\pi\lambda A^2 \times \frac{1}{r}. \tag{B.1.5}$$

Having obtained $f_{R1}(r)$ and $f_{R2}(r)$, I move on to evaluate $\Pr\left[\frac{Phr^{-\alpha}}{I_d+\sigma^2} > \gamma\right]$ in (B.1.1)

as

$$\begin{aligned}\Pr\left[\frac{Phr^{-\alpha}}{I_d+N_0}>\gamma\right] &= \mathbb{E}_{I_d}\left\{\Pr\left[h>\frac{\gamma r^{\alpha}(I_d+\sigma^2)}{P}\right]\right\}\\ &= \mathbb{E}_{I_d}\left\{\exp\left(-\frac{\gamma r^{\alpha}(I_d+\sigma^2)}{P}\right)\right\}\\ &= \exp\left(-\frac{\gamma r^{\alpha}\times\sigma^2}{P}\right)\mathcal{L}_{I_d}\left(\frac{\gamma r^{\alpha}}{P}\right),\end{aligned} \tag{B.1.6}$$

where $\mathcal{L}_{I_d}$ is the Laplace transform of RV I_d evaluated at s.

The proof of Theorem 1 is completed by plugging Eq. (B.1.3), Eq. (B.1.5), and Eq. (B.1.6) into Eq. (4.2.4).

B.2 Proof of Lemma 4.2.1

Based on the considered UAS, it is straightforward to derive $\mathcal{L}_{I_{d1}}$ as

$$\begin{aligned}\mathcal{L}_{I_{d1}}(s) &= \mathbb{E}_{[\Phi,\{h_i\}]}\left\{exp\left(-s\sum_{i\in\Phi/b_0}Ph_id^{-\alpha}\right)\right\}\\ &\overset{(a)}{=} \exp\left(-2\pi\lambda\int_r^{\infty}(1-\mathbb{E}_{[h]}\{\exp(-sPhu^{-\alpha})\})udu\right)\\ &\overset{(b)}{=} \exp\left(-2\pi\lambda\int_r^{\infty}(1-\mathbb{E}_{[h]}\{\exp(-r^{\alpha}\gamma hu^{-\alpha})\})udu\right),\end{aligned} \tag{B.2.1}$$

where the step (a) is obtained from [5] and the step (b) is plugging $s=r^{\alpha}\gamma P^{-1}$ into Eq. (B.2.1).

The part in Eq. (B.2.1) $\left(\mathbb{E}_{[h]}\left\{exp(-r^{-\alpha}\gamma hu^{-\alpha})\right\}\right)$ considers interferences from both social and non-social paths, thus, $\mathcal{L}_{I_d}(s)$ should be further derived as

$$\begin{aligned}&\mathcal{L}_{I_{d1}}(s) =\\ &\exp\left(-2\pi\lambda\int_r^{\infty}\mathrm{P_S}(u)\left\{1-\mathbb{E}_{[h]}\left\{\exp(\frac{-\gamma h}{r^{\alpha}u^{\alpha}})\right\}\right\}udu\right)\times\\ &\exp\left(-2\pi\lambda\int_r^{\infty}\mathrm{P_{NS}}(u)\left\{1-\mathbb{E}_{[h]}\left\{\exp(\frac{-\gamma h}{r^{\alpha}u^{\alpha}})\right\}\right\}udu\right),\end{aligned} \tag{B.2.2}$$

where $\mathrm{P_{NS}}(u) = 1 - \mathrm{P_S}(u)$. Plugging Eq. (4.1.3) into Eq. (B.2.2), I can get

$$\begin{aligned}
&\mathcal{L}_{I_{d1}}(s) = \\
&\exp\left(-2\pi\lambda \int_r^\infty \left\{1 - \mathbb{E}_{[h]}\left\{\exp(\frac{-\gamma h}{r^\alpha u^\alpha})\right\}\right\} udu\right) \\
&= \exp\left(-2\pi\lambda \times \int_r^\infty \left\{1 - \frac{1}{1 + r^\alpha \gamma u^{-\alpha}}\right\} udu\right) \\
&= \exp\left(\frac{-2\pi\lambda r^2 \gamma}{\alpha - 2} {}_2F_1\left[1, 1 - \frac{2}{\alpha}; 2 - \frac{2}{\alpha}; -\gamma\right]\right),
\end{aligned} \tag{B.2.3}$$

where ${}_2F_1[\cdot,\cdot;\cdot;\cdot]$ is the hyper-geometric function [91] and $\alpha > 2$.

B.3 Proof of Lemma 4.2.2

From Appendix B.2, the second part of Eq. (B.1.1) can be expressed as

$$\begin{aligned}
&\int_A^\infty \Pr\left[\frac{Phr^{-\alpha}}{I_d + \sigma^2} > \gamma\right] f_{R2}(r)dr \\
&= \int_A^\infty \exp\left(-\frac{\gamma \times r^\alpha \times \sigma^2}{P}\right) \mathcal{L}_{I_{d2}}\left(\frac{\gamma \times r^\alpha}{P}\right),
\end{aligned} \tag{B.3.1}$$

where $\mathcal{L}_{I_{d2}}(s)$ also needs to consider the interferences from both social and non-social paths.

Thus $\mathcal{L}_{I_{d2}}(s)$ can be expressed as

$$\begin{aligned}
&\mathcal{L}_{I_{d2}}(s) = \\
&\exp\left(-2\pi\lambda\int_r^\infty (1-\mathbb{E}_{[h]}\{\exp(-r^\alpha\gamma h u^{-\alpha})\})udu\right) \\
&=\exp\left(-2\pi\lambda\int_r^\infty \frac{A^2}{u^2}\left\{1-\mathbb{E}_{[h]}\{\exp(\frac{-\gamma h}{r^\alpha u^\alpha})\right\}udu\right)\times \\
&\exp\left(-2\pi\lambda\int_A^\infty \frac{u^2-A^2}{u^2}\left\{1-\mathbb{E}_{[h]}\{\exp(\frac{-\gamma h}{r^\alpha u^\alpha})\right\}udu\right) \\
&= \exp\left(-2\pi\lambda\gamma^2\frac{1}{\alpha}\left(\ln\left(1+\frac{1}{\gamma}\right)-\ln\left(\frac{1}{\gamma}\right)\right)\right) \\
&\times \exp\left(\frac{-2\pi\lambda A^{2-\alpha}r^\alpha\gamma}{\alpha-2}\times\nabla_2(\alpha,A,r,\gamma)\right)\times \\
&\exp\left(2\pi\lambda A^2\frac{1}{\alpha}\left(\ln(1+\frac{A^\alpha r^{-\alpha}}{\gamma})-\ln(\frac{A^\alpha r^{-\alpha}}{\gamma})\right)\right), \\
&\qquad\qquad\qquad\qquad\qquad\qquad\qquad\qquad (r>A),
\end{aligned} \tag{B.3.2}$$

where $\nabla_2(\alpha,A,r,\gamma) = {}_2F_1\left[1,1-\frac{2}{\alpha};2-\frac{2}{\alpha};-A^{-\alpha}r^\alpha\gamma\right]$, ${}_2F_1[\cdot,\cdot;\cdot;\cdot]$ is the hyper-geometric function [91] and $\alpha > 2$.

B.4 Proof of Lemma 4.3.1

In this appendix, I first prove that the proposed algorithm possesses the moderation property. That is, the magnitude of decrement of any action probability is bounded by a certain value.

From Eq. (4.3.7), the amount that a probability decrease is computed by

$$p_j(t) - p_j(t+1) = \frac{\Delta}{F-K(t)} = \frac{1}{F\delta}\times\frac{1}{F-K(t)} < \frac{1}{F\delta}, \tag{B.4.1}$$

so the magnitude of decrement is bounded by the value $1/F\delta$ and the proposed algorithm possesses the moderation property.

Then I prove that the proposed algorithm possesses the monotony property. That

is, if there exists an index i and a time instant $t' < \infty$, such that

$$d_i(t) > d_j(t), \ for \ j \neq i \ and \ t > t', \tag{B.4.2}$$

then there exists an integer F_0 such that for all $F > F_0$, $p_i(t) \to 1$ with probability one as $t \to \infty$. Consider

$$\Delta p_i(t) = E[p_i(t+1) - p_i(t)|\mathbf{o}(t)], \tag{B.4.3}$$

where $\mathbf{o}(t)$ is the estimator vector.

From Eq. (4.3.7), $p_i(t+1)$ can be expressed as:

$$\begin{aligned} p_i(t+1) &= p_i(t) + \frac{\Delta}{K(t)}, \\ &\quad if \ \alpha_j \ is \ chosen \ and \ d_i > d_j. \\ p_i(t+1) &= 1 - \sum_{j \neq i} (p_j(t) - \frac{\Delta}{F}) \\ &= p_i(t) + \frac{\Delta(F-1)}{F}, \\ &\quad if \ \alpha_i \ is \ chosen \ and \ d_i \ is \ max. \end{aligned} \tag{B.4.4}$$

Hence, for all $t > t'$ and $F > K(t) \geq 1$, $\Delta p_i(t)$ can be expressed by:

$$\begin{aligned} &\Delta p_i(t) \\ &= \sum_{j \neq i} \frac{\Delta}{K(t)} \times p_j(t) + \Delta \times \frac{(F-1)}{F} \times p_i(t) \\ &= \frac{\Delta}{K(t)}(1 - p_i(t)) + \Delta \times \frac{(F-1)}{F} \times p_i(t) \\ &> \frac{\Delta}{K(t)} + \Delta \times p_i(t) \times (\frac{K(t)^2 - K(t) - K(t)}{FK(t)}) \\ &\geq \Delta - \Delta \frac{P_i(t)}{F} = \Delta \times (1 - \frac{P_i(t)}{F}) > 0. \end{aligned} \tag{B.4.5}$$

Therefore, $p_i(t)$ is a submartingale and according to the submartingale convergence theorem [92], $p_i(t)$ will converge to one with probability one. Therefore, the monotony property of the algorithm is proved.

Appendix C

Proofs of Chapter 5

C.1 Proof of Theorem 5.3.1

When transmission between UAV-BS and UE is LoS, two conditions should be satisfied: 1) The distance between UE and UAV-BS is r, and there is no UAV-BS of LoS path within r. 2) There is no UAV-BS of NLoS path within r_1. Based on these conditions, $f^{\mathrm{L}}(r)$ is computed as [52]

$$\begin{aligned} f^{\mathrm{L}}(r) = & \exp\left(-\int_0^{r_1}\left(1-\Pr^{\mathrm{L}}(u)\right)2\pi u\lambda du\right) \\ & \times \exp\left(-\int_0^{r}\Pr^{\mathrm{L}}(u)\,2\pi u\lambda du\right) \\ & \times \Pr^{\mathrm{L}}(r)\times 2\pi r\lambda. \end{aligned} \tag{C.1.1}$$

When transmission between UAV-BS and UE is NLoS, two conditions should be satisfied: 1) The distance between UE and UAV-BS is r, and there is no UAV-BS of NLoS path within r. 2) There is no UAV-BS of LoS path within r_2. So $f^{\mathrm{NL}}(r)$ can

be derived as

$$\begin{aligned} f^{\mathrm{NL}}(r) = &\exp\left(-\int_0^{r_2} \Pr^{\mathrm{L}}(u)\, 2\pi u\lambda du\right) \\ &\times \exp\left(-\int_0^{r} \left(1-\Pr^{\mathrm{L}}(u)\right) 2\pi u\lambda du\right) \\ &\times \left(1-\Pr^{\mathrm{L}}(r)\right) \times 2\pi r\lambda. \end{aligned} \tag{C.1.2}$$

the CDF of associated UAV-BS located at r from UE is $1-\exp\left(-\int_0^r \Pr^{\mathrm{L}}(u) 2\pi u\lambda du\right)$, and PDF is

$$f^{\mathrm{L}}(r) = \exp\left(-\int_0^{r} \Pr^{\mathrm{L}}(u) 2\pi u\lambda du\right) \Pr^{\mathrm{L}}(r) 2\pi r\lambda. \tag{C.1.3}$$

Considering the probability of event C^{NL} conditioned on associated UAV-BS located at r km from UE, it can be derived as

$$\Pr\left[C^{\mathrm{NL}} \middle| R^{\mathrm{L}} = r\right] = \exp\left(-\int_0^{r_1} \left(1-\Pr^{\mathrm{L}}(u)\right) 2\pi u\lambda du\right). \tag{C.1.4}$$

$\Pr\left[\mathrm{SINR} > \gamma \,|r\right]$ conditioned on r can be expressed as

$$\begin{aligned} \Pr\left[\frac{P\zeta^{\mathrm{L}}(r)g}{I_r+N_0} > \gamma\right] =& \mathbb{E}_{[I_r]}\left\{g > \frac{\gamma\left(I_r+N_0\right)}{P\zeta^{\mathrm{L}}(r)}\right\} \\ =& \mathbb{E}_{[I_r]}\left\{\bar{F}_G\left(\frac{\gamma\left(I_r+N_0\right)}{P\zeta^{\mathrm{L}}(r)}\right)\right\}, \end{aligned} \tag{C.1.5}$$

where $\bar{F}_G$ is the CCDF of g which has an exponential distribution. So $\bar{F}_G = \exp(-g)$ and $\Pr\left[\mathrm{SINR} > \gamma \,|r\right]$ can be further expressed as

$$\begin{aligned} \Pr\left[\frac{P\zeta^{\mathrm{L}}(r)g}{I_r+N_0} > \gamma\right] &= \mathbb{E}_{[I_r]}\left\{\exp\left(-\frac{\gamma\left(I_r+N_0\right)}{P\zeta^{\mathrm{L}}(r)}\right)\right\} \\ &= \exp\left(-\frac{\gamma N_0}{P\zeta^{\mathrm{L}}(r)}\right) \mathbb{E}_{[I_r]}\left\{\exp\left(-\frac{\gamma I_r}{P\zeta^{\mathrm{L}}(r)}\right)\right\} \\ &= \exp\left(-\frac{\gamma N_0}{P\zeta^{\mathrm{L}}(r)}\right) \mathcal{L}_{I_r}\left(\frac{\gamma}{P\zeta^{\mathrm{L}}(r)}\right). \end{aligned} \tag{C.1.6}$$

Then $\Pr\left[\frac{P\zeta^{\mathrm{NL}}(r)g}{I_r+N_0} > \gamma\right]$ can be derived in a similar way:

$$
\begin{aligned}
&\Pr\left[\frac{P\zeta^{\mathrm{NL}}(r)g}{I_r+N_0}>\gamma\right] \\
&=\exp\left(-\frac{\gamma N_0}{P\zeta^{\mathrm{NL}}(r)}\right)\mathbb{E}_{[I_r]}\left\{\exp\left(-\frac{\gamma I_r}{P\zeta^{\mathrm{NL}}(r)}\right)\right\} \\
&=\exp\left(-\frac{\gamma N_0}{P\zeta^{\mathrm{NL}}(r)}\right)\mathcal{L}_{I_r}\left(\frac{\gamma}{P\zeta^{\mathrm{NL}}(r)}\right).
\end{aligned}
\tag{C.1.7}
$$

Bibliography

[1] H. Zhang, N. Liu, X. Chu, K. Long, A.-H. Aghvami, and V. C. Leung, "Network slicing based 5g and future mobile networks: Mobility, resource management, and challenges," *IEEE Communications Magazine*, vol. 55, no. 8, pp. 138–145, 2017.

[2] Cisco, "Visual networking index forecast, 2015–2020," 2015.

[3] D. López-Pérez, M. Ding, H. Claussen, and A. H. Jafari, "Towards 1 gbps/ue in cellular systems: Understanding ultra-dense small cell deployments," *IEEE Communications Surveys & Tutorials*, vol. 17, no. 4, pp. 2078–2101, 2015.

[4] A. Damnjanovic, J. Montojo, Y. Wei, T. Ji, T. Luo, M. Vajapeyam, T. Yoo, O. Song, and D. Malladi, "A survey on 3gpp heterogeneous networks," *IEEE Wireless Communications*, vol. 18, no. 3, pp. 10–21, June 2011.

[5] J. G. Andrews, F. Baccelli, and R. K. Ganti, "A tractable approach to coverage and rate in cellular networks," *IEEE Transactions on Communications*, vol. 59, no. 11, pp. 3122–3134, 2011.

[6] H. S. Dhillon, R. K. Ganti, F. Baccelli, and J. G. Andrews, "Modeling and analysis of k-tier downlink heterogeneous cellular networks," *IEEE Journal on Selected Areas in Communications*, vol. 30, no. 3, pp. 550–560, April 2012.

[7] S. Lee and K. Huang, "Coverage and economy of cellular networks with many base stations," *IEEE Communications Letters*, vol. 16, no. 7, pp. 1038–1040, 2012.

[8] M. D. Renzo, W. Lu, and P. Guan, "The intensity matching approach: A tractable stochastic geometry approximation to system-level analysis of cellular networks," *IEEE Transactions on Wireless Communications*, vol. 15, no. 9, pp. 5963–5983, Sept 2016.

[9] S. M. Yu and S.-L. Kim, "Downlink capacity and base station density in cellular networks," in *Modeling & Optimization in Mobile, Ad Hoc & Wireless Networks (WiOpt), 2013 11th International Symposium on*. IEEE, 2013, pp. 119–124.

[10] M. Ding, D. Lopez-Perez, G. Mao, and Z. Lin, "Study on the idle mode capability with los and nlos transmissions," *arXiv preprint arXiv:1608.06694*, 2016.

[11] C. Ma, Z. Lin, L. Marini, J. Li, and B. Vucetic, "Learning automaton based distributed caching for mobile social networks," in *IEEE Wireless Communications and Networking Conference (WCNC)*. IEEE, 2016.

[12] Z. Gao, L. Dai, and Z. Wang, "Channel estimation for mmwave massive mimo based access and backhaul in ultra-dense network," in *Communications (ICC), 2016 IEEE International Conference on*. IEEE, 2016, pp. 1–6.

[13] S. Hur, T. Kim, D. J. Love, J. V. Krogmeier, T. A. Thomas, and A. Ghosh, "Multilevel millimeter wave beamforming for wireless backhaul," in *GLOBECOM Workshops (GC Wkshps), 2011 IEEE*. IEEE, 2011, pp. 253–257.

[14] ——, "Millimeter wave beamforming for wireless backhaul and access in small cell networks," *IEEE transactions on communications*, vol. 61, no. 10, pp. 4391–4403, 2013.

[15] S. Han, I. Chih-Lin, Z. Xu, S. Wang *et al.*, "Reference signals design for hybrid analog and digital beamforming." *IEEE communications letters*, vol. 18, no. 7, pp. 1191–1193, 2014.

[16] M. Chen and A. Ksentini, "Cache in the air: exploiting content caching and delivery techniques for 5g systems," *IEEE Communications Magazine*, p. 132, 2014.

[17] L. Zhang, M. Xiao, G. Wu, and S. Li, "Efficient scheduling and power allocation for d2d-assisted wireless caching networks," *IEEE Transactions on Communications*, vol. PP, no. 99, pp. 1–1, 2016.

[18] H. Zhang, Y. Dong, J. Cheng, M. J. Hossain, and V. C. Leung, "Fronthauling for 5g lte-u ultra dense cloud small cell networks," *IEEE Wireless Communications*, vol. 23, no. 6, pp. 48–53, 2016.

[19] M. Ji, G. Caire, and A. F. Molisch, "Fundamental limits of caching in wireless d2d networks," *IEEE Transactions on Information Theory*, vol. 62, no. 2, pp. 849–869, Feb 2016.

[20] ——, "The throughput-outage tradeoff of wireless one-hop caching networks," *IEEE Transactions on Information Theory*, vol. 61, no. 12, pp. 6833–6859, Dec 2015.

[21] ——, "Wireless device-to-device caching networks: Basic principles and system performance," *IEEE Journal on Selected Areas in Communications*, vol. 34, no. 1, pp. 176–189, Jan 2016.

[22] P. Li and S. Guo, "Incentive mechanisms for device-to-device communications," *IEEE Network*, vol. 29, no. 4, pp. 75–79, July 2015.

[23] Z. Zheng, T. Wang, L. Song, Z. Han, and J. Wu, "Social-aware multi-file dissemination in device-to-device overlay networks," in *Computer Communications*

Workshops (INFOCOM WKSHPS), 2014 IEEE Conference on, April 2014, pp. 219–220.

[24] C. Zhang and W. Zhang, "Spectrum sharing for drone networks," *IEEE Journal on Selected Areas in Communications*, vol. 35, no. 1, pp. 136–144, 2017.

[25] B. Galkin, J. Kibilda, and L. A. DaSilva, "Deployment of uav-mounted access points according to spatial user locations in two-tier cellular networks," in *Wireless Days (WD), 2016*. IEEE, 2016, pp. 1–6.

[26] R. I. Bor-Yaliniz, A. El-Keyi, and H. Yanikomeroglu, "Efficient 3-d placement of an aerial base station in next generation cellular networks," in *Communications (ICC), 2016 IEEE International Conference on*. IEEE, 2016, pp. 1–5.

[27] M. Ding and D. L. Pérez, "Please lower small cell antenna heights in 5g," in *Global Communications Conference (GLOBECOM), 2016 IEEE*. IEEE, 2016, pp. 1–6.

[28] M. Ding and D. López-Pérez, "On the performance of practical ultra-dense networks: The major and minor factors," *arXiv preprint arXiv:1701.07964*, 2017.

[29] L. Marini, J. Li, and Y. Li, "Distributed caching based on decentralized learning automata," in *IEEE International Conference on Communications (ICC)*. IEEE, 2015, pp. 3807–3812.

[30] J. Hu, L.-L. Yang, and L. Hanzo, "Delay analysis of social group multicast-aided content dissemination in cellular system," *IEEE Transactions on Communications*, vol. 64, no. 4, pp. 1660–1673, 2016.

[31] M. Haenggi, *Stochastic geometry for wireless networks*. Cambridge University Press, 2012.

[32] M. Afshang and H. S. Dhillon, "Poisson cluster process based analysis of hetnets with correlated user and base station locations," *IEEE Transactions on Wireless Communications*, vol. 17, no. 4, pp. 2417–2431, April 2018.

[33] Y. Kishiyama, A. Benjebbour, T. Nakamura, and H. Ishii, "Future steps of lte-a: evolution toward integration of local area and wide area systems," *IEEE Wireless Communications*, vol. 20, no. 1, pp. 12–18, February 2013.

[34] P. Bahl, M. T. Hajiaghayi, K. Jain, S. V. Mirrokni, L. Qiu, and A. Saberi, "Cell breathing in wireless lans: Algorithms and evaluation," *IEEE Transactions on Mobile Computing*, vol. 6, no. 2, pp. 164–178, Feb 2007.

[35] H.-S. Jo, Y. J. Sang, P. Xia, and J. G. Andrews, "Outage probability for heterogeneous cellular networks with biased cell association," in *Global Telecommunications Conference (GLOBECOM 2011), 2011 IEEE*. IEEE, 2011, pp. 1–5.

[36] A. Damnjanovic, J. Montojo, Y. Wei, T. Ji, T. Luo, M. Vajapeyam, T. Yoo, O. Song, and D. Malladi, "A survey on 3gpp heterogeneous networks," *IEEE Wireless Communications*, vol. 18, no. 3, 2011.

[37] D. Lopez-Perez, I. Guvenc, G. De la Roche, M. Kountouris, T. Q. Quek, and J. Zhang, "Enhanced intercell interference coordination challenges in heterogeneous networks," *IEEE Wireless Communications*, vol. 18, no. 3, 2011.

[38] M. Bennis, M. Debbah, and H. V. Poor, "Ultra-reliable and low-latency wireless communication: Tail, risk and scale," *arXiv preprint arXiv:1801.01270*, 2018.

[39] B. Soret, P. Mogensen, K. I. Pedersen, and M. C. Aguayo-Torres, "Fundamental tradeoffs among reliability, latency and throughput in cellular networks," in *Globecom Workshops (GC Wkshps), 2014*. IEEE, 2014, pp. 1391–1396.

[40] G. Durisi, T. Koch, and P. Popovski, "Toward massive, ultrareliable, and low-latency wireless communication with short packets," *Proceedings of the IEEE*, vol. 104, no. 9, pp. 1711–1726, 2016.

[41] M. Luvisotto, Z. Pang, and D. Dzung, "Ultra high performance wireless control for critical applications: Challenges and directions," *IEEE Transactions on Industrial Informatics*, vol. 13, no. 3, pp. 1448–1459, 2017.

[42] M. Peng, C. Wang, J. Li, H. Xiang, and V. Lau, "Recent advances in underlay heterogeneous networks: Interference control, resource allocation, and self-organization," *IEEE Communications Surveys Tutorials*, vol. 17, no. 2, pp. 700–729, Secondquarter 2015.

[43] P. Bhat, S. Nagata, L. Campoy, I. Berberana, T. Derham, G. Liu, X. Shen, P. Zong, and J. Yang, "Lte-advanced: an operator perspective," *IEEE Communications Magazine*, vol. 50, no. 2, pp. 104–114, February 2012.

[44] M. Yu, Z. Wang, S. Wang, and X. Xu, "Architecture design for service network deployment, customization and execution," in *2014 International Conference on Service Sciences*, May 2014, pp. 13–18.

[45] Z. Wang, X. Xu, and X. Wang, "Mass customization oriented and cost-effective service network," in *International IFIP Working Conference on Enterprise Interoperability*. Springer, 2013, pp. 172–185.

[46] A. J. Dietrich, S. Kirn, and V. Sugumaran, "A service-oriented architecture for mass customization amp;mdash;a shoe industry case study," *IEEE Transactions on Engineering Management*, vol. 54, no. 1, pp. 190–204, Feb 2007.

[47] B. Zhuang, D. Guo, and M. L. Honig, "Energy-efficient cell activation, user association, and spectrum allocation in heterogeneous networks," *IEEE Journal on Selected Areas in Communications*, vol. 34, no. 4, pp. 823–831, April 2016.

[48] Q. Ye, B. Rong, Y. Chen, M. Al-Shalash, C. Caramanis, and J. G. Andrews, "User association for load balancing in heterogeneous cellular networks," *IEEE Transactions on Wireless Communications*, vol. 12, no. 6, pp. 2706–2716, June 2013.

[49] M. Di Renzo, "Stochastic geometry modeling and analysis of multi-tier millimeter wave cellular networks," *IEEE Transactions on Wireless Communications*, vol. 14, no. 9, pp. 5038–5057, 2015.

[50] M. Di Renzo, A. Guidotti, and G. E. Corazza, "Average rate of downlink heterogeneous cellular networks over generalized fading channels: A stochastic geometry approach," *IEEE Transactions on Communications*, vol. 61, no. 7, pp. 3050–3071, 2013.

[51] X. Zhang and J. G. Andrews, "Downlink cellular network analysis with multi-slope path loss models," *IEEE Transactions on Communications*, vol. 63, no. 5, pp. 1881–1894, 2015.

[52] M. Ding, P. Wang, D. López-Pérez, G. Mao, and Z. Lin, "Performance impact of los and nlos transmissions in dense cellular networks," *IEEE Transactions on Wireless Communications*, vol. 15, no. 3, pp. 2365–2380, 2016.

[53] A. AlAmmouri, J. G. Andrews, and F. Baccelli, "Sinr and throughput of dense cellular networks with stretched exponential path loss," *arXiv preprint arXiv:1703.08246*, 2017.

[54] J. Li, Y. Chen, Z. Lin, W. Chen, B. Vucetic, and L. Hanzo, "Distributed caching for data dissemination in the downlink of heterogeneous networks," *IEEE Transactions on Communications*, vol. 63, no. 10, pp. 3553–3568, 2015.

[55] Z. Hu, Z. Zheng, T. Wang, L. Song, and X. Li, "Caching as a service: Small-cell caching mechanism design for service providers," *IEEE Transactions on Wireless Communications*, vol. 15, no. 10, pp. 6992–7004, Oct 2016.

[56] E. Bastug, M. Bennis, and M. Debbah, "Living on the edge: The role of proactive caching in 5g wireless networks," *IEEE Communications Magazine*, vol. 52, no. 8, pp. 82–89, 2014.

[57] C. Ma, M. Ding, H. Chen, Z. Lin, G. Mao, and X. Li, "Socially aware distributed caching in device-to-device communication networks," in *Globecom Workshops (GC Wkshps), 2016 IEEE*. IEEE, 2016, pp. 1–6.

[58] Z. Chen, Y. Liu, B. Zhou, and M. Tao, "Caching incentive design in wireless d2d networks: A stackelberg game approach," *arXiv preprint arXiv:1603.00244*, 2016.

[59] H. Zhang, Y. Qiu, X. Chu, K. Long, and V. Leung, "Fog radio access networks: Mobility management, interference mitigation and resource optimization," *arXiv preprint arXiv:1707.06892*, 2017.

[60] D. Wu, J. Yan, H. Wang, D. Wu, and R. Wang, "Social attribute aware incentive mechanism for device-to-device video distribution," *IEEE Transactions on Multimedia*, 2017.

[61] X. Zhang, Y. Li, Y. Zhang, J. Zhang, H. Li, S. Wang, and D. Wang, "Information caching strategy for cyber social computing based wireless networks," *IEEE Transactions on Emerging Topics in Computing*, vol. 5, no. 3, pp. 391–402, July 2017.

[62] A. Fotouhi, M. Ding, and M. Hassan, "Dynamic base station repositioning to

improve spectral efficiency of drone small cells," in *2017 IEEE 18th International Symposium on A World of Wireless, Mobile and Multimedia Networks (WoWMoM)*, June 2017, pp. 1–9.

[63] C. Zhang and W. Zhang, "Spectrum sharing for drone networks," *IEEE Journal on Selected Areas in Communications*, vol. 35, no. 1, pp. 136–144, Jan 2017.

[64] F. Ono, H. Ochiai, and R. Miura, "A wireless relay network based on unmanned aircraft system with rate optimization," *IEEE Transactions on Wireless Communications*, vol. 15, no. 11, pp. 7699–7708, 2016.

[65] M. Gruber, "Role of altitude when exploring optimal placement of uav access points," in *Wireless Communications and Networking Conference (WCNC), 2016 IEEE*. IEEE, 2016, pp. 1–5.

[66] R. I. Bor-Yaliniz, A. El-Keyi, and H. Yanikomeroglu, "Efficient 3-d placement of an aerial base station in next generation cellular networks," in *2016 IEEE International Conference on Communications (ICC)*, May 2016, pp. 1–5.

[67] M. Mozaffari, W. Saad, M. Bennis, and M. Debbah, "Drone small cells in the clouds: Design, deployment and performance analysis," in *Global Communications Conference (GLOBECOM), 2015 IEEE*. IEEE, 2015, pp. 1–6.

[68] M. Alzenad, A. El-Keyi, F. Lagum, and H. Yanikomeroglu, "3d placement of an unmanned aerial vehicle base station (uav-bs) for energy-efficient maximal coverage," *IEEE Wireless Communications Letters*, 2017.

[69] M. Mozaffari, W. Saad, M. Bennis, and M. Debbah, "Unmanned aerial vehicle with underlaid device-to-device communications: Performance and tradeoffs," *IEEE Transactions on Wireless Communications*, vol. 15, no. 6, pp. 3949–3963, 2016.

[70] A. K. Gupta, X. Zhang, and J. G. Andrews, "Sinr and throughput scaling in ultradense urban cellular networks," *IEEE Wireless Communications Letters*, vol. 4, no. 6, pp. 605–608, Dec 2015.

[71] Q. Wu, Y. Zeng, and R. Zhang, "Joint trajectory and communication design for multi-uav enabled wireless networks," *IEEE Transactions on Wireless Communications*, vol. 17, no. 3, pp. 2109–2121, 2018.

[72] Y. Zeng, R. Zhang, and T. J. Lim, "Throughput maximization for uav-enabled mobile relaying systems," *IEEE Transactions on Communications*, vol. 64, no. 12, pp. 4983–4996, 2016.

[73] Y. Zeng and R. Zhang, "Energy-efficient uav communication with trajectory optimization," *IEEE Trans. Wireless Commun*, vol. 16, no. 6, pp. 3747–3760, 2017.

[74] J. Lyu, Y. Zeng, and R. Zhang, "Cyclical multiple access in uav-aided communications: A throughput-delay tradeoff," *IEEE Wireless Communications Letters*, vol. 5, no. 6, pp. 600–603, 2016.

[75] Y. Li, B. Cao, and C. Wang, "Handover schemes in heterogeneous lte networks: challenges and opportunities," *IEEE Wireless Communications*, vol. 23, no. 2, pp. 112–117, 2016.

[76] R. Balakrishnan and I. Akyildiz, "Local anchor schemes for seamless and low-cost handover in coordinated small cells," *IEEE Transactions on Mobile Computing*, vol. 15, no. 5, pp. 1182–1196, 2016.

[77] H.-S. Jo, Y. J. Sang, P. Xia, and J. G. Andrews, "Heterogeneous cellular networks with flexible cell association: A comprehensive downlink sinr analysis," *IEEE Transactions on Wireless Communications*, vol. 11, no. 10, pp. 3484–3495, 2012.

[78] C. Ma, M. Ding, H. Chen, Z. Lin, G. Mao, and D. Lopez-Perez, "On the performance of multi-tier heterogeneous cellular networks with idle mode capability," *arXiv preprint arXiv:1704.02176*, 2017.

[79] J.-S. Ferenc and Z. Néda, "On the size distribution of poisson voronoi cells," *Physica A: Statistical Mechanics and its Applications*, vol. 385, no. 2, pp. 518–526, 2007.

[80] A. Hinde and R. Miles, "Monte carlo estimates of the distributions of the random polygons of the voronoi tessellation with respect to a poisson process," *Journal of Statistical Computation and Simulation*, vol. 10, no. 3-4, pp. 205–223, 1980.

[81] S. Singh, H. S. Dhillon, and J. G. Andrews, "Offloading in heterogeneous networks: Modeling, analysis, and design insights," *IEEE Transactions on Wireless Communications*, vol. 12, no. 5, pp. 2484–2497, 2013.

[82] I. S. Gradshteyn and I. M. Ryzhik, *Table of integrals, series, and products*. Academic press, 2014.

[83] 3GPP, "TR 36.828: Further enhancements to LTE Time Division Duplex (TDD) for Downlink-Uplink (DL-UL) interference managemnet and traffic adapataion," June 2012.

[84] J. Liu, M. Sheng, L. Liu, and J. Li, "Effect of densification on cellular network performance with bounded pathloss model," *IEEE Communications Letters*, vol. 21, no. 2, pp. 346–349, 2017.

[85] M. Ding, D. López-Pérez, G. Mao, and Z. Lin, "Ultra-dense networks: Is there a limit to spatial spectrum reuse?" *arXiv preprint arXiv:1704.00399*, 2017.

[86] D. Liben-Nowell, J. Novak, R. Kumar, P. Raghavan, and A. Tomkins, "Geographic routing in social networks," *Proceedings of the National Academy of*

Sciences of the United States of America, vol. 102, no. 33, pp. 11 623–11 628, 2005.

[87] N. B. Ellison *et al.*, "Social network sites: Definition, history, and scholarship," *Journal of Computer-Mediated Communication*, vol. 13, no. 1, pp. 210–230, 2007.

[88] L. Fu, W. Huang, X. Gan, F. Yang, and X. Wang, "Capacity of wireless networks with social characteristics," *IEEE Transactions on Wireless Communications*, vol. 15, no. 2, pp. 1505–1516, Feb 2016.

[89] B. Zhang, Y. Li, D. Jin, P. Hui, and Z. Han, "Social-aware peer discovery for d2d communications underlaying cellular networks," *IEEE Transactions on Wireless Communications*, vol. 14, no. 5, pp. 2426–2439, May 2015.

[90] F. Wang, Y. Li, Z. Wang, and Z. Yang, "Social community aware resource allocation for d2d communications underlaying cellular networks," *IEEE Transactions on Vehicular Technology*, vol. PP, no. 99, pp. 1–1, 2015.

[91] D. Zwillinger, *Table of integrals, series, and products.* Elsevier, 2014.

[92] M. Agache and B. J. Oommen, "Generalized pursuit learning schemes: new families of continuous and discretized learning automata," *IEEE Transactions on Systems, Man, and Cybernetics, Part B: Cybernetics*, vol. 32, no. 6, pp. 738–749, 2002.

[93] A.-L. Barabási and R. Albert, "Emergence of scaling in random networks," *science*, vol. 286, no. 5439, pp. 509–512, 1999.

[94] M. I. Ashraf, M. Bennis, W. Saad, and M. Katz, "Exploring social networks for optimized user association in wireless small cell networks with device-to-device communications," in *IEEE Wireless Communications and Networking Conference Workshops (WCNCW).* IEEE, 2014, pp. 224–229.

[95] L. C. Freeman, "A set of measures of centrality based on betweenness," *Sociometry*, pp. 35–41, 1977.

[96] B. Latané, J. H. Liu, A. Nowak, M. Bonevento, and L. Zheng, "Distance matters: Physical space and social impact," *Personality and Social Psychology Bulletin*, vol. 21, no. 8, pp. 795–805, 1995.

[97] T. Zhou, L. Lü, and Y.-C. Zhang, "Predicting missing links via local information," *The European Physical Journal B-Condensed Matter and Complex Systems*, vol. 71, no. 4, pp. 623–630, 2009.

[98] C. F. Aliferis, A. Statnikov, I. Tsamardinos, S. Mani, and X. D. Koutsoukos, "Local causal and markov blanket induction for causal discovery and feature selection for classification part i: Algorithms and empirical evaluation," *Journal of Machine Learning Research*, vol. 11, no. Jan, pp. 171–234, 2010.

[99] 3GPP, "Tr 36.828 (v11.0.0): Further enhancements to lte time division duplex (tdd) for downlink-uplink (dl-ul) interference management and traffic adaptation," 2016.

[100] M. Ding, D. L. Pérez, and G. Mao, "A new capacity scaling law in ultra-dense networks," *arXiv preprint arXiv:1704.00399*, 2017.

[101] A. Fotouhi, M. Ding, and M. Hassan, "Dynamic base station repositioning to improve spectral efficiency of drone small cells," *arXiv preprint arXiv:1704.01244*, 2017.

[102] Y. Zhou and W. Zhuang, "Performance analysis of cooperative communication in decentralized wireless networks with unsaturated traffic," *IEEE Transactions on Wireless Communications*, vol. 15, no. 5, pp. 3518–3530, 2016.